

# CEBAF Program Advisory Committee Six (PAC6) Proposal Cover Sheet

This proposal must be received by close of business on April 5, 1993 at:

CEBAF  
User Liaison Office  
12000 Jefferson Avenue  
Newport News, VA 23606

## Proposal Title

"Photoreactions on  $^3\text{He}$ "

## Contact Person

**Name:** Dr. B.L. Berman  
**Institution:** The George Washington University  
**Address:** 725-21st Street, N.W., Room 105  
**Address:**  
**City, State ZIP/Country:** Washington, D.C. 20052  
**Phone:** (202) 994-7192 **FAX:** (202) 994-3001  
**E-Mail → BITnet:** BERMAN@GWUVM **Internet:** BERMAN@GWUVM.GWU.EDU

If this proposal is based on a previously submitted proposal or letter-of-intent, give the number, title and date:

## CEBAF Use Only

Receipt Date: 4/5/93 Log Number Assigned: PR 93-044

By: gp

# Photoreactions on ${}^3\text{He}$

**B.L. Berman\***†‡, C. Bennhold, W.J. Briscoe, P.L. Cole, J.P. Connelly, K.S. Dhuga,  
W.R. Dodge, W.C. Parke, S.L. Rugari, and Z. Papandreou  
Center for Nuclear Studies, The George Washington University  
Washington, DC, 20052

**P. Corvisiero\***, M. Anghinolfi, N. Efimkin, L. Mazzaschi, V. Mokeev, G. Ricco,  
M. Ripani, M. Sanzone, M. Taiuti, and A. Zucchiatti  
INFN - Sezione di Genova e Dipartimento di Fisica dell'Università  
I-16146 Genova, Italy

**G. Audit\***, J-M. Laget, and B. Saghai  
Centre d'Etudes Nucleaires de Saclay, F-91191 Gif-sur-Yvette, France

N. Bianchi, G.P. Capitani, E. De Sanctis, A. Deppman, A. Ebolese, A. Fantoni,  
P. Levi Sandri, V. Muccifora, E. Polli, A.R. Reolon, and P. Rossi  
INFN - Laboratori Nazionali di Frascati, I-00044 Frascati, Italy

C.E. Hyde-Wright  
Department of Physics, University of Washington, Seattle, WA 98195

J.M. Lambert  
Department of Physics, Georgetown University, Washington, DC 20057

S.J. Greene  
Meson Physics Division, Los Alamos National Laboratory, Los Alamos, NM, 87545

\* Co-Spokesperson

† Will present proposal

‡ Contact person

## **Abstract**

We propose to study the behavior of the nucleon resonances in nuclei, the effects of the nuclear three-body force at short distances, the small component of the nuclear wave function involving the delta-isobar configuration. These are the aspects of nuclear physics that can be studied best by means of the interaction of real photons below about 1.5 GeV with  $^3\text{He}$  with the CLAS. We request 400 hours of beam time with a liquid- $^3\text{He}$  target, of which 150 hours represent overlap with Experiment 91-014.

## 1. Introduction

${}^3\text{He}$  is the only stable nucleus that fulfills the four requirements for our proposed study: a) it has a binding energy per nucleon more than twice as large as  ${}^2\text{H}$ , making it more typical of nuclear matter; b) it has enough nucleons so that one can study the influence of nearby hadronic matter on the N-N force; c) it has few enough nucleons so that its properties and behavior can be treated rigorously by theoretical calculations in the continuum; and d) it can be studied in the laboratory without the onerous task of dealing with a radioactive target. (There are a number of important measurements that one could, and should, make which require the use of a  ${}^3\text{H}$  target, but these are not the subject of the present proposal.)

The reduced photon wavelengths for energies between 0.5 and 5 GeV (which we take to be typical for CEBAF) range from about half the radius of the nucleon (0.4 fm) to one-tenth of this value. The internucleon spacing in  ${}^3\text{He}$  is only slightly greater than the diameter of the nucleon (in free space). Thus we expect an intimate connection between the presence of the other two nucleons and the occurrence of an excitation or decay process which takes place on the first. For example, at the lower side of this range of energies, the resonance region up to 2 GeV, we expect to observe a measurable influence of the nearby nucleons on the propagation and decay of a resonance which is photo-excited on the struck nucleon. On the other hand, at the higher side of this energy range, the situation is not so clear: will the nucleus behave merely as a collection of free nucleons, or will we be able to see quark-structure effects in the nucleus that do not occur in the free nucleon?

This proposal focuses on three kinds of physical phenomena: resonances in nuclei, three-body force effects, and the  $\Delta$ -isobar part of the nuclear wave function. Each of these phenomena is studied in various exclusive reaction channels. In addition, data for certain other reaction channels which will be acquired simultaneously bear upon several other problems of current interest in nuclear physics.

Recent total photoabsorption data on Be and C for photon energies from 0.2 to 1.1 GeV show very strong (35% in cross section) suppression in the region of the  $D_{13}$  and  $F_{15}$  resonances. This suppression is in strong contrast to the  $\Delta$  resonance, which shows only Fermi-broadening effects. We will study the possible suppression of the photoabsorption cross section in  ${}^3\text{He}$  by detecting the exclusive N- $\pi$  and N- $\pi$ - $\pi$  channels.

The large difference in the behavior of the  $\Delta$  versus the  $D_{13}$  and  $F_{15}$  resonances is puzzling, since their lifetimes in free space are not very different. This difference might be caused by the different quark structures of these resonances. Consider, for example, a harmonic-oscillator quark model. The N and the  $\Delta$  have essentially identical quark wave functions in space. The  $D_{13}$  and  $F_{15}$ , however, include p- and d-orbit oscillator states, respectively. We therefore expect the  $D_{13}$  and  $F_{15}$  resonances to have larger rms radii than the  $\Delta$ . Thus the higher resonances are damped by color opacity--bigger objects interact more strongly with the nuclear medium.

The reactions  ${}^3\text{He}(\gamma, ppn)$  and  ${}^3\text{He}(\gamma, NNN\pi)$  in which all three nucleons carry high momentum necessarily require that all three nucleons be involved in the interaction. This can be due to ground-state correlations, final-state interactions, and three-body currents. In later sections, we discuss specific kinematic signatures for the contributions from three-body-force effects.

## 2. Resonances in Nuclei

### A. Previous Work

There have been very few previous studies of the behavior of resonances in nuclei. Recent measurements of the photon absorption cross sections for  ${}^9\text{Be}$ ,  ${}^{12}\text{C}$ , and  ${}^{238}\text{U}$  at Frascati (Bia93, Ang93) and Mainz (AudPC, KnePC) have shown that the  $D_{13}$  and  $F_{15}$  resonances are damped much more than expected from the Fermi motion of the nucleons in the nucleus alone. Figure 1 shows the new experimental data for Be and C. The continuous line is the result of a calculation (MokPC) which takes into account the broadening of resonances due to Fermi motion. A realistic momentum distribution has been used (CioPC) (for  ${}^{12}\text{C}$ ), and different helicity amplitudes for neutron and proton photon coupling have been considered. The effect of reducing both the  $D_{13}$  and  $F_{15}$  resonances by the same factor (0.8 in amplitude) also is shown in Fig. 1. The agreement between the calculation (dashed line) and the experimental data is quite good, and suggests that baryon resonances higher than the  $\Delta(1232)$  are damped or suppressed by some nuclear-medium effect. This effect was observed, however, in a purely inclusive channel. Our objective here is to examine the propagation and the attenuation of the  $D_{13}$  and  $F_{15}$  resonances produced in the  ${}^3\text{He}$  nucleus. With the CLAS, the most important exclusive channels can be identified and measured.

In the constituent quark-model description, N and  $\Delta$  states consist of three quarks in their lowest (s-wave) states, while the  $N^*$  resonances are due to the excitation of one or more quarks to a higher level: the excitation of one quark to the 1p or 1d level produces the  $D_{13}$  and  $F_{15}$  resonances, respectively. In this picture, the higher levels are more sensitive to modifications of the quark potential. Quark tunneling becomes more and more probable as the energy increases, whether or not the potential well is modified, so that the E1 and E2 transition strengths to the  $D_{13}$  and  $F_{15}$  resonances should be very sensitive to the quark-confinement size parameter  $1/\alpha$ .

The theoretical and experimental information available on the M1 resonance  $P_{33}(1232)$ , the E1 resonance  $D_{13}(1520)$ , and the E2 resonance  $F_{15}(1680)$  is summarized in Table 1. The existing experimental data on these resonances, namely, the mass difference  $M^*-M$  (relative to the nucleon mass  $M$ ), the total cross section integrated over the resonance  $\Sigma$ , and the helicity amplitudes  $A_{1/2}$  and  $A_{3/2}$  are compared with the corresponding predictions of the constituent quark model of Isgur and Karl (Isg78-79).

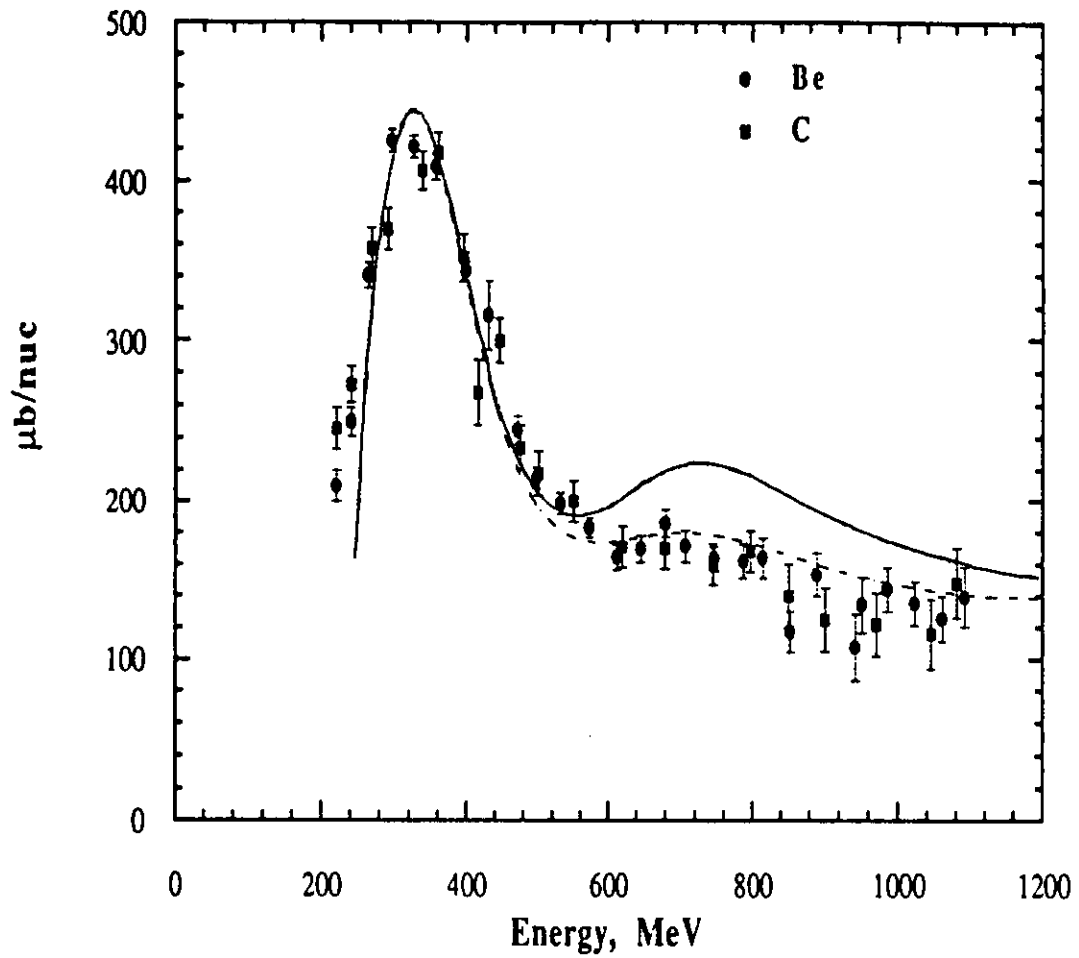


**Fig. 1.** Total photon absorption cross section per nucleon for Be (circles) and C (squares). The solid curve is a fit to the average of the free proton and neutron cross sections, broadened by the Fermi motion for C. The dashed curve results from attenuating the  $D_{13}$  and  $F_{15}$  amplitudes each by 20%.

[The cross section is proportional to the sum of the squares of the helicity amplitudes.] The comparison shows, in addition to the remarkably good agreement, the sensitivity of each state to the model parameters. The mass splitting  $M^*-M$  between the  $\Delta$  and the proton is almost completely determined by the spin-dependent terms in the Hamiltonian. Conversely, the E1 and E2 transition strengths to the  $D_{13}$  and  $F_{15}$  resonances, respectively, are very sensitive to the quark-confinement parameter  $1/\alpha$ , reasonable agreement being obtained for  $1/\alpha \cong 0.5$  fm. [This value is close to the hard core radius of the N-N potential and quite different from the one obtained by fitting the harmonic-oscillator proton rms radius  $\langle r^2 \rangle_{ho} = 1/\alpha^2$ , which leads to a value for  $1/\alpha$  of 0.86 fm.]

Electric dipole and quadrupole sum rules state that the integrated E1 cross section is proportional to  $1/\alpha^2$ , and the integrated E2 cross section is proportional to  $1/\alpha^4$  (Bri87,88). For this reason, the dependence of the  $D_{13}$  and  $F_{15}$  resonance strengths on the confinement parameter is strong, and it will be extremely interesting to obtain exclusive-channel experimental data for these resonances inside  ${}^3\text{He}$  in order to explain whether and to what extent the presence of neighboring nucleons modifies the baryon resonances. No such data exist at present.

The use of the CLAS will naturally lead to a good measurement of the dominant  ${}^3\text{He}$  photodisintegration and photoproduction channels with at most one neutral particle in the final state. The sum of the cross sections for all of the principal exclusive channels measured in this experiment will therefore provide a good approximation for the total photonuclear absorption cross sections for  ${}^3\text{He}$ . Ciofi (CioPC) has calculated the momentum distributions of the nucleons in  ${}^3\text{He}$ , shown in Fig. 2. We have used these to compute the total photon absorption cross section for  ${}^3\text{He}$ , where the  $D_{13}$  and  $F_{15}$  resonances have been broadened by Fermi motion, but not suppressed; this prediction is shown in Fig. 3. It will become clear from the results of the measurements proposed here whether the assumption of no suppression in  ${}^3\text{He}$  is justified.

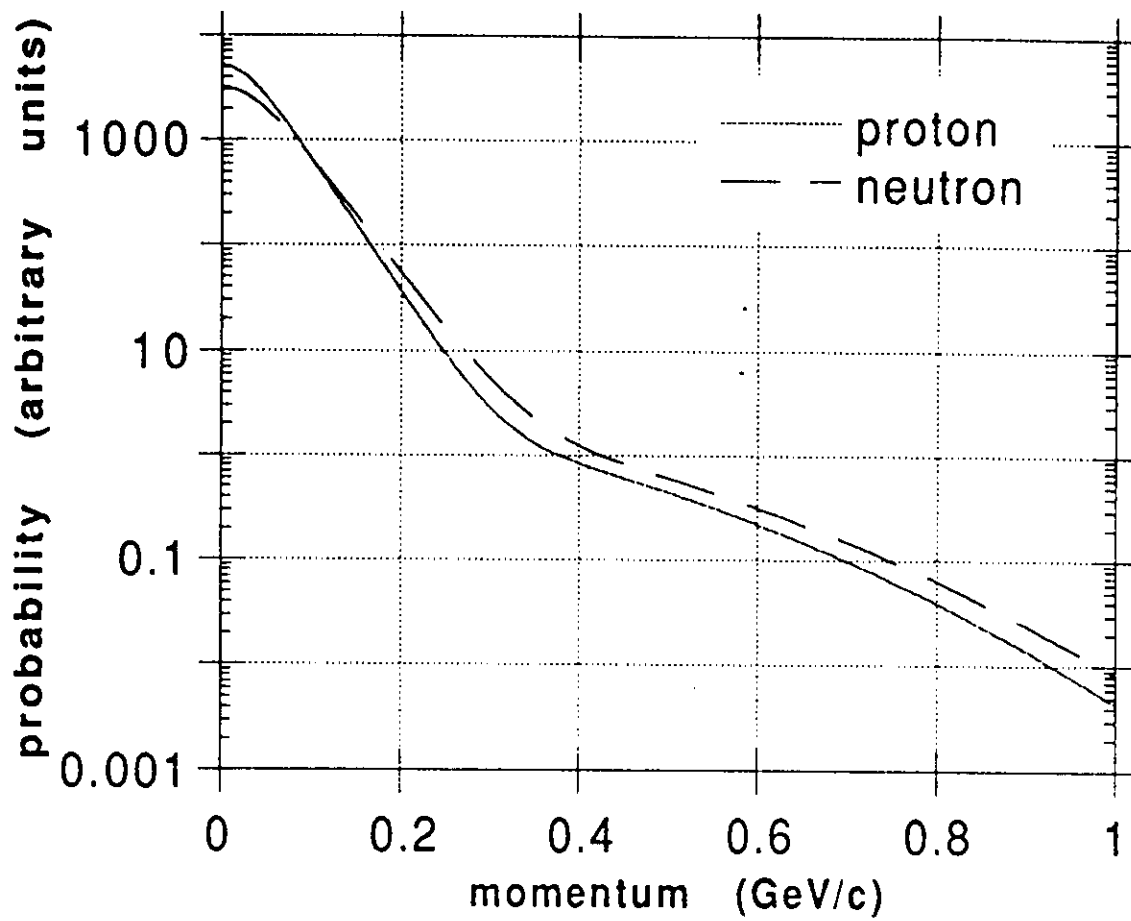


**Fig. 2.** Momentum distributions of protons (solid line) and neutrons (dashed line) in  $^3\text{He}$ , from (CioPC).

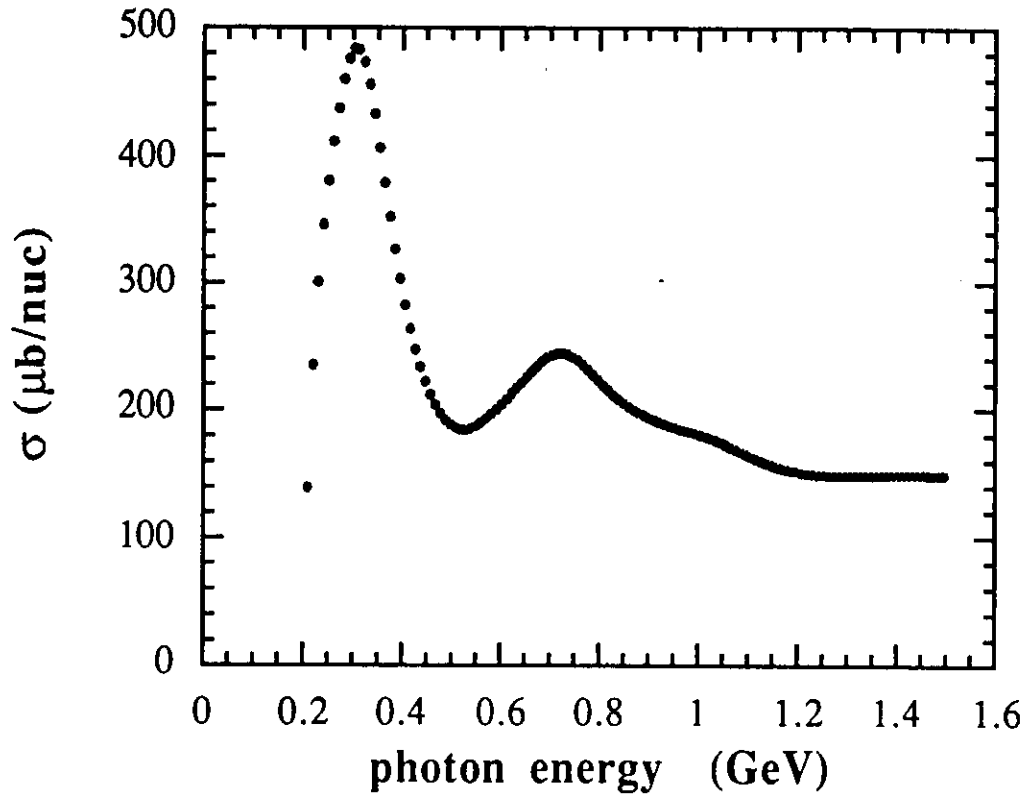


**Fig. 3.** Total photon absorption cross section per nucleon for  ${}^3\text{He}$ , predicted from the free-nucleon cross sections, broadened by Fermi motion.

**Table 1**  
Resonance Absorption Data

		Proton		Neutron	
		Expt	Thy	Expt	Thy
M1	M*-M [MeV]	292	300	292	300
	$\Sigma$ (1232) [mb-MeV]	63	52	65	52
	$A_{1/2}$ (1232) [ $\text{GeV}^{-1/2} \cdot 10^{-3}$ ]	-141±5	-103		-103
	$A_{3/2}$ (1232) [ $\text{GeV}^{-1/2} \cdot 10^{-3}$ ]	-258±11	-179		-179
E1	M*-M [MeV]	580	595	580	595
	$\Sigma$ (1520) [mb-MeV]	32	42	13	25
	$A_{1/2}$ (1520) [ $\text{GeV}^{-1/2} \cdot 10^{-3}$ ]	-22±10	-23	-65±13	-45
	$A_{3/2}$ (1520) [ $\text{GeV}^{-1/2} \cdot 10^{-3}$ ]	167±10	128	-144±14	-122
E2	M*-M [MeV]	798	775	798	775
	$\Sigma$ (1680) [mb-MeV]	19	27	15	8
	$A_{1/2}$ (1680) [ $\text{GeV}^{-1/2} \cdot 10^{-3}$ ]	-17±10	0	31±13	26
	$A_{3/2}$ (1680) [ $\text{GeV}^{-1/2} \cdot 10^{-3}$ ]	127±12	91	-30±14	-25

## B. The Event Generator

We wrote an event-generator code which takes into account all of the principal  $1\pi, 2\pi, 3\pi, \dots$  channels in the interaction of real photons with nucleons in  $^3\text{He}$ . The Fermi motion of nucleons inside the nucleus is accounted for by the use of a realistic momentum distribution in  $^3\text{He}$  (CioPC, Fig. 2). Different channels are weighted proportional to their cross sections, and for all of the one- and two-pion channels the resonant amplitude and the continuum (Born + background) terms are considered separately.

In particular, for the one-pion channels, we follow the phenomenological analysis of Walker (Wal69), which fits the existing experimental data on the nucleon very well, as can be seen in Fig. 4. The helicity amplitudes  $A_{\lambda\mu}(\theta, \phi)$ , where  $\lambda$  and  $\mu$  are the initial- and final-state helicities, respectively, are given separately for resonant, Born, and background terms as a function of the pion center-of-mass angles  $\theta$  and  $\phi$ . The resonant term is assumed to have a Breit-Wigner shape

$$A(W) = A(W_0) (k_0 q_0 / kq)^{1/2} (W_0 \Gamma^{1/2} \Gamma_\gamma^{1/2}) / (s - s_0 - iW\Gamma)$$

The eight helicity amplitudes  $A_{\lambda\mu}$  are not independent--the four with  $\lambda_k = -1$  are simply related to the four with  $\lambda_k = +1$  by parity symmetry. Thus, only four helicity amplitudes are used:

$$\begin{aligned} H_1 &= A_{3/2, 1/2} & H_2 &= A_{1/2, 1/2} \\ H_3 &= A_{3/2, -1/2} & H_4 &= A_{1/2, -1/2} \end{aligned}$$

Each of these is the sum of Born, resonant, and background terms

$$H = H_{\text{Born}} + H_{\text{Res}} + H_{\text{bkgd}}$$

The differential cross section can be written as

$$d\sigma(\theta)/d\Omega = \frac{1}{2} q/k \sum |H_i|^2$$

where  $q$  and  $k$  are the magnitude of the pion and photon center-of-mass momenta. From these calculations it is therefore possible to describe in a realistic way the angular distribution and to study in a quantitative way the effect of any damping of resonances in nuclear matter.

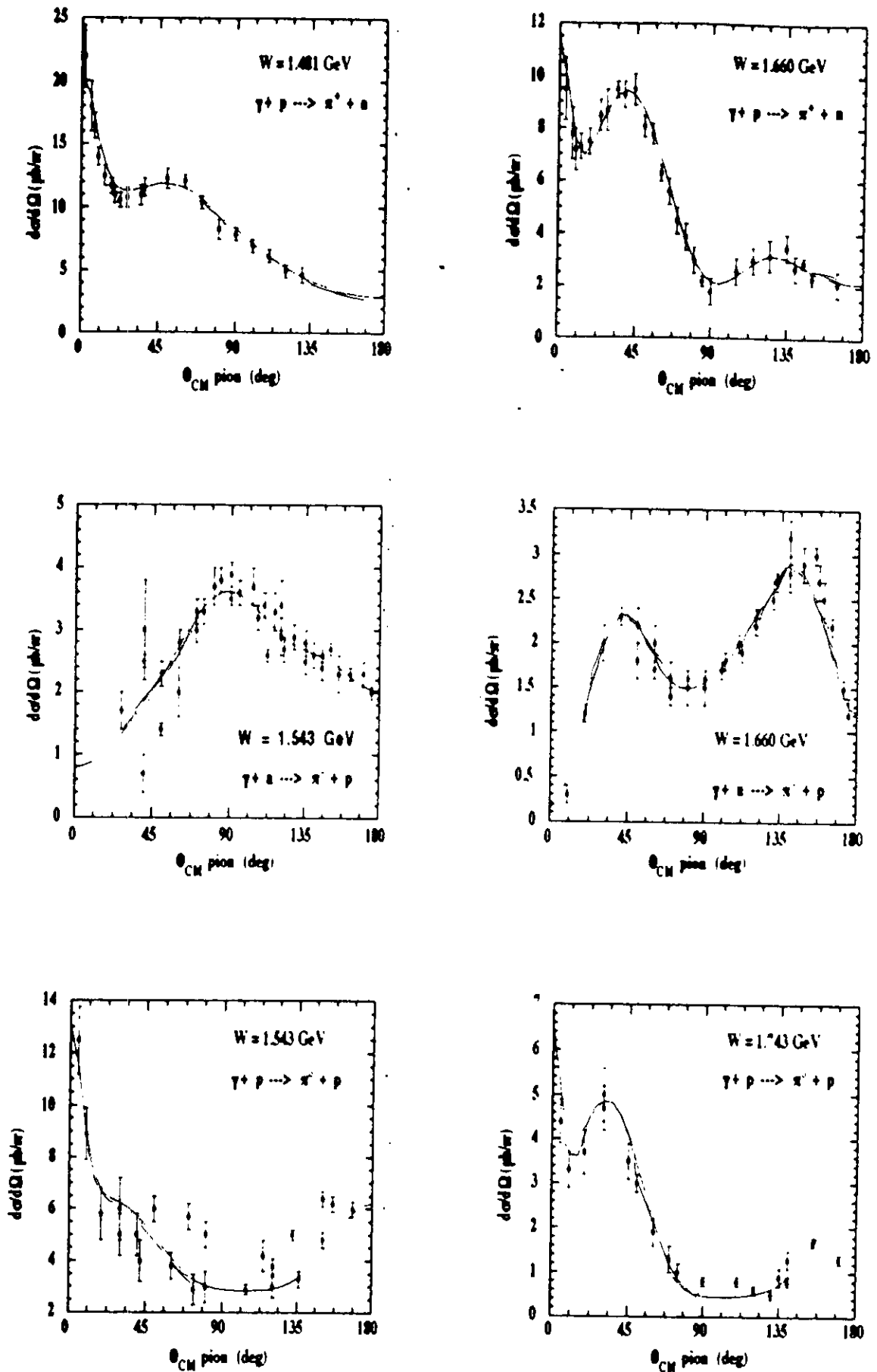


Fig. 4. Differential cross sections for photopion production on the free nucleons calculated from the helicity-amplitude formulation near the  $D_{13}$  and  $F_{15}$

Two-pion events are described using a code (RipPC) where both the  $\Delta$ - $\pi$  and the  $\rho$ -N production are treated including the most important Feynman diagrams, namely, the contact term, pion-in-flight, t-channel  $\Delta$  exchange, direct Born term, and s-channel resonance for the  $\Delta$ - $\pi$  reactions, plus diffractive scattering, pion exchange, and s-channel resonance term for the  $\rho$ -N reactions. The results have been normalized to existing  $\Delta^{++}$ - $\pi^-$  and  $\rho^0$ -p experimental data. Two-pion phase-space events are described using the currently available data tables.

Phase-space processes for three- and four-pion production which may be a relevant background for the channels investigated here have been included, weighted by their relative cross sections.

### C. Single-pion photoproduction--the ( $\gamma, \pi N$ ) channel

All of the prominent  $N^*$  resonances above the  $\Delta$  have branching ratios for the single-pion channel which are of the order of 50%. The understanding of the structure of the resonances in few-body systems requires therefore an accurate investigation of the one-pion decay channels. Starting from a phenomenological description (Wal69, Met74) of all of the single-pion photoproduction channels on the free nucleon, we find that the size and even the shape of the differential cross sections are very sensitive to the resonance strength. Figure 5 shows that for both E1 and E2 transitions, an attenuation of 10-30% is clearly apparent near the resonant peaks, although very little effect is seen at very large and small angles where nonresonant terms are dominant. Therefore, we propose to measure the attenuation, if any, of the  $D_{13}$  and  $F_{15}$  resonances in  $^3\text{He}$  through the angular distribution of pions for all of the exclusive one-pion channels where at most one neutral particle is present in the final state, i.e.,

$^3\text{He}(\gamma, \pi^0 p)pn$ , where only resonant terms contribute, and

$^3\text{He}(\gamma, \pi^+ n)pn$  and

$^3\text{He}(\gamma, \pi^- p)pp$ , where both Born and resonant terms contribute.

The CLAS acceptances for N- $\pi$  coincidence detection are shown in Fig. 6 as a function of the pion laboratory angle at the  $D_{13}$  and  $F_{15}$  energy values. The reaction  $^3\text{He}(\gamma, \pi^0 n)pp$  has a rather low acceptance (due to the limited geometrical acceptance of CLAS for photons and neutrons) which can, however, be increased (by a factor of about three) if only one photon from  $\pi^0$  decay is detected and we know, from missing-mass and missing-

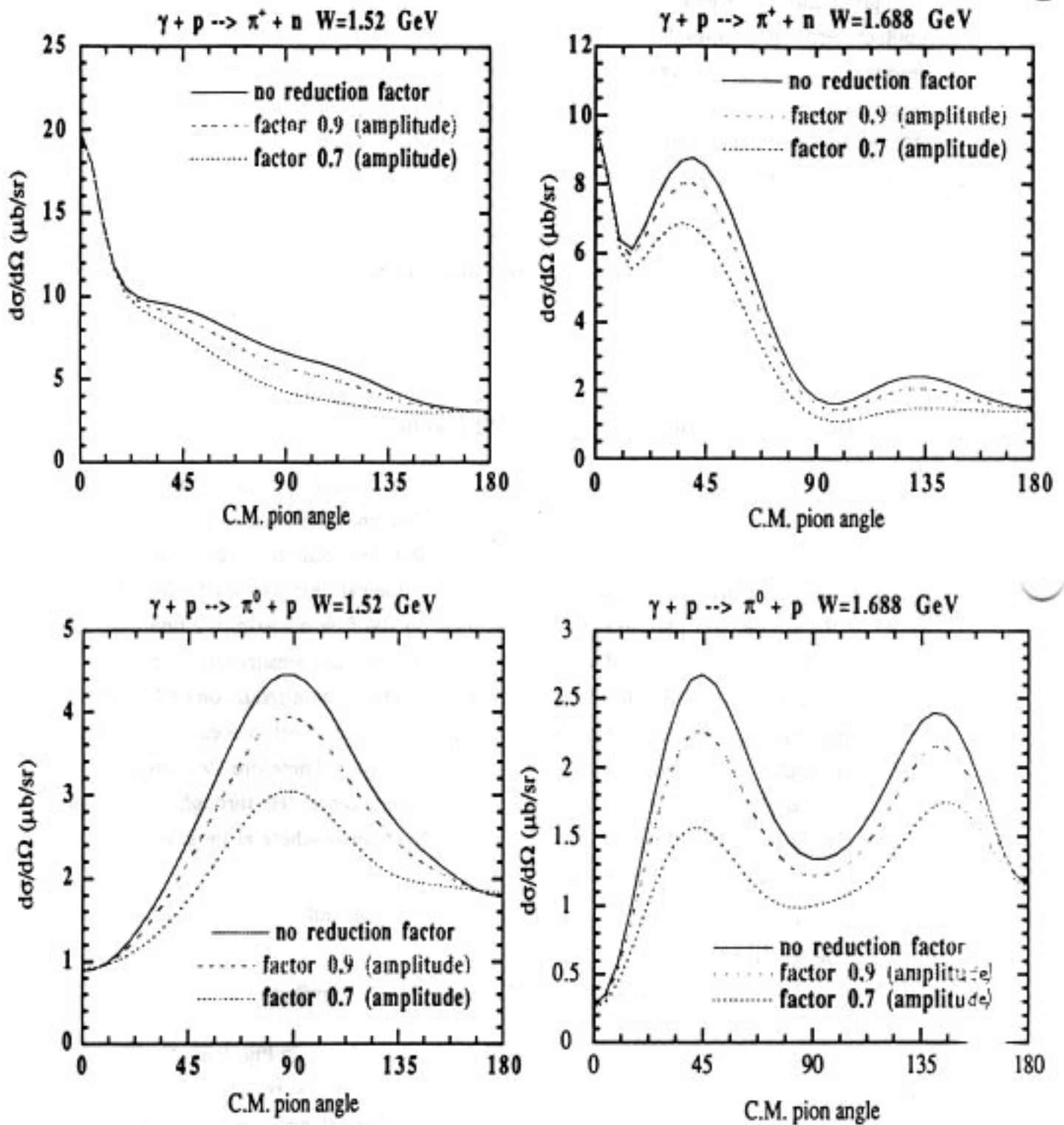


Fig. 5. Differential cross sections for (top)  $\gamma + p \rightarrow \pi^+ + n$  and (bottom)  $\gamma + p \rightarrow \pi^0 + p$  (solid lines), compared with what they would be if the resonant amplitudes for the  $D_{13}$  (left) and  $F_{15}$  (right) resonances were reduced by 10% (dashed lines) and by 30% (dotted lines).

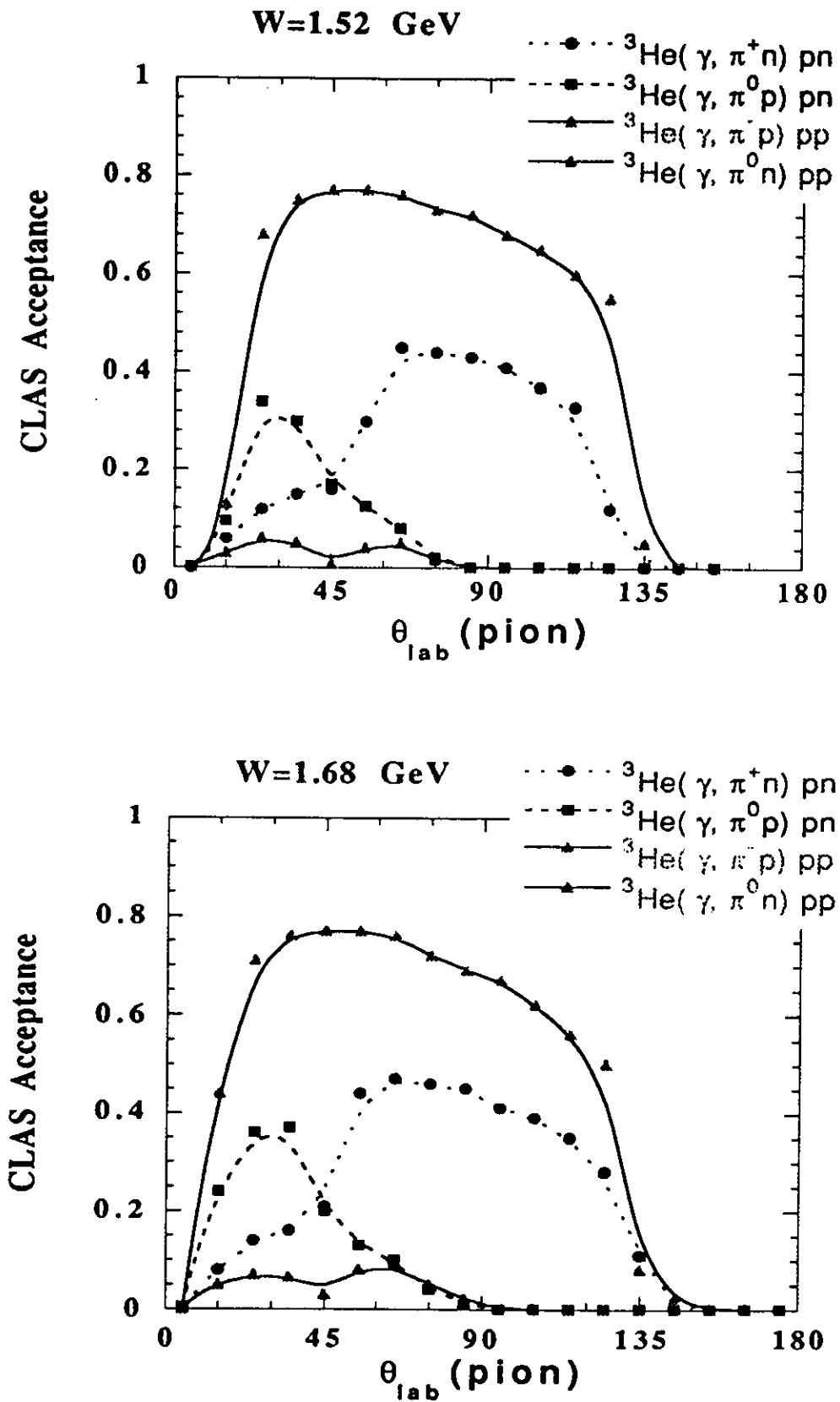


Fig. 6. CLAS acceptance computations for the single-pion decay channels of the  $D_{13}$  (top) and  $F_{15}$  (bottom) resonances, when both the pion and the nucleon are

momentum reconstruction, that the other photon has been lost. One-pion exclusive channels can be identified unambiguously through the invariant mass reconstruction  $W$ , shown in Fig. 7, where

$$W^2 = m_N^2 + m_\pi^2 + 2E_N E_\pi - 2\mathbf{p}_N \cdot \mathbf{p}_\pi$$

Expected counting rates per  $\text{g/cm}^2$  of target thickness are presented in Fig. 8, assuming a  $\Delta\theta$  bin of  $10^\circ$ , a total photon intensity of  $10^7 \text{ s}^{-1}$  in the  $0.35E_0 - 0.95E_0$  tagging energy interval, and a  $\Delta k/k$  energy bin of 2%. Simulations were done taking into account all of the possible multipion photoproduction channels where the resonant part of the transition amplitude for the  $1\pi$  channels was multiplied by reduction factors of 0.9 and 0.7. Figure 9 shows the expected total counts obtained with the CLAS for the  ${}^3\text{He}(\gamma, \pi^0 p)pn$  and  ${}^3\text{He}(\gamma, \pi^+ n)pn$  reactions as a function of the pion laboratory angle at the  $D_{13}$  and  $F_{15}$  energy values. The error bars include both the statistical uncertainty (evaluated for 300 hours of beam time) and a systematic uncertainty assumed to be 5%. These measurements will be carried out for incident photon energies between 0.5 and 1.5 GeV, well above the peak of the  $\Delta$  at  $\sim 300$  MeV (the principal interfering process). From the reconstruction of the invariant mass of the events it also will be possible to measure the energy dependence of each one-pion cross section. It should be emphasized that, due to the large solid-angle coverage of the CLAS, it will be possible to measure a reduction of the resonance amplitude which is less than 10%. This means that we are extremely sensitive to nuclear-medium effects on the excitation of the resonances, and therefore we can obtain more precise results than previously possible.

A revealing picture of the high sensitivity of this measurement is given in Fig. 10. Here the hypothesis was made that the photon interacts with a single nucleon in  ${}^3\text{He}$ , the other two being spectators. We can reconstruct the momentum (due to Fermi motion) of the target nucleon from the tagged-photon energy and the measured pion and nucleon momenta. The laboratory differential cross section is obtained from measuring the pion angular distribution and from the CLAS acceptance, and is boosted to the CM frame. The three different sets of points in Fig. 10 refer to the reconstruction of events generated by attenuating the resonant part of the process by the quoted factors.

Of course, this process is particularly easy to study when all of the product particles are charged. Therefore, the  ${}^3\text{He}(\gamma, \pi^- ppp)$  case, for which all three protons and the negative pion are detected and where the missing energy is shown to be insufficient to have produced a second pion, will yield unambiguous, high-statistics data. If reasonable

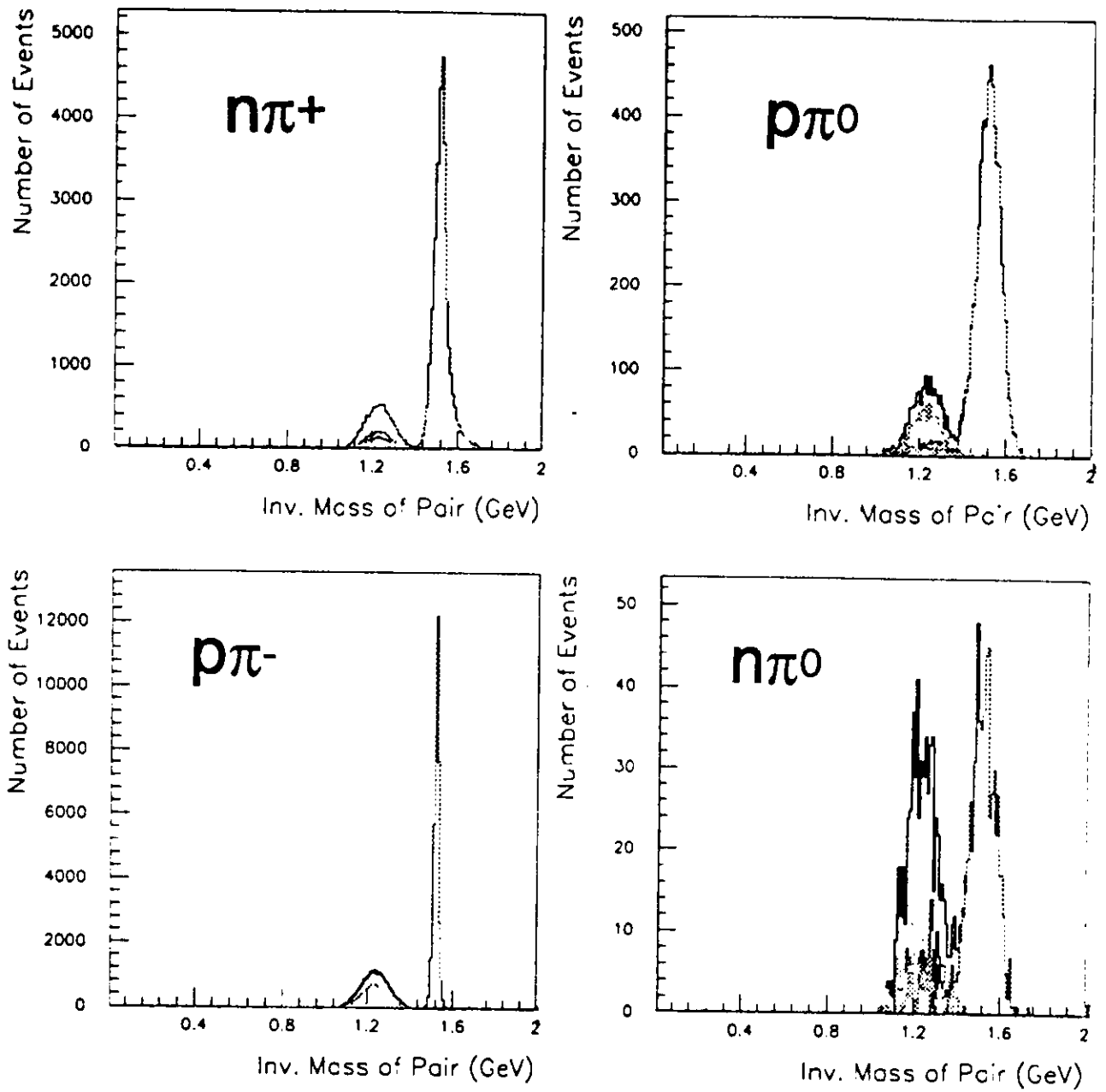


**Fig. 7.** Invariant mass of the N- $\pi$  pair from decay of the  $D_{13}$  resonance. The lower-mass peaks result from two-pion decay events where only one is detected.

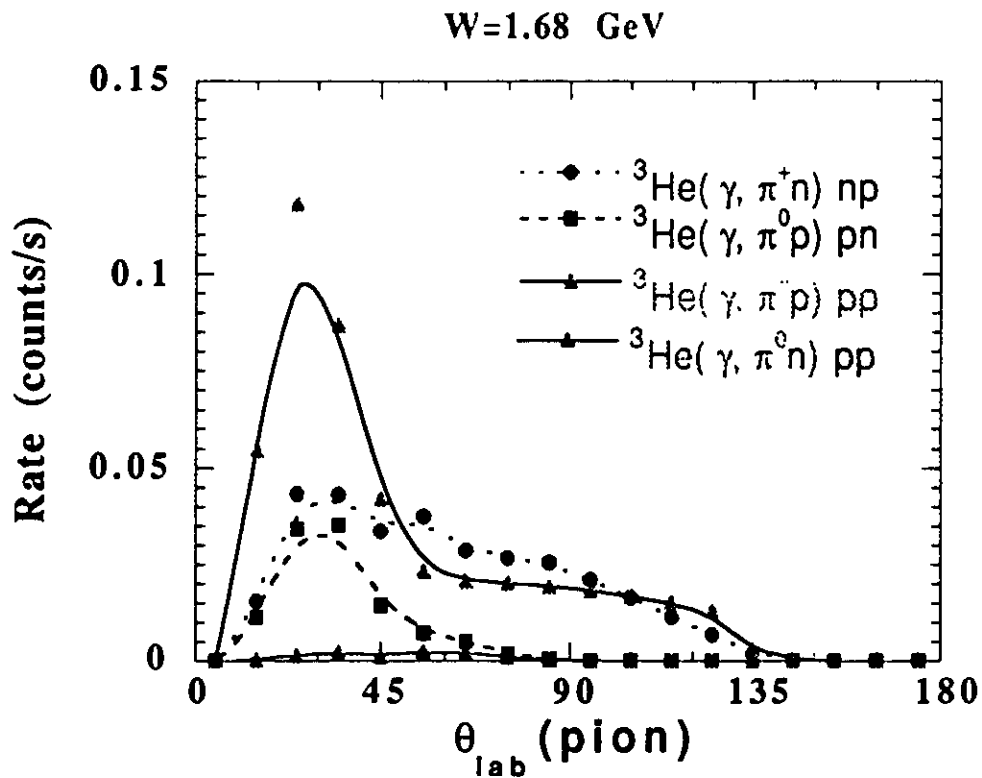
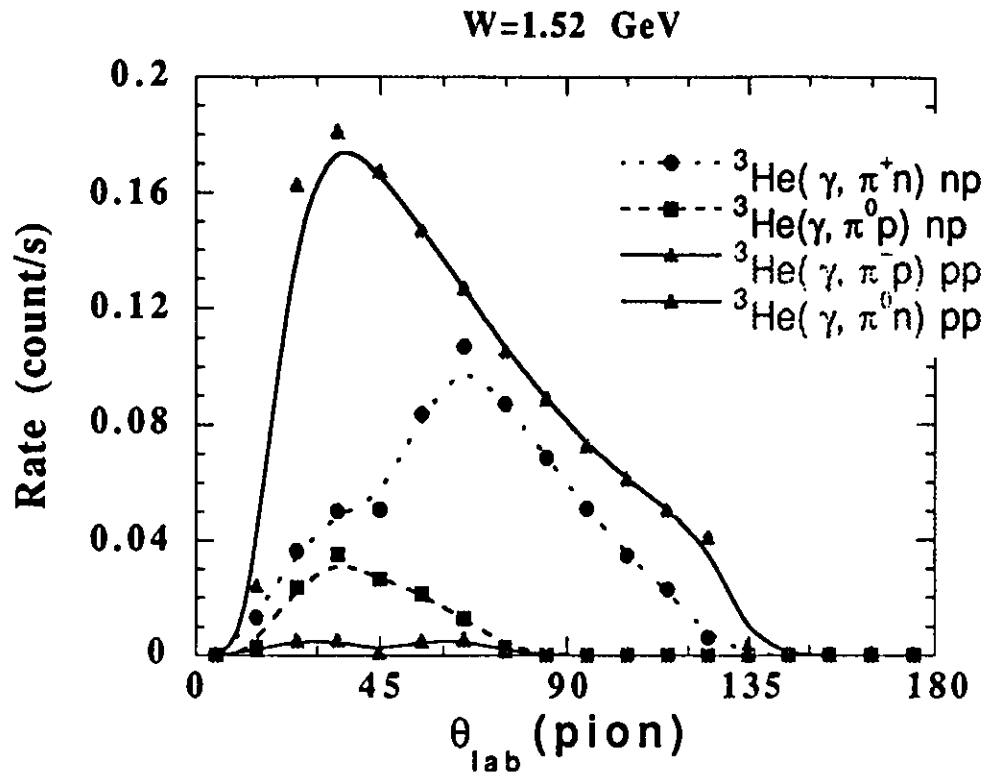


**Fig. 8.** Predicted counting rates per  $\text{gm}/\text{cm}^2$   $^3\text{He}$ -target thickness for the single-pion decay channels of the  $D_{13}$  (top) and  $F_{15}$  (bottom) resonances. No reduction factor has been applied.

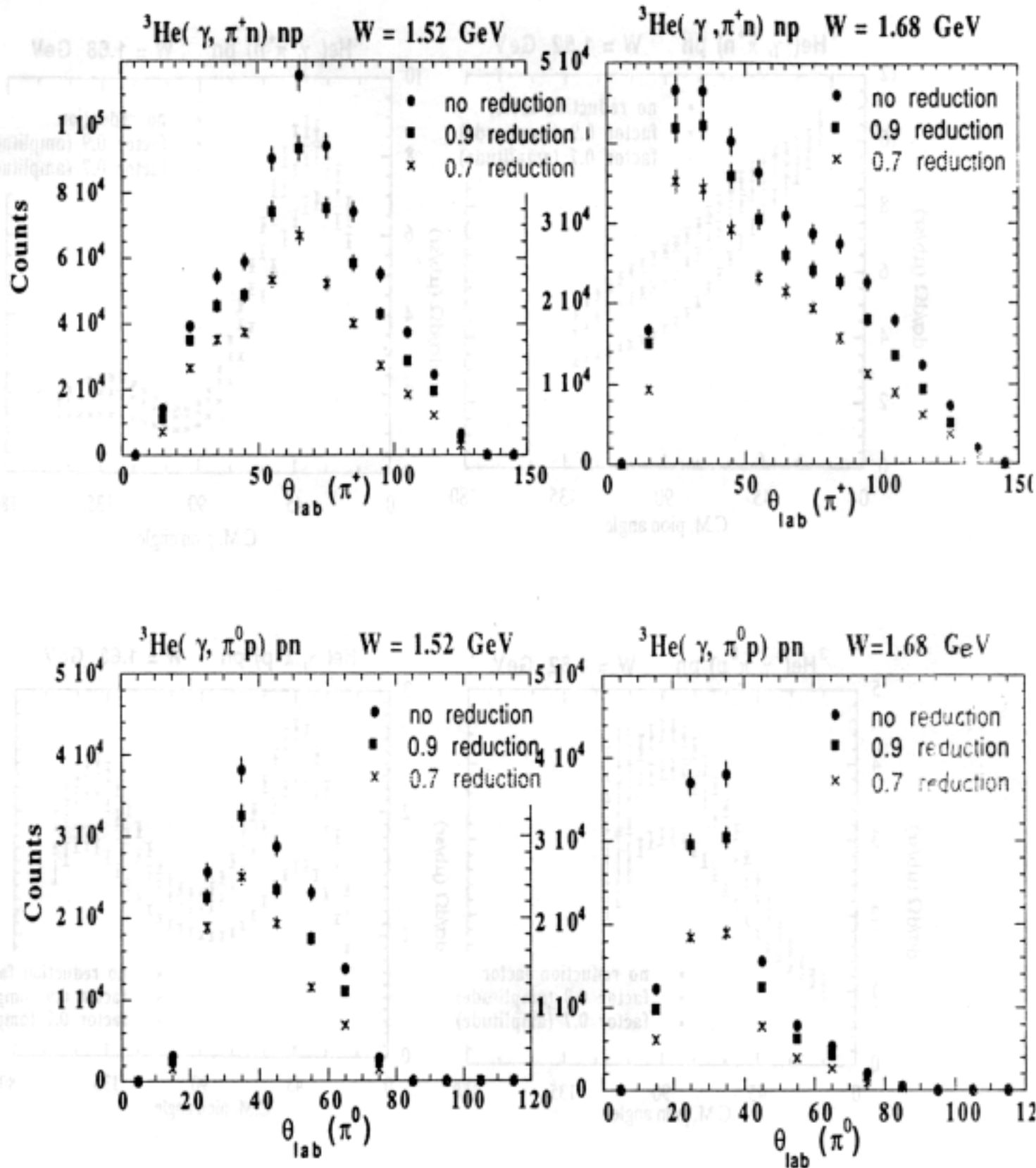


Fig. 9. Total counts predicted per  $\text{gm}/\text{cm}^2$   ${}^3\text{He}$ -target thickness for the  $D_{13}$  (left) and  $F_{15}$  (right) resonances decaying via the  $\pi^+$ -n channel (top) and the  $\pi^0$ -p channel (bottom), for 300 hours of data acquisition. The predicted values are computed for reduction factors of zero, 10%, and 30%, as indicated.

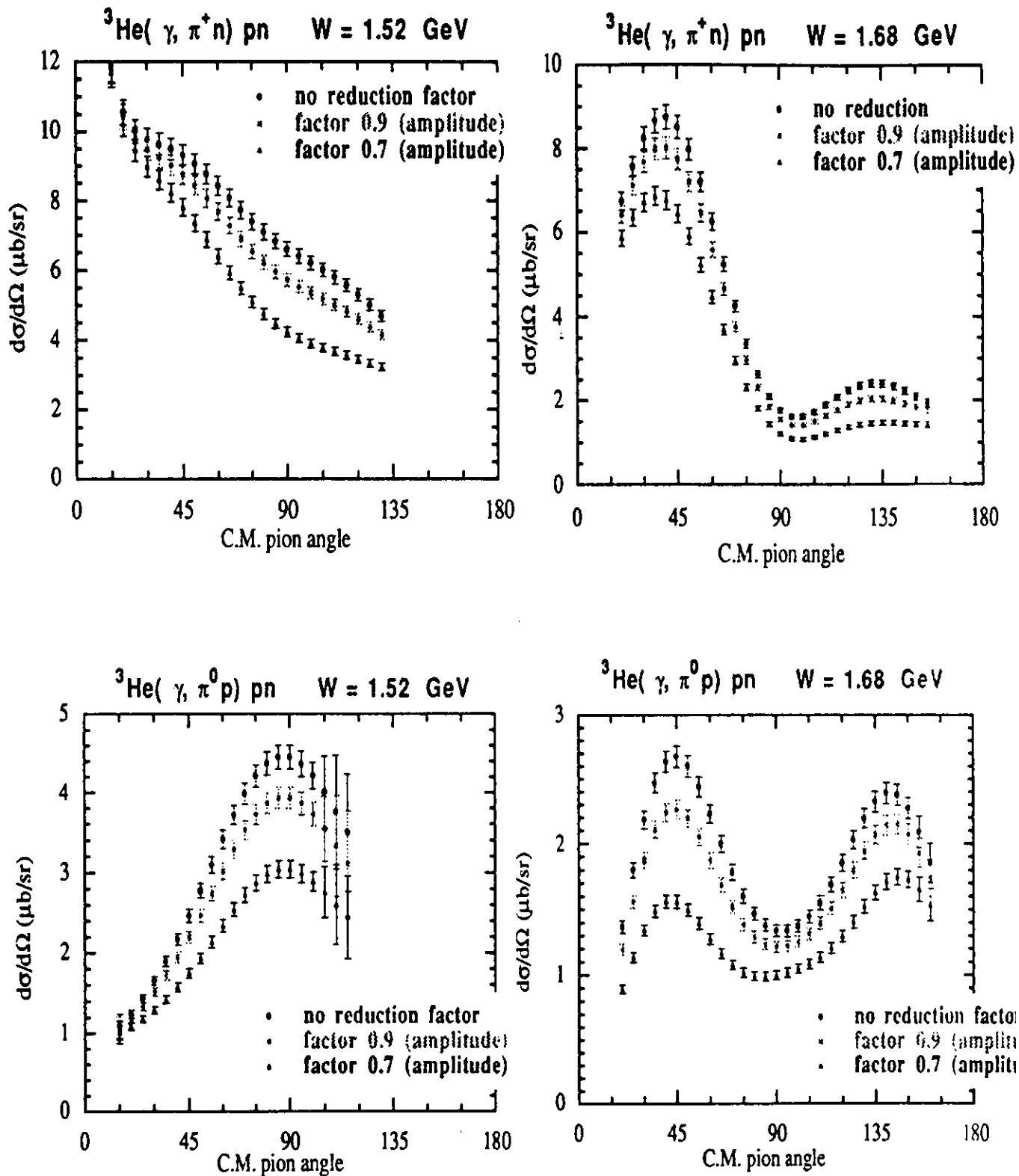


Fig. 10. Simulated differential cross sections for the  $\pi^+$ -n (top) and  $\pi^0$ -p (bottom) decay channel resulting from the values plotted in Fig. 9.

data for the other  $(\gamma, 1\pi 3N)$  channels ( $\pi^+pnn$  and  $\pi^0ppn$ ) can be obtained, as indicated above, then the study of the  $(\pi^-ppp)$  channel should be particularly fruitful. [Another interesting possibility arising from the full detection of  $(\gamma, \pi^-ppp)$  channel lies in the investigation of all of the possible combinations of invariant mass of two- and three-particle resonances. Besides the well known  $\Delta^0$  production channel, two-proton dibaryon states or even more exotic  $pp\pi^-$  resonances can be searched for in the energy range between 1 and 2 GeV (see Sec. 5 below).]

#### D. Two-pion photoproduction--the $(\gamma, \pi\pi N)$ channel

Whether a resonance higher in excitation energy than the  $\Delta(1232)$  decays into a  $\Delta$  plus a  $\pi$ , or into a nucleon plus a  $\rho$  meson, the result is a two-pion event from two sequential two-body decay processes, which can therefore be reconstructed from the observed kinematics. With the liquid  $^3\text{He}$  target, since low-momentum spectator nucleons cannot be detected efficiently with the CLAS, the target nucleon (the proton or neutron which absorbed the photon) cannot be identified unambiguously, unless all of the outgoing particles are detected. We therefore restrict our analysis to those channels with three charged particles in the final state, namely,

$$\begin{aligned} &^3\text{He}(\gamma, \Delta^{++}\pi^-)pn, (\Delta^{++} \rightarrow p\pi^+) \\ &^3\text{He}(\gamma, \Delta^0\pi^+)pn, (\Delta^0 \rightarrow p\pi^-), \text{ and} \\ &^3\text{He}(\gamma, \rho^0 p)pn, (\rho^0 \rightarrow \pi^+\pi^-), \end{aligned}$$

or with at most one neutral particle in the final state, namely,

$$^3\text{He}(\gamma, \Delta^0\pi^0)pp, (\Delta^0 \rightarrow p\pi^-),$$

where the  $\Delta$  decay into two charged particles and its reconstruction is therefore easier.

The CLAS acceptance for detecting the three charged particles is shown in Fig. 11, both for the  $\Delta^{++}$  and the  $\rho^0$  channels. The invariant-mass reconstructions for the pairs  $p\pi^+$ ,  $p\pi^-$ , and  $\pi^+\pi^-$  from events generated with a probability proportional to their cross section at  $W = 1.68$  GeV are shown in Fig. 12. The different channels overlap, and a partial separation is possible only through a fitting procedure. For this procedure, the  $\Delta$  and  $\rho$  are assumed to have a Breit-Wigner shape with fixed widths, while the shapes of the backgrounds are deduced from the simulation; their relative strengths, as well as the  $\Delta$  and

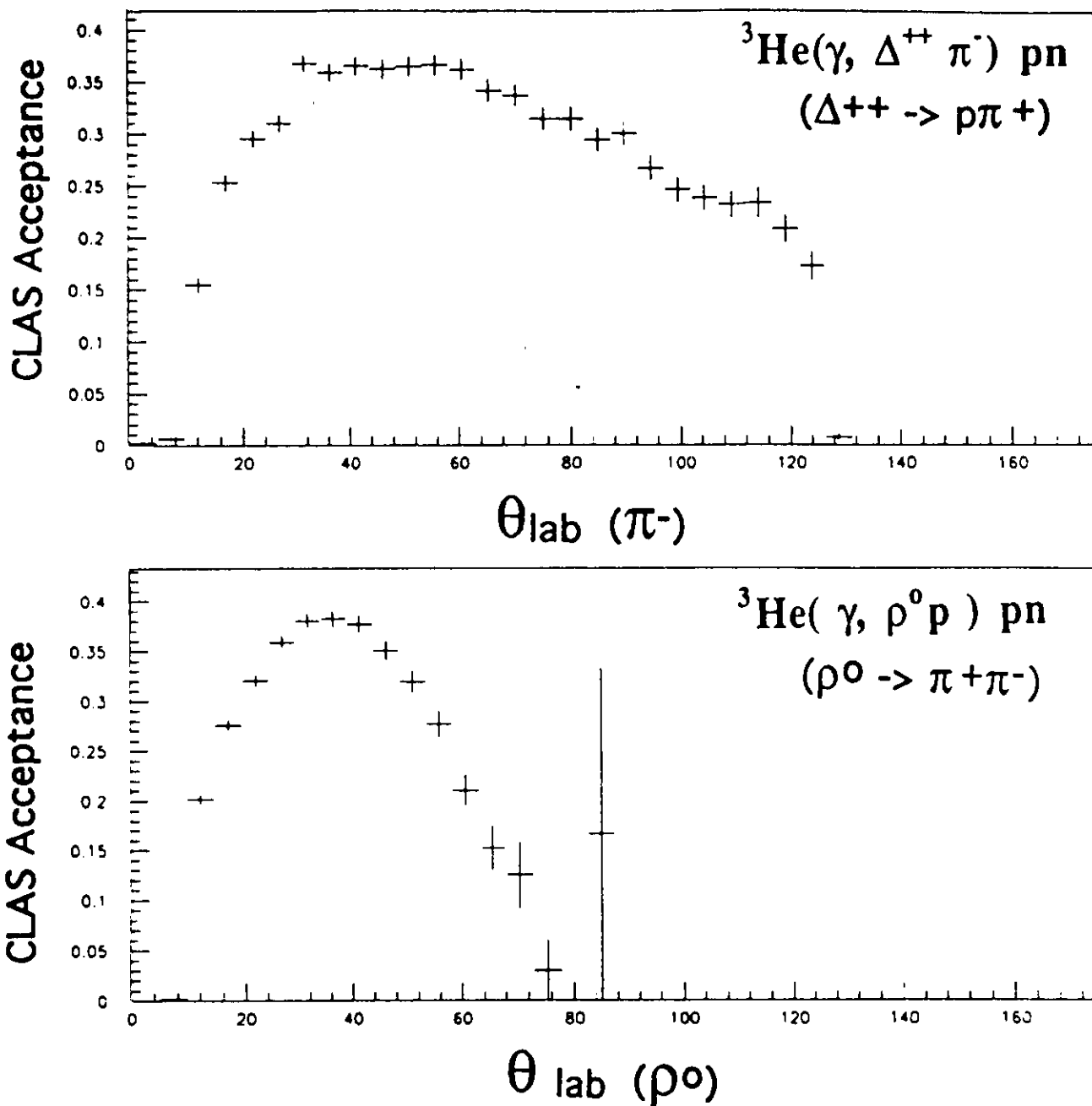
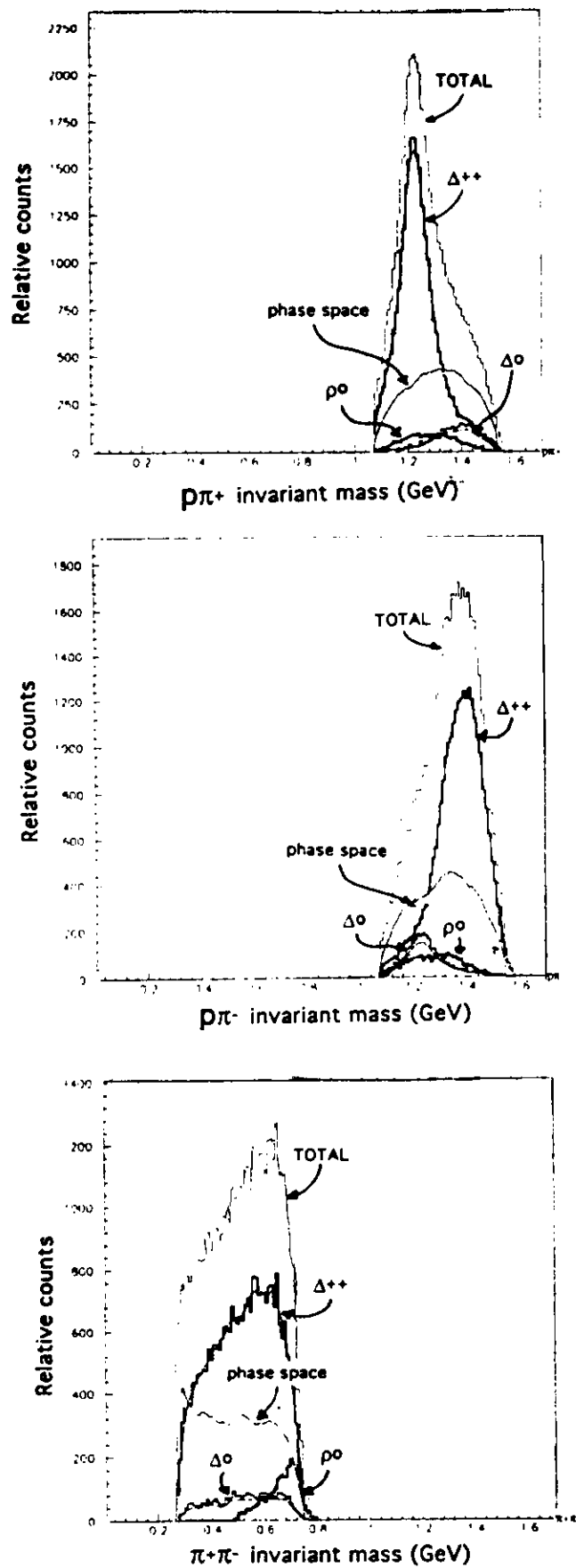


Fig. 11. CLAS acceptance computations for the decay channels of the  $F_{15}$  resonance that result in a  $p\pi^+\pi^-$  final state and all three particles are detected. The top figure shows the acceptance for the  $\Delta^{++}\pi^-$  channel; the bottom, for the  $p\rho^0$  channel.



**Fig. 12.** Relative invariant mass distributions for decay channels of the  $F_{15}$  resonance that result in a  $p\pi^+\pi^-$  final state and all three particles are detected. The top figure shows the invariant mass of the  $p\pi^+$  pair; the middle one, the  $p\pi^-$  pair; the bottom one, the  $\pi^+\pi^-$  pair.

$\rho$  peak heights, are free parameters. The backgrounds arise from phase space and from misidentified combinations of two particles from a three-particle final state. A correlated analysis for the  $\Delta^{++}\pi^-$ ,  $\Delta^0\pi^+$ , and  $\rho^0\pi^0$  reconstruction from the  $p\pi^+\pi^-$  final state has been done. Table 2 shows the comparison among the relative weights of the different channels obtained from the correlated fit, together with their uncertainties; the results are clearly good, and a systematic analysis of the total cross section for the  $2\pi$  processes should therefore be possible in the  $D_{13}$  and  $F_{15}$  energy region.

**Table 2**

Invariant-Mass Analysis for  $p\pi^+$ ,  $p\pi^-$ , and  $\pi^+\pi^-$  Pairs from the  $p\pi^+\pi^-$  Final State

Channel	CLAS Reconstruction	Recognized
$\Delta^{++}\pi^-$	26124	$26082 \pm 330$
$\Delta^0\pi^+$	2941	$2429 \pm 232$
$\rho^0\pi^0$	2362	$2422 \pm 166$
$\pi^+\pi^-\pi^0$	14101	$14538 \pm 514$

The situation becomes even better at higher photon energy, where a larger kinematical region is accessible to the background events, and separation of the  $\Delta$  and  $\rho$  is easier. Moreover, the  $\rho$  production here is favored, and its study is clearly more interesting at higher energy, where the effects of the nuclear medium on the vector-meson-dominance mechanism can be tested. Channels can be separated by fitting the experimental data with the sum of the different processes, each of them with fixed energy dependence and variable strength.

For the  $\Delta^0\pi^0$  channel, the interfering nonresonant production processes (the Born terms) are absent, and the resonant decays can be identified unambiguously. The branching ratio to this channel is low, and unfortunately also the CLAS acceptance is lower than for the other  $2\pi$  channels, due to the presence of a  $\pi^0$ . We hope, however, to disentangle it from the background due to other channels using a similar fitting technique. A detailed study of this interesting channel is still in progress.

### 3. Three-Body-Force Effects

#### A. General approach

The three-nucleon part of the  $^3\text{He}$  wave function is dominated at low energies, and correspondingly long distances, by the two-body N-N force, to the extent that the very existence of a three-body component of the strong nuclear force is still a subject of debate (Ber86, Wei90-92). Our objective here is to demonstrate the existence and to delineate some of the properties of any nuclear three-body force which manifests itself with reasonable probability at the shorter distances that will be accessible at CEBAF.

One of the central problems of nuclear physics is the elucidation of the interaction between nucleons in the presence of other nucleons--the delineation of the properties of the many-body nuclear force. The study of the three-body nuclei, in a sense, embodies the nuclear many-body problem in its purest form, provided only that the nuclear four-body force be substantially weaker (and/or of shorter range) than the three-body force. The recognition of this fact is not new (Ber64), but it remains current. With the availability of high-duty-factor electron beams at the MIT/Bates and NIKHEF accelerators and the approaching advent of CEBAF, the study of three-body forces at short distances is fast becoming a reality.

#### B. Theoretical approach

The few-body approach to the nucleon-nucleus interaction begins with the free N-N force. Then, by studies of the properties of three-nucleon nuclei, N-d reactions and scattering, and three-nucleon final-state interactions (for example, following N-d breakup or the three-body breakup of  $^3\text{H}$  and  $^3\text{He}$  following photo- or electro-excitation), one attempts to elucidate the effects of the nuclear three-body force upon the N-N interaction. This in turn gives rise to three-body modifications of the two-body nuclear force inside nuclei (both finite nuclei and nuclear matter). A number of such attempts have been made. However, a distinction should be made between real three-body forces and the model three-body forces used until now that may suffer from inappropriate or oversimplified approximations in dealing with a real two-body force. Real three-body forces must exist; they correspond to one nucleon interacting with a third nucleon (by pion exchange or

some other mechanism) while at the same time still off shell from its interaction with the second nucleon. In addition, the convergence of a hierarchy of two-, three-, and four-body forces is almost guaranteed by the short-range nature of the N-N force.

As the energy increases, the number of open channels becomes very large, continuum processes become dominant, and calculations that are both exact and complete become more and more difficult. To date, none has been done in the GeV region, and it is clear that an enormous computational effort is required to do so. Therefore, a different approach has been taken by Laget (Lag85-89). Diagrams that are likely to be dominant are computed in kinematical regions that are likely to enhance three-body mechanisms. Although there is no claim of either exactitude or completeness in these calculations, there is a great deal of thought given to the conditions under which the desired effects are likely to be most important, with two very important consequences: (1) the dominant terms are not omitted from the calculation; and (2) the experimentalist derives valuable guidance in deciding where to concentrate his or her experimental effort.

In a more complete treatment, the contributions of full three-body rescattering to the photodisintegration amplitude might be performed in the manner of Gibson and Lehman (Gib84), wherein the electromagnetic interaction is treated as the Born driving term in a Lipmann-Schwinger equation for the full amplitude. The rescattering amplitude would be found separately by solving the appropriate Faddeev equation. This method requires representations of the N-N interaction which must reproduce the two-body data and be in a form which allows a complete calculation in a reasonable time on currently available supercomputers. Such representations are at hand as separable expansions of the N-N interaction which reproduce the results of the Paris potential. These have been used to construct precise bound-state wave functions of  $^3\text{He}$  (Par91) and have been used consistently in photodisintegration processes (Fon92). In this method, the Born contribution comes from the photodisintegration into three free particles. However, in the experiment proposed here, with photon energies in the GeV region, a large number of multipole terms in an expansion of the electromagnetic field will contribute to the breakup amplitude. An alternative is to use the full electromagnetic field interacting with both nucleons and exchanged mesons, abandoning the use of Siegert's Theorem. This type of calculation would be on the forefront of what is possible with current methods and computers. One saving grace is that relativistic corrections are minimized in the central region of phase space of the outgoing nucleons (see below) where each carries about the

same energy. This is the same region where three-body effects are expected to be the strongest.

In the meantime, we need to use the tools that we have available. Figure 13 shows the diagrams used in the calculation of the three-nucleon photodisintegration, from (Aud89,91). Diagrams g and h are true three-body meson-exchange currents, which can be associated with three-body forces. A diagram with  $\rho$  exchange in both legs should also be added at high energies, although it is not clear whether it is critical to do so at energies below 1.5 GeV.

### C. Three-body photodisintegration - the $(\gamma,pp)n$ channel

In order to enhance three-body effects, one must seek to minimize the effects of the ordinary two-body channels. The most straightforward way to accomplish this is to require that each of the three nucleons be emitted with large center-of-mass energy and momentum, and perhaps also that the plane defined by any pair of nucleon momenta not include the direction of the incident photon. This is sometimes known as the "star" configuration, discussed in several papers in (Ber86). In this way one seeks to distinguish a true three-body correlation from two sequential two-body interactions. Kinematically, in addition to the above, we need only to assure ourselves that the missing energy is less than the pion rest mass, so that we know that a pion was not created in the reaction process. We therefore propose to measure the photodisintegration of  ${}^3\text{He}$  into two protons and a neutron, under all of the above kinematic conditions for energies from about 0.3 to 1.5 GeV. By comparing the results with phase-space predictions, we can ascertain the magnitude and kinematic signatures, if any, of three-body-force effects.

Using the diagrams shown in Fig. 13, we have calculated the  ${}^3\text{He}(\gamma,ppn)$  cross section for  $E_\gamma = 800$  MeV for several sets of coplanar star kinematics (polar angle  $\theta = 0^\circ$ ), where the azimuthal angle  $\phi$  (relative to the emitted neutron) is allowed to vary. The angles  $\theta$  and  $\phi$  in the star geometry are defined in Fig. 14. In the center-of-momentum system,  $\theta$  is the polar angle of the plane of the star relative to the photon direction, and  $\phi$  is the azimuthal angle of the neutron in the star plane. Let the subscripts 1 and 2 refer to the two outgoing protons and  $\mathbf{p}_n$  be the momentum of the outgoing neutron. Then the laboratory cross section for the  ${}^3\text{He}(\gamma,pp)n$  reaction is expressed in terms of a reduced cross section by

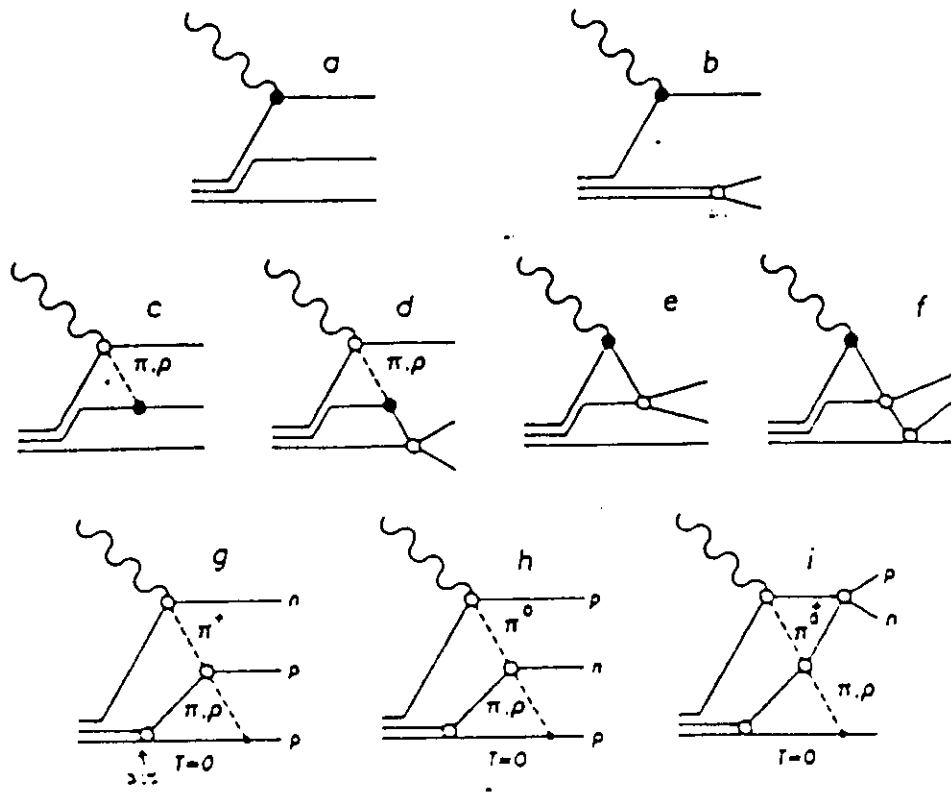


**Fig. 13.** Diagrams used in the calculation of the  ${}^3\text{He}(\gamma,ppn)$  cross section.

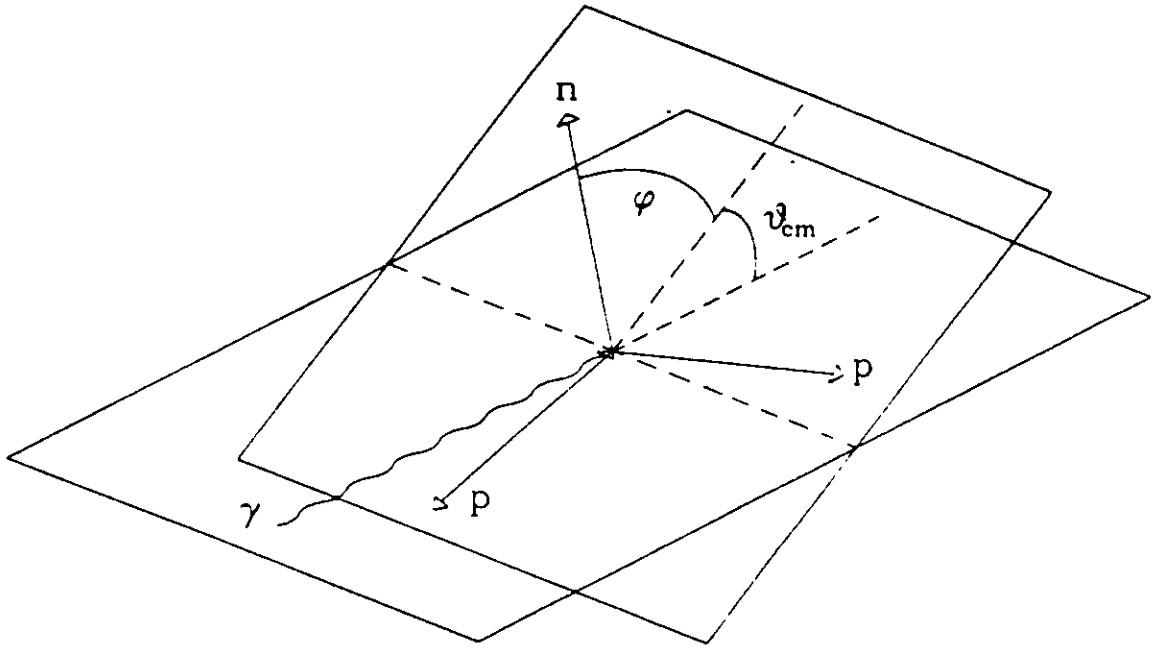


**Fig. 14.** Schematic representation of the star configuration.

$$d^3\sigma/[dp_1d\Omega_1d\Omega_2]_{lab} = K \cdot d^2\sigma/(dp_n[d\Omega_1]_{cm}).$$

Here, K is a kinematical factor that depends only on the energies and momenta of the nucleons. The 2-body and (2+3)-body reduced cross sections and their ratio are given in Table 3 and shown in Fig.15, omitting the MEC contribution because it is very small. It is readily apparent that the place to look for three-body-force effects is near  $\phi = 30^\circ$ , where the triangular singularity of the triangular graph has its maximum effect.

**Table 3**

Three-Nucleon Photodisintegration Cross Sections

$\phi$	K	2-body reduced cross section	(2+3)-body reduced cross section	(2+3)-body and 2-body cross-section ratio
(deg)	(GeV <sup>2</sup> )	$\mu\text{b}/[\text{sr}^2-(\text{GeV}/c)^3]$	$\mu\text{b}/[\text{sr}^2-(\text{GeV}/c)^3]$	
0	0.64	0.52	1.02	2.0
15	0.60	0.14	0.82	6.1
30	0.54	0.07	1.30	18.6
45	0.48	0.07	0.96	12.9
60	0.47	0.08	0.48	5.8
75	0.50	0.13	0.35	2.8
120	1.11	0.49	0.55	1.1
180	1.32	0.25	0.34	1.4

Extensive background and acceptance studies have been carried out for the  ${}^3\text{He}(\gamma,pp)n$  reaction for the CLAS. Details of these studies are given in the Appendix. Here, we summarize the principal results, namely, (a) the techniques that we have developed for distinguishing between the  ${}^3\text{He}(\gamma,pp)n$  and  ${}^3\text{He}(\gamma,pp)n\pi^0$  reactions, and (b) how to extract star-configuration events from the three-nucleon background.

The primary difficulty in identifying the p-p-n channel is in efficiently separating the pionic and non-pionic events without unduly sacrificing the acceptance. The events

$$\Theta = 0^\circ, E_\gamma = 0.8 \text{ GeV}$$

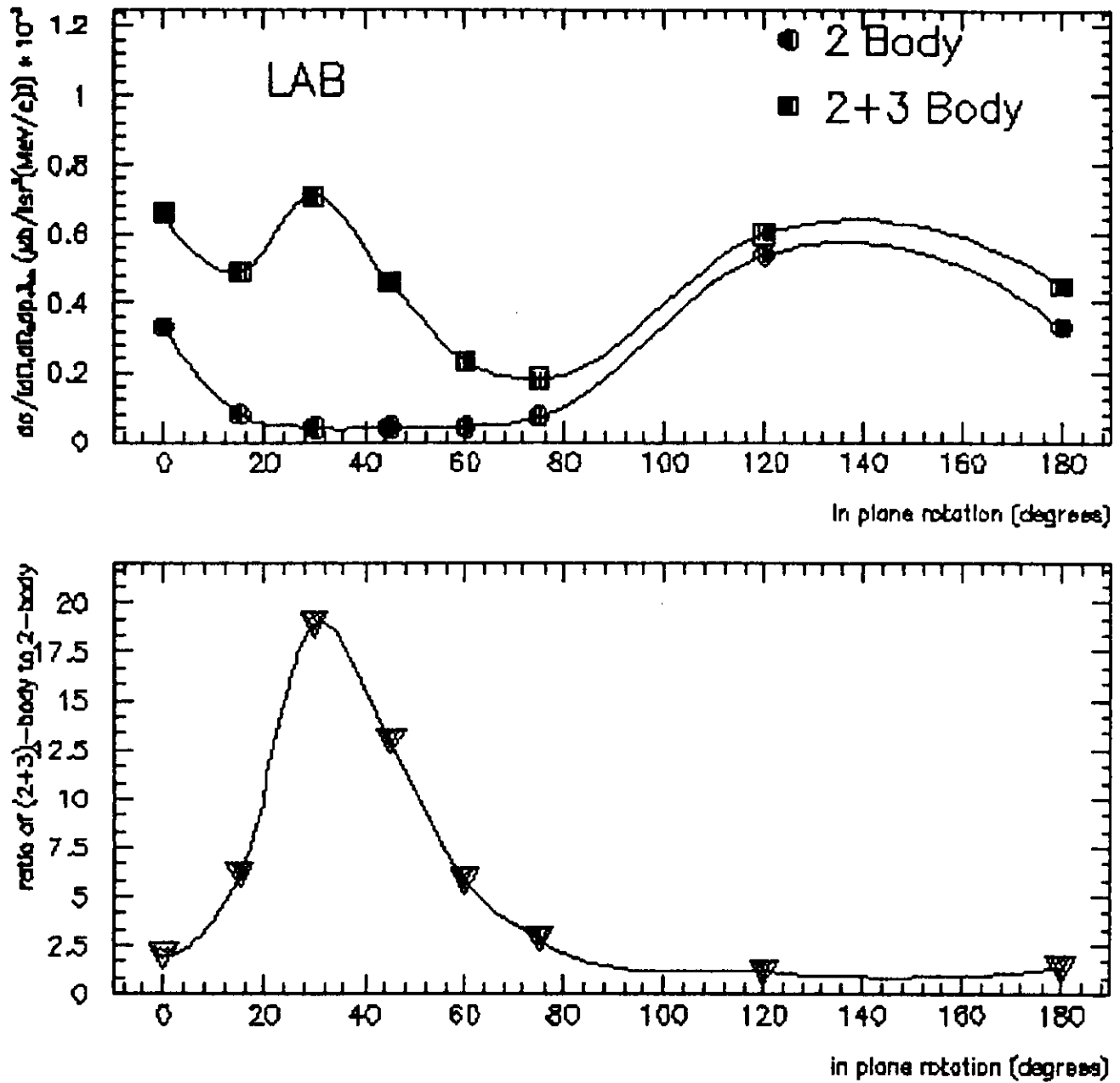


Fig. 15. Calculated (2+3)-body and 2-body cross sections (top) and their ratio (bottom) for  $\theta = 0^\circ$  as a function of  $\phi$  in the star configuration (see text).

were generated uniformly in phase space, Lorentz boosted to the laboratory frame, and fed into the CLAS simulation program FASTMC. For our pionic and non-pionic studies, we generated 60,000 and 100,000 events, respectively. A p-p coincidence defines the minimum condition for an accepted event. The overall acceptance for  ${}^3\text{He}(\gamma,pp)X$  is approximately 60% for both  $E_\gamma = 0.8$  and 1.3 GeV, and is independent of magnetic field strength for positive polarity. We developed powerful cuts which enable us to identify the p-p-n channel unambiguously (see the Appendix). In Fig. 16, we overlay the distributions of the missing mass squared for the p-p-n and p-p-n- $\pi^0$  channels. Only half a percent of the  ${}^3\text{He}(\gamma,pp)n\pi^0$  events survive a cut set at  $1.1 (\text{GeV}/c^2)^2$ , and demanding that the reconstructed photon energy  $E_\gamma^{\text{rcn}}$  be within 40 MeV of the tagged-photon energy leaves *only 13 events* of the 60,000 generated. This value is to be compared with an acceptance of 23% for the p-p-n channel after imposing these two tight cuts.

In order to search for star-configuration candidates, we employ the formalism of triangular Dalitz plots. We note that the outgoing nucleons produced in a star event all have equal energies in the center-of-momentum frame. This implies that after boosting to the lab frame, the kinetic energies of the star nucleons must satisfy the relationship

$$\frac{2}{3} \sqrt{\frac{[\sum T_i^2 - \sum_{i<j} T_i T_j]}{(\sum T_i)^2}} \leq \frac{\beta\gamma \sqrt{(E_{\text{cm}})^2 - 9m^2}}{3 \gamma E_{\text{cm}} - 3m} \equiv r$$

Figure 17 shows the CLAS acceptance for star events in the form of a triangular Dalitz plot. It can be seen from Fig. 17 that the vast majority of the star events fall within a well defined boundary (a circle), whereas phase-space events fill the whole of the Dalitz triangle, as shown in Fig. 18. Imposing this condition alone eliminates approximately 50% of the three-nucleon phase-space background, and a much larger fraction of the three-nucleon events dominated by two-body forces. This latter statement follows from the fact that two-body forces result in events that are dominated either by a spectator nucleon or by quasi-two-body breakup, and hence tend to populate the periphery of the Dalitz plot. We next invoke a cut on the invariant mass squared. The invariant masses of the three pairs of nucleons must be equal. After demanding that the nucleons satisfy the above kinematic relation, making a change of variables in the lab frame, and applying an invariant-mass cut, the details of which are given in the Appendix, we find that we can eliminate at least 99.4% of the p-p coincidence background. In this way we greatly enhance the star signal over the remaining three-nucleon background.

${}^3\text{He}(\gamma,pp)n$  vs.  ${}^3\text{He}(\gamma,pp)n\pi^0$  ( $E_\gamma = 1.3$  GeV,  $B/B_0 = +1.0$ )

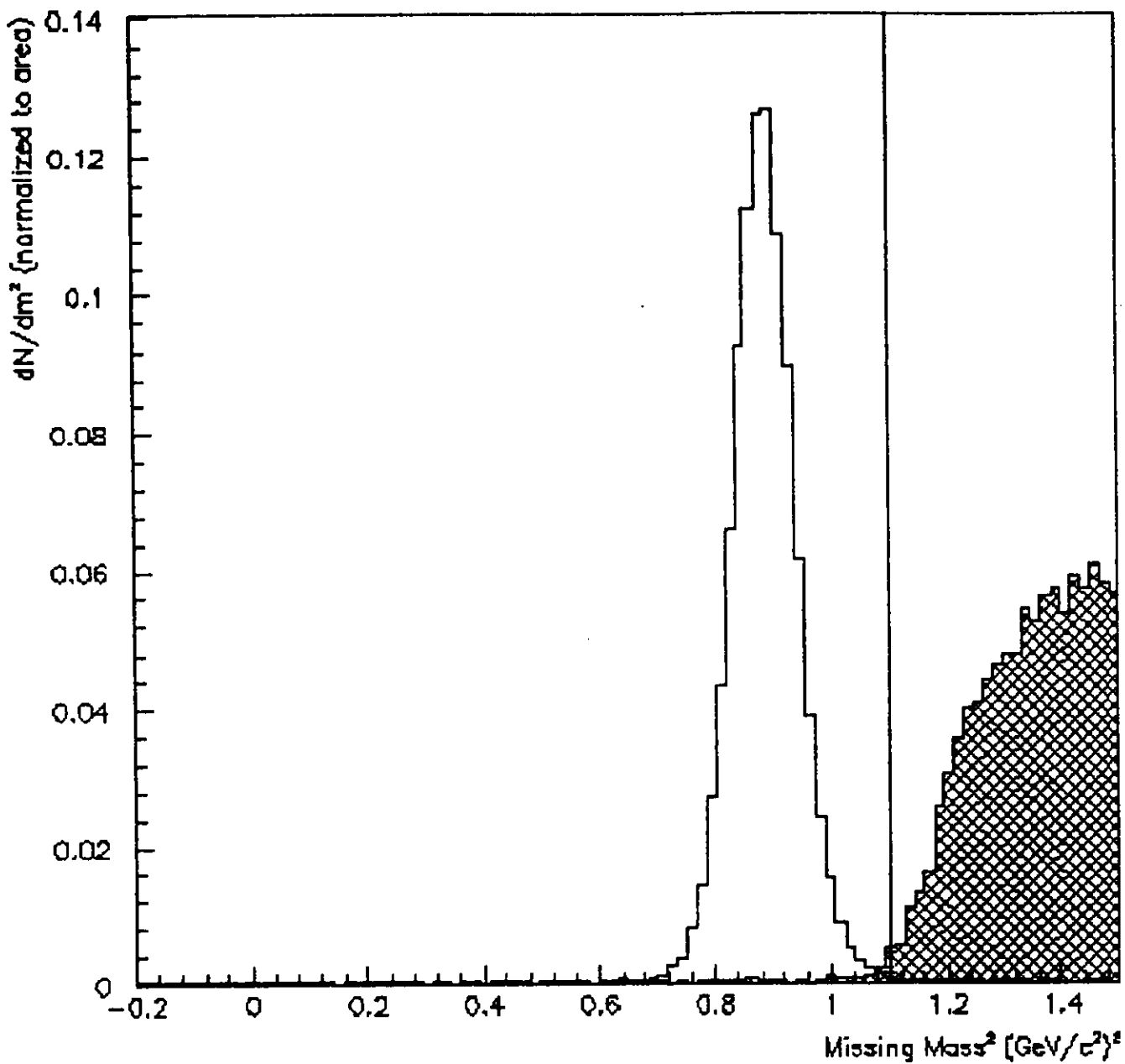


Fig. 16. Missing-mass plot for the  ${}^3\text{He}(\gamma,pp)n$  and  ${}^3\text{He}(\gamma,pp)n\pi^0$  channels.

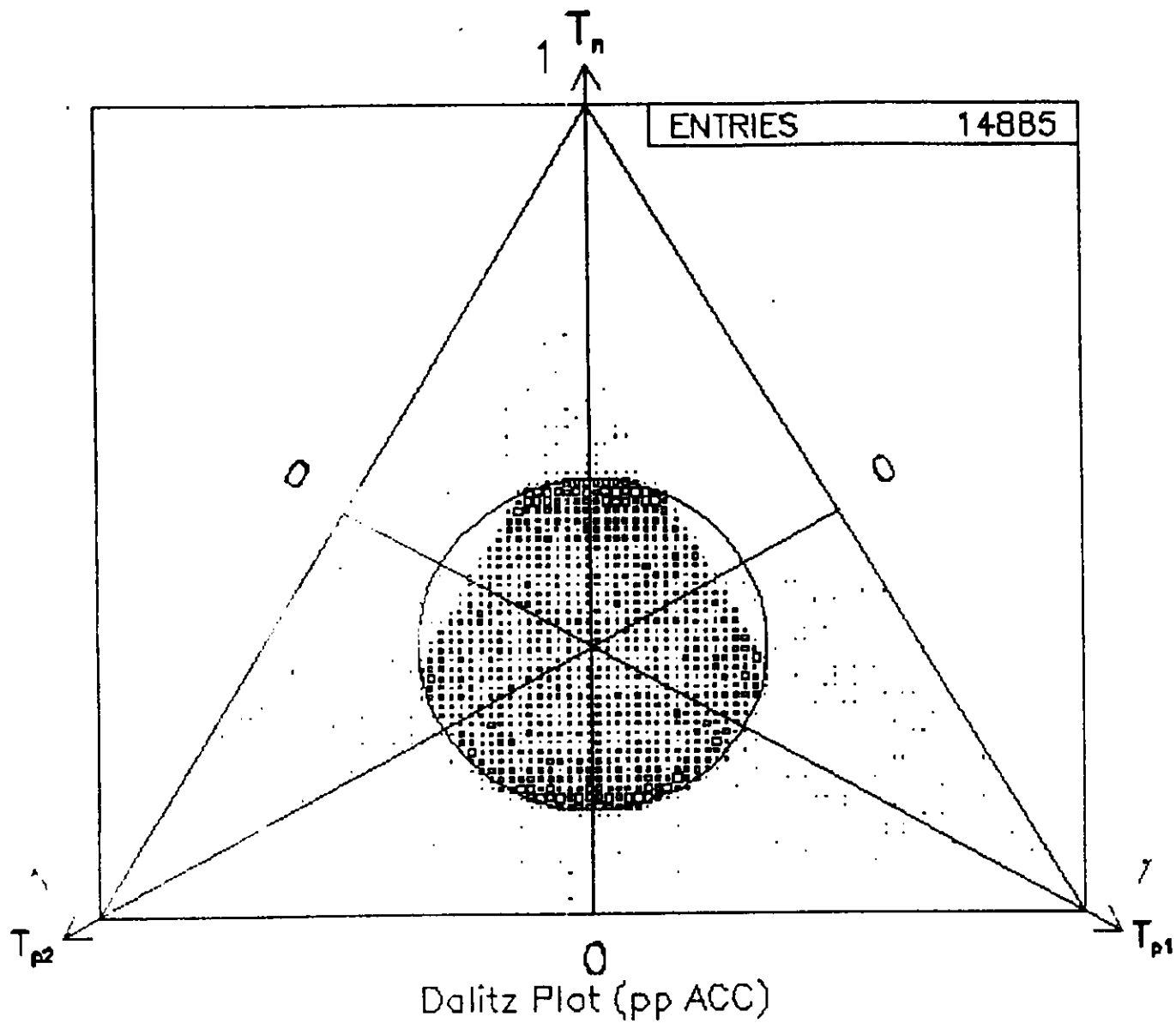


Fig. 17. CLAS acceptance plot, in the form of a three-axis Dalitz plot, for the star configuration.

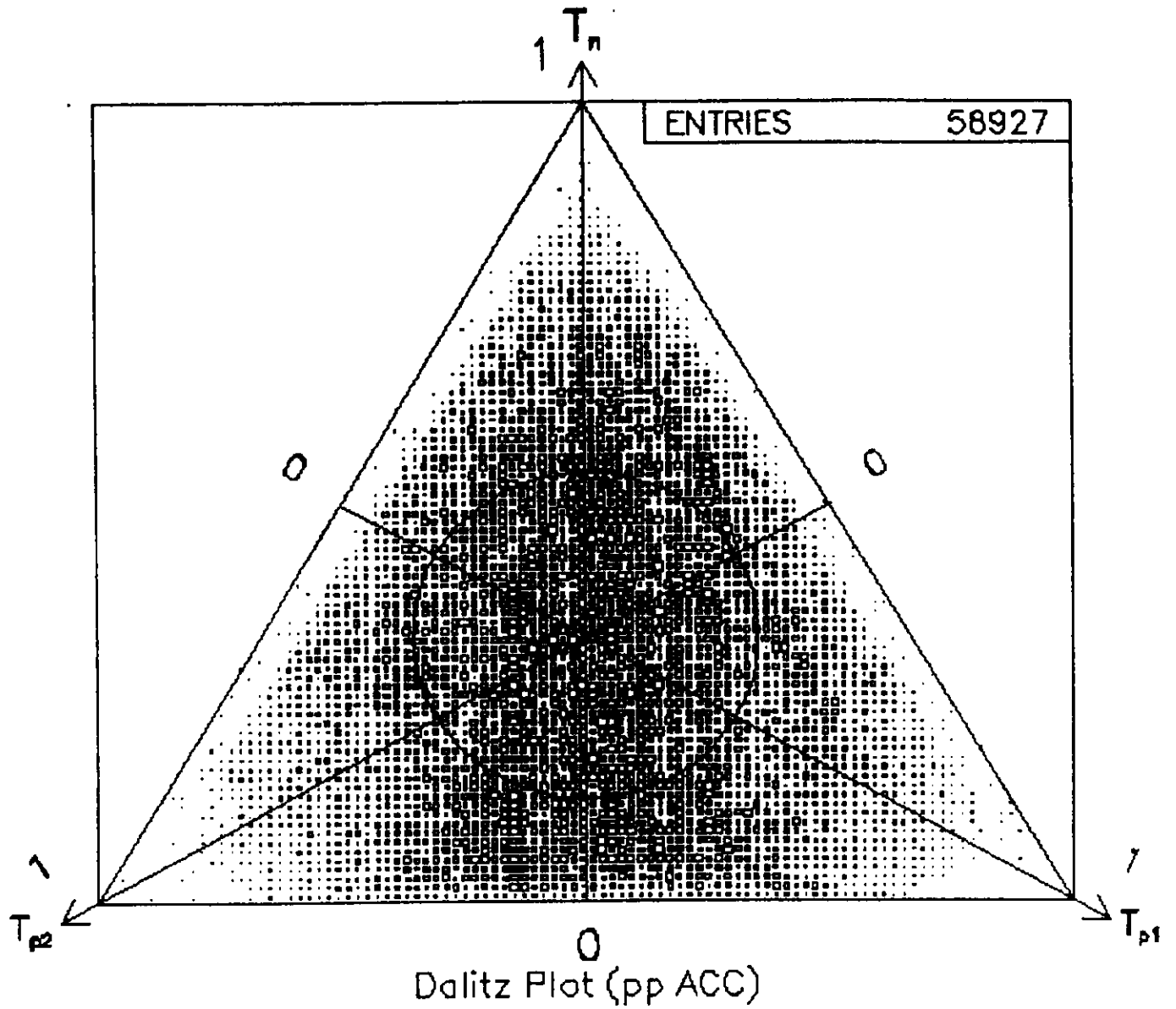


Fig. 18. CLAS acceptance plot, in the form of a three-axis Dalitz plot, for phase space.

The counting rate  $N$  for the  ${}^3\text{He}(\gamma, pp)n$  reaction in the star configuration is estimated from the data in Table 3. It is given by

$$N = N_\gamma N_T d^3\sigma/[dp_1 d\Omega_1 d\Omega_2]_{\text{lab}} \Delta p \Delta\Omega_1 \Delta\Omega_2 \varepsilon$$

where:

- $N_\gamma = 10^7 \text{ s}^{-1}$
- $N_T = 1 \text{ g/cm}^2$
- $d^3\sigma/[dp_1 d\Omega_1 d\Omega_2]_{\text{lab}} \approx 0.5 \text{ nb}/[(\text{MeV}/c) - \text{sr}^2]$
- $\Delta p = (2/3)\beta\gamma E_{\text{cm}}$ , where  $\beta = E_\gamma/(M_{{}^3\text{He}} + E_\gamma)$ , and  $\gamma = (1 - \beta^2)^{-1/2}$
- $\Delta\Omega_1 = \Delta\Omega_2 = 2\pi(\cos 7^\circ - \cos 140^\circ) = 3.52\pi$
- $\varepsilon$  (for p-p coincidences) = 0.6

This yields a total counting rate, integrated over solid angle and momentum, of  $25 \text{ s}^{-1}$  at  $E_\gamma = 0.8 \text{ GeV}$ , which we take to be representative.

We plan to bin the star candidates as follows:

1. 20 bins of 50 MeV in  $E_\gamma$
2. 4 bins of  $22.5^\circ$  in  $\theta$  ( $0^\circ < \theta < 90^\circ$ )
3. 20 bins of  $9^\circ$  in  $\phi$  for each proton ( $0^\circ < \phi < 180^\circ$ )

This gives 32,000 bins.

Since  $25 \text{ s}^{-1} = 90,000 \text{ hr}^{-1}$ , we expect approximately 2.8 counts per bin per hour. Data acquisition for 400 hours then yields about 1100 counts per bin, resulting in a statistical uncertainty of 3%.

#### **D. Three-nucleon correlations in $\pi$ photoproduction - the $(\gamma, \pi 3N)$ channel**

Another way of determining the presence of possible three-body-force effects in  ${}^3\text{He}$  is to search for correlations of three nucleons recoiling from a single-pion photoproduction event. This procedure should be able to distinguish between true three-nucleon correlations and the sequential two-body interactions arising from

photoproduction of deltas or other resonances. Then, having discarded the events where one of the nucleons is associated with the pion, as from a delta decay (see Sec. 2 above), we can compare the remaining events with phase-space predictions to determine the magnitude and possible kinematic signatures of three-body-force effects. Again, this procedure is particularly easy to carry out when all of the product particles are charged, as is the case for the  ${}^3\text{He}(\gamma, \pi^- ppp)$  reaction. Three-body correlation studies, including the important N-N- $\Delta$  channel, and the associated CLAS acceptance calculations, are currently underway.

## 4. Small Parts of the Nuclear Wave Function

There are certain unexplored, and hence more speculative, topics in nuclear physics which will be accessible to experiment only at CEBAF, both for the energy range covered and because of the power of the CLAS detector. Our objective here is to discover the existence and to explore the nature of the small parts of the nuclear wave function that manifest themselves primarily at small distances. In particular, since at low energies the  ${}^3\text{He}$  wave function is dominated by the NNN configuration, we wish to ascertain whether and to what extent, at GeV energies,  $\Delta\text{NN}$  configurations might play a role.

If one wishes to find a  $\Delta\text{NN}$  part of the  ${}^3\text{He}$  wave function, the most definitive demonstration is the direct knockout of a delta. Estimates of the probability of such a configuration vary from less than a few tenths of a percent (Abd90) to several percent (Lag92) (roughly the ratio of the N and  $\Delta$  binding energies), and are momentum-dependent as well. Clearly, one needs to distinguish the  $\Delta$ -knockout events from the far more likely  $\Delta$ -production events; but because  $\Delta$ -photoproduction from nucleons can result only in  $\Delta^+$  and  $\Delta^0$  production, it is possible to identify the  $\Delta$ -knockout process by observing  $\Delta^{++}$  production. We also can impose the additional kinematic restriction, if needed, that we detect a high-momentum recoil neutron, which guarantees that the other neutron be a spectator. Also, since the probability for knocking a pre-existing delta out of the nucleus depends on the momentum distribution of the deltas inside the nucleus, we can, with the use of monochromatic photons and with measurement of the angular distribution of the knocked-out deltas, map out the momentum distribution as a further and more stringent test of the theoretical calculations.

### A. The $\Delta^{++}$ component in the ${}^3\text{He}$ ground state

For many years the nucleus has been viewed as a system of non-composite nucleons which move nonrelativistically and interact through instantaneous two-body potentials. Mesonic and internal nucleonic degrees of freedom were considered frozen until it became clear that the electromagnetic properties of nuclei cannot be described in this picture alone. To reproduce the electromagnetic form factors properly, especially for few-nucleon systems like  ${}^3\text{He}$  and  ${}^3\text{H}$ , requires the inclusion of meson-exchange currents

(MEC), thus serving as evidence for mesons inside nuclei. On the other hand, it is well known that explicit  $\Delta$  production is an important channel in pion scattering and pion photoproduction from nuclei. Applying the  $\Delta$ -hole model to these reactions has taught us much about the nature of the  $\Delta$ -N and  $\Delta$ -nucleus interactions. Since most of the attraction between two nucleons (and therefore the binding of nuclei) comes from the two-pion exchange, allowing intermediate deltas as shown in Fig. 19, the nuclear ground-state wave function should contain  $\Delta$  and perhaps  $N^*$  components. However, until now there has been no conclusive evidence for these components, because  $\Delta$  creation on a quasifree nucleon overwhelmed the knockout signal of a preformed  $\Delta$ . The photoproduction of  $\Delta^{++}$  on  ${}^3\text{He}$  offers us a way to overcome this drawback, provided that the contributions of two-step processes are small. We therefore propose to measure the cross section of the  ${}^3\text{He}(\gamma, p\pi^+)nn$  reaction, where the  $p$ - $\pi^+$  system reconstructs to a  $\Delta^{++}$ .

Few-nucleon systems are the natural place to start searching for  $\Delta$  components because their wave functions can be obtained exactly. The deuteron as a  $T = 0$  system permits only the even less probable  $\Delta$ - $\Delta$  components, which leaves  ${}^3\text{He}$  as the obvious choice. Faddeev calculations for the trinucleon with realistic N-N and N- $\Delta$  interactions include transitions such as  $p + p \rightarrow \Delta^{++} + n$  in the ground-state wave function (Haj83a). Since the  $p$ - $p$  pair is mostly in the  ${}^1S_0$  state, the  $\Delta$  wave function in  ${}^3\text{He}$  has a dominant D-wave component. The peak of the  $\Delta$  momentum distribution is predicted to be approximately 400 MeV/c, as shown in Fig. 20 (Str87). Thus, the  $\Delta$ -knockout contribution should exhibit a maximum around  $P_R = 400$  MeV/c. Here,  $P_R$  denotes the momentum of the recoiling neutron in the pair, which is equivalent to the momentum of the  $\Delta$  before the interaction. The probability of the  $\Delta$ -N-N component in  ${}^3\text{He}$  has been calculated to be about 2.4% (Str87) which, using the isospin relations for the delta  $P(nn\Delta^{++}) : P(np\Delta^+) : P(pp\Delta^0) = 3 : 2 : 1$ , gives  $P(nn\Delta^{++}) \cong 1.2\%$ .

The clearest signature of a  $\Delta^{++}$  component in the  ${}^3\text{He}$  ground state would be the spectrum of the  $\Delta^{++}$  emitted at a given angle  $\theta_\Delta$  in the  ${}^3\text{He}(\gamma, p\pi^+)nn$  reaction, as shown in Fig. 21. The peak in Fig. 21 corresponds to the absorption of a photon by a  $\Delta^{++}$ - $n$  pair nearly at rest in  ${}^3\text{He}$ . The top of the peak corresponds to kinematics where this pair is at rest (i.e., the second neutron is also at rest) and where the momentum of the first neutron (in the pair) is opposite to the momentum of the  $\Delta^{++}$  before it absorbs the photon. The width of the peak is simply the reflection of the Fermi motion of the pair in the ground state of  ${}^3\text{He}$ . In the calculation shown in Fig. 21 (Lag92), this  $\Delta$ - $n$  component [Fig. 22(d)] has been generated by a  $\pi$  and  $\rho$  meson-exchange interaction in a  $p$ - $p$  pair. It has

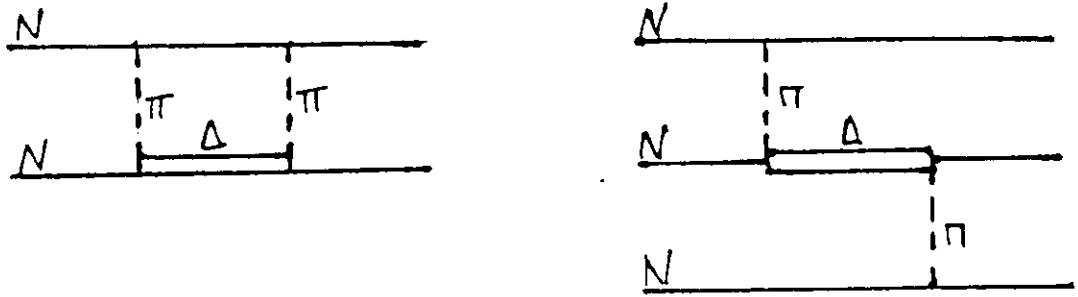


**Fig. 19.** The  $\Delta$  contribution to the two- and three-body forces.

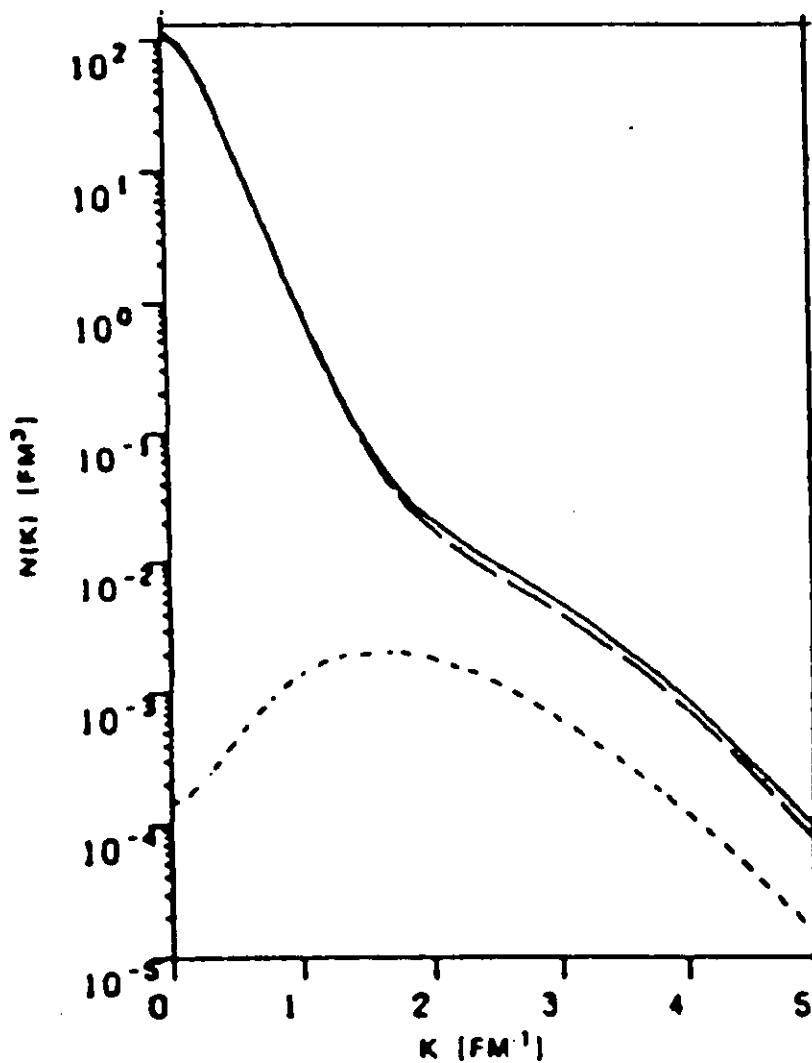


**Fig. 20.** Momentum distributions in the three-nucleon bound state. The nucleonic distributions arising from a calculation with (solid curve) and without (dashed curve) a  $\Delta$  isobar are compared with the distribution of the  $\Delta$  (short-dashed curve). The calculation makes use of the Paris potential as the purely nucleonic reference.

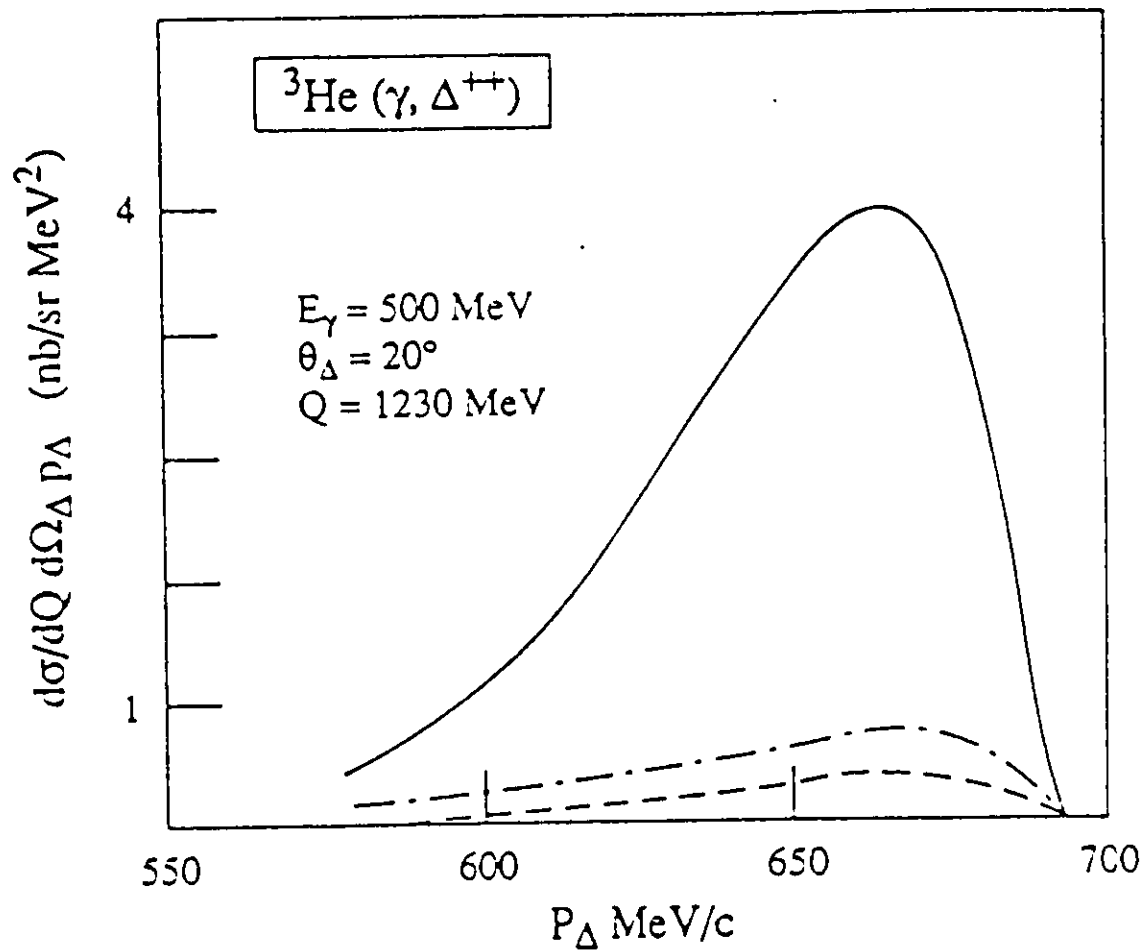


**Fig. 21.** The spectrum of the  $\Delta^{++}$  emitted in the  ${}^3\text{He}(\gamma, \Delta^{++})$  reaction. The dashed curve includes only N-N rescattering mechanisms, while the dot-dashed curve includes  $\pi$ -N rescattering as well. The full curve takes into account the contributions of the  $\Delta$  component and the associated exchange currents.

been shown (Haj83b) that this perturbative treatment leads to results very similar to the full coupled-channel treatment. To insure gauge invariance, meson-exchange currents associated with the  $\Delta$  component also have been taken into account: the  $\pi$ - $\Delta$  contact term [Fig. 22(c)] has been computed explicitly, while the pion-photoelectric term is already contained in the pion-rescattering term [Fig. 22(b)]. The contribution of mechanisms involving three nucleons [Fig. 22(e)] is not taken into account in this calculation, but should result in a sizable effect at lower  $\Delta$  momentum, since the momentum is shared among three rather than between two baryons.

The contribution of the two-step processes depicted in Figs. 22(a) and (b) are predicted to be much reduced compared to the  $\Delta$ -knockout reaction. The nucleon-rescattering diagram shown in Fig. 22(a) includes processes such as  $\gamma + p \rightarrow n + \pi^+$  followed by charge exchange of the neutron,  $n + p \rightarrow p + n$ . While this reaction will give a contribution to the  ${}^3\text{He}(\gamma, p\pi^+)nn$  cross section, the final  $p$ - $\pi^+$  pair would not reconstruct to a  $\Delta^{++}$ . The situation is different for the case of pion rescattering, shown in Fig. 22(b). Again, one can have  $\gamma + p \rightarrow n + \pi^+$  here, but now the  $\pi^+$  can rescatter on the second proton to form a  $\Delta^{++}$  which would subsequently decay. Laget (Lag92) has calculated this pion-rescattering contribution to be larger than the nucleon-rescattering term but still much smaller than the  $\Delta$ -knockout term, as can be seen in Fig. 21. Moreover, the magnetic moment of a  $\Delta$  is proportional to its charge, except for any anomalous contribution, and because of the ratio of the relevant isospin coupling coefficients, this rescattering contribution is suppressed compared with the  $\Delta^{++}$  knockout and associated MEC contributions. Finally, the pion-rescattering contributions decrease with increasing photon energy because the elementary cross sections for the reactions  $\gamma + p \rightarrow n + \pi^+$  and  $\pi^+ + p \rightarrow p + \pi^+$  are much smaller above the  $\Delta$  energy region than inside it. [We note as well that at higher  $E_\gamma$ , the  $(\gamma, \pi^+)$  and  $(\pi^+, \pi^+)$  processes will proceed, not by forming the  $\Delta$ , but rather a higher resonance, such as the  $D_{13}$ .] The reason that the contribution of the multiple-scattering series decreases with increasing photon energy is that whereas the  $\Delta$ -knockout amplitude (and its associated MEC) depends on the momentum of the undetected neutron in the active pair, the various rescattering amplitudes involve a nuclear transition form factor which depends primarily on the momentum of the incident photon.

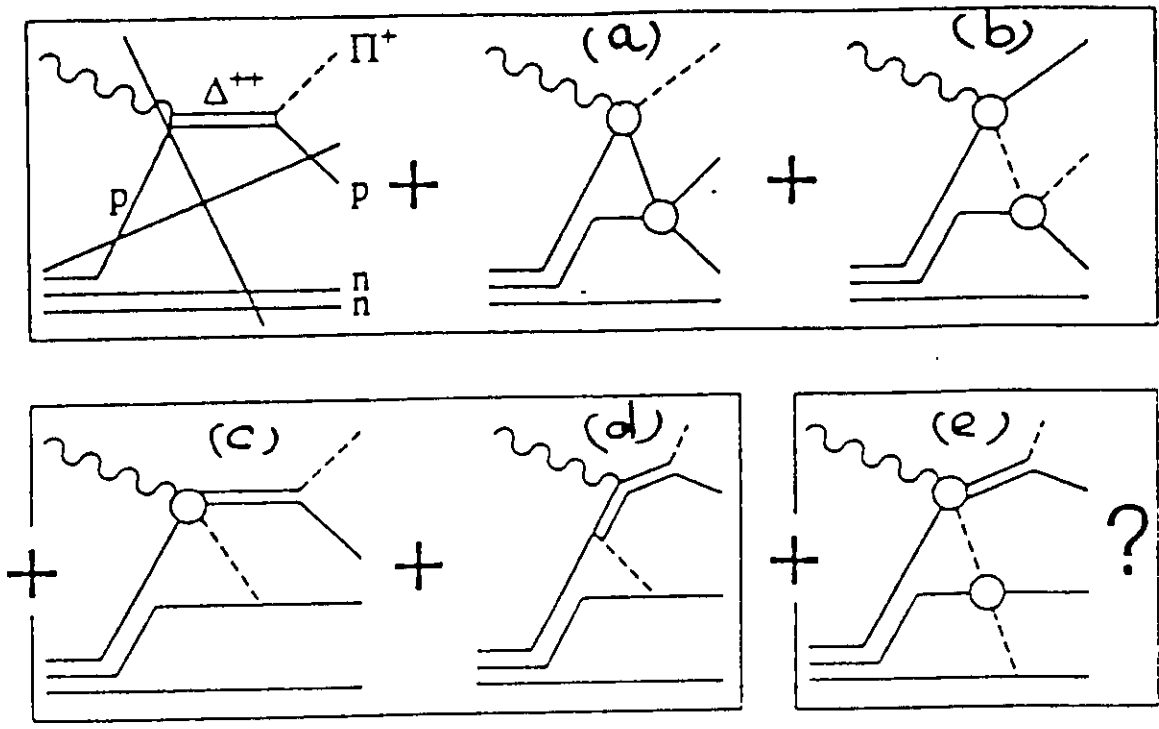


**Fig. 22.** The mechanisms which lead to a  $\Delta$  component in the wave function and the associated meson-exchange currents (bottom). The top part depicts the multiple-scattering mechanisms which contribute to the background of the  ${}^3\text{He}(\gamma, \Delta^{++})$  reaction.

## B. Delta knockout--the $(\gamma, \Delta^{++})$ channel

We propose to measure the cross section for the  ${}^3\text{He}(\gamma, p\pi^+)nn$  reaction with tagged photons from 320 MeV to at least 1 GeV: this energy range allows one to determine the momentum distribution of a  $\Delta^{++}$  inside  ${}^3\text{He}$  having momentum between 100 MeV/c and 1 GeV/c. The detection in CLAS of a proton and a  $\pi^+$  in coincidence defines the mass  $M_\Delta$ , the momentum  $P_\Delta$ , and the angle  $\theta_\Delta$  of the emitted  $\Delta^{++}$ .

As can be seen in Fig. 21, the signature of a  $\Delta$  component is a peak in the spectrum of the momentum of the emitted  $\Delta$ . Consequently, the resolution for the reconstructed momentum  $P_\Delta$  of the emitted  $\Delta$  should be much better than 50 MeV/c. A simulation with the FASTMC code shown in Fig. 23 yields the result that this resolution is  $\Delta P_\Delta \cong 10$  MeV/c, for all of the kinematics covered by this study. This is good enough to map out this peak. The resolution for the mass  $M_\Delta$  of the  $\Delta$  is  $\cong 3$  MeV, with no broadening in the simulation. The efficiency for detecting a p and a  $\pi^+$  at  $E_\gamma = 0.5$  GeV is about 40%.

We will take advantage of the fact that the same value of  $P_\Delta$  can be obtained for different values of the incoming photon energy, by varying the angle of the emitted  $\Delta$ , in order to determine the variation of the measured momentum distribution with the transferred momentum. This will allow us to unravel any possible corrections resulting from background mechanisms.

The counting rate  $N$  is related to the cross section through the relation

$$N = N_T N_\gamma (d^3\sigma/dM_\Delta dP_\Delta d\Omega_\Delta) dM_\Delta dP_\Delta d\Omega_\Delta \varepsilon.$$

Assuming the following:

- Target thickness:  $N_T = 1 \text{ g/cm}^2$
- Number of photons in  $\Delta E_\gamma = 10 \text{ MeV}$  :  $N_\gamma = 10^5 \text{ s}^{-1}$
- Average cross section:  $d\sigma = 1 \text{ nb/sr/MeV}^2/c^3$
- CLAS acceptance:  $\varepsilon = 0.4$
- $M_\Delta = 10 \text{ MeV}$
- $P_\Delta = 10 \text{ MeV/c}$
- $\Omega_\Delta = 2\pi \cdot 5^\circ \cong 0.5 \text{ sr}$

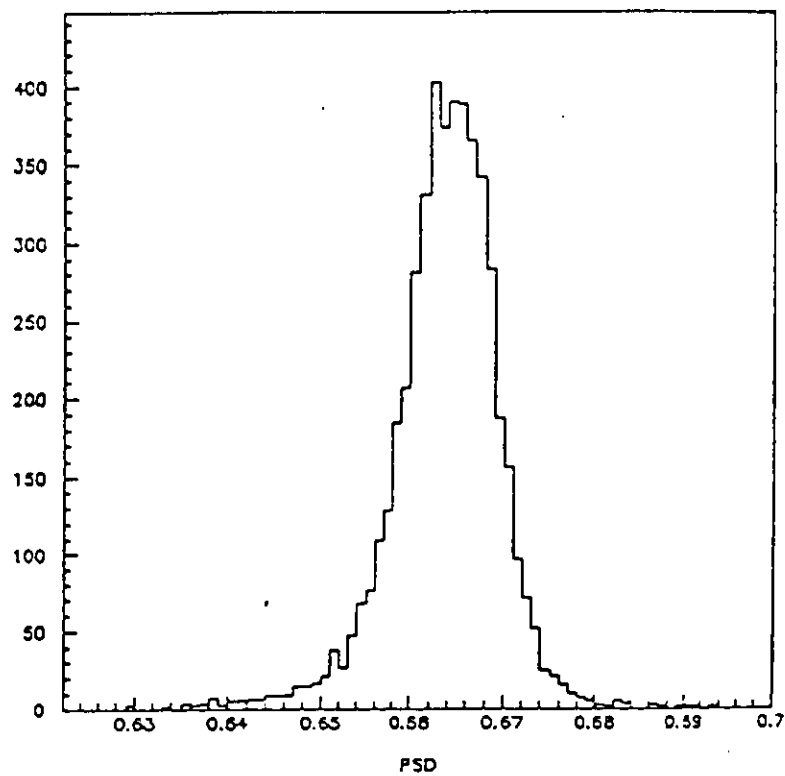
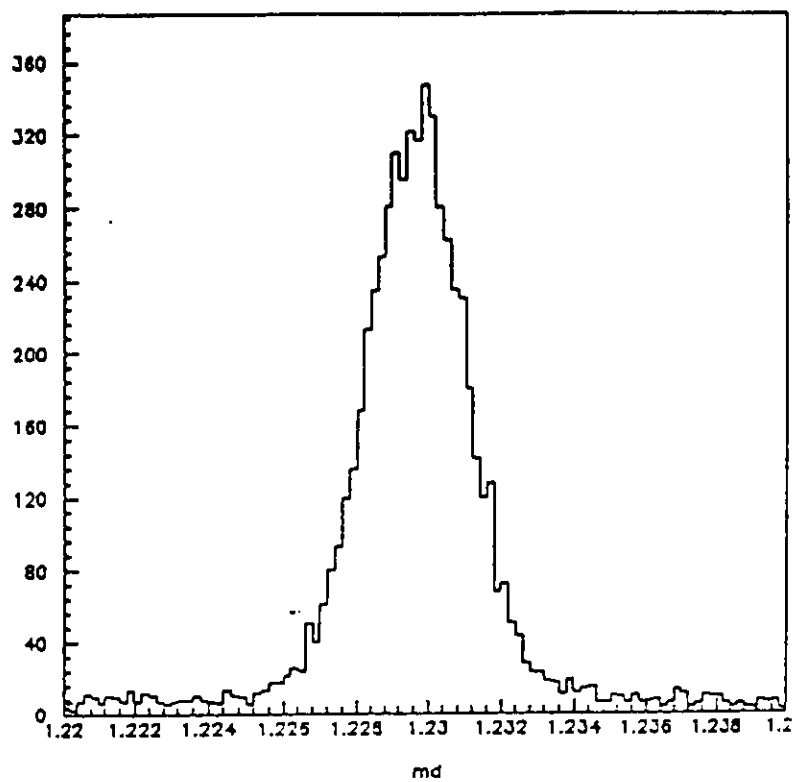


**Fig. 23.** Mass and momentum resolution of the  $\Delta^{++}$ , as reconstructed by FASTMC from the detected  $p-\pi^+$  pair, at the top of the peak in Fig. 21.

we get  $N = 4 \cdot 10^{-4} \text{ s}^{-1} \cong 1.4 \text{ hr}^{-1}$ , which corresponds to approximately  $7 \text{ hr}^{-1}$  in the peak, and it is the area of the peak which is proportional to the momentum distribution of the  $\Delta$ .

If we tag between 320 and 1020 MeV (i.e., 70 energy bins of  $\Delta E_\gamma = 10 \text{ MeV}$ ), and if we measure  $\theta_\Delta$  between  $10^\circ$  and  $110^\circ$  (i.e., 20 angular bins of  $\Delta\theta_\Delta = 5^\circ$ ), the total number of counts obtained will be of the order of  $2000 \text{ hr}^{-1}$ . This leads to about  $5 \cdot 10^5$  counts in 250 hours.

### C. Delta knockout--the $(\gamma, \Delta^{++}n)$ channel

In order to disentangle the events resulting from the three-body-force diagram (e) in Fig. 22, we need to detect low-momentum  $\Delta^{++}$  events as well (the low-momentum tail in Fig. 21). This requires the detection of the recoil neutron in addition to the  $\Delta^{++}$  reconstructed from the p and  $\pi^+$ . Also, because the  $\Delta$  is so broad (120 MeV), it is possible that some of the  $\Delta^{++}$  events determined only from p- $\pi^+$  reconstructions might be contaminated with accidental p- $\pi^+$  coincidences. Therefore, we propose to measure the  ${}^3\text{He}(\gamma, p\pi^+)n$  reaction channel, where the detected neutron is not a spectator. These neutrons can readily be distinguished, as can be seen in Fig. 24, and we merely need to eliminate the very-low-momentum spectator neutrons.

We applied the following cuts:

1. We demand that the two mass-identified particles be positively charged, be measured in any one of the three drift chambers, and deposit energy in the TOF scintillator array. Furthermore, the particles must pass the following mass-squared criteria:
  - (a) for the  $\pi^+$ ,  $m^2 < 0.15 \text{ (GeV/c}^2\text{)}^2$ ; and
  - (b) for the proton,  $m^2 > 0.65 \text{ (GeV/c}^2\text{)}^2$ .
2. The invariant mass of the proton and  $\pi^+$  must be within 50 MeV of the mass of the  $\Delta^{++}$ .
3. An energetic recoil neutron must be detected in the shower-counter array, and satisfy the following two conditions:

- (a) that  $|\mathbf{p}_n| > 0.4 \text{ GeV/c}$ ; and

momenta of recoil and spectator neutrons for  $\Delta^{++}$  knockout

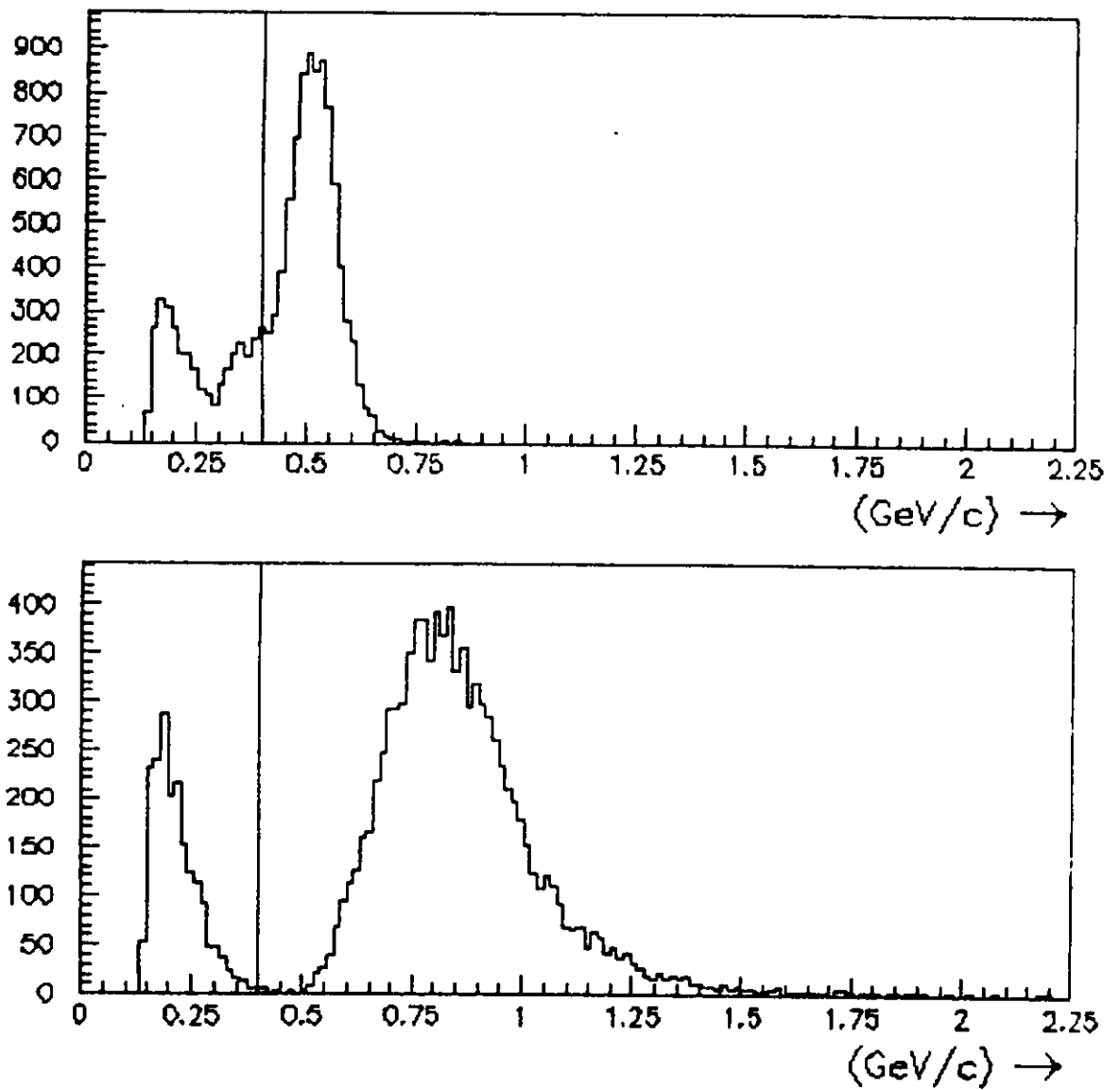


Fig. 24. Momentum distributions for the recoil and spectator neutrons from the  ${}^3\text{He}(\gamma, \Delta^{++}n)n$  reaction.

(b) that the reconstructed velocity be less than  $0.95c$ .

Cut 1 demands that we have a two-charged-particle coincidence and that the masses reconstruct to a proton and a  $\pi^+$ . Cut 2 focuses only on potential  $\Delta^{++}$  candidates. We modified FASTMC to allow for neutral detection (Col93). Our version of FASTMC also includes the backward shower counters, which in our studies, span from  $45^\circ$  to  $112^\circ$  in polar angle and subtend an interval of  $60^\circ$  in azimuthal angle. Cut 3a eliminates spectator neutrons, and Cut 3b insures that the detected neutral particle is not a decay photon.

For our studies we simulated the  $\Delta^{++}$  knockout by distributing the  $\Delta^{++}$  and recoil neutron uniformly in phase space, endowing the spectator neutron with a Fermi-momentum distribution, and assuming that the  $\Delta^{++}$  was on-shell. We generated 60,000 events at two magnetic-field operating points ( $B/B_0 = +0.25$  and  $+1.00$ ), for an incident photon energy of  $E_\gamma = 0.5$  GeV. The resulting acceptances are 3.5% and 4.1% for the two magnetic-field settings, respectively. Figure 25 shows resulting invariant-mass distribution of the  $\Delta^{++}$ .

Invariant mass of ( $p\pi^+$ ) with energetic neutron detected

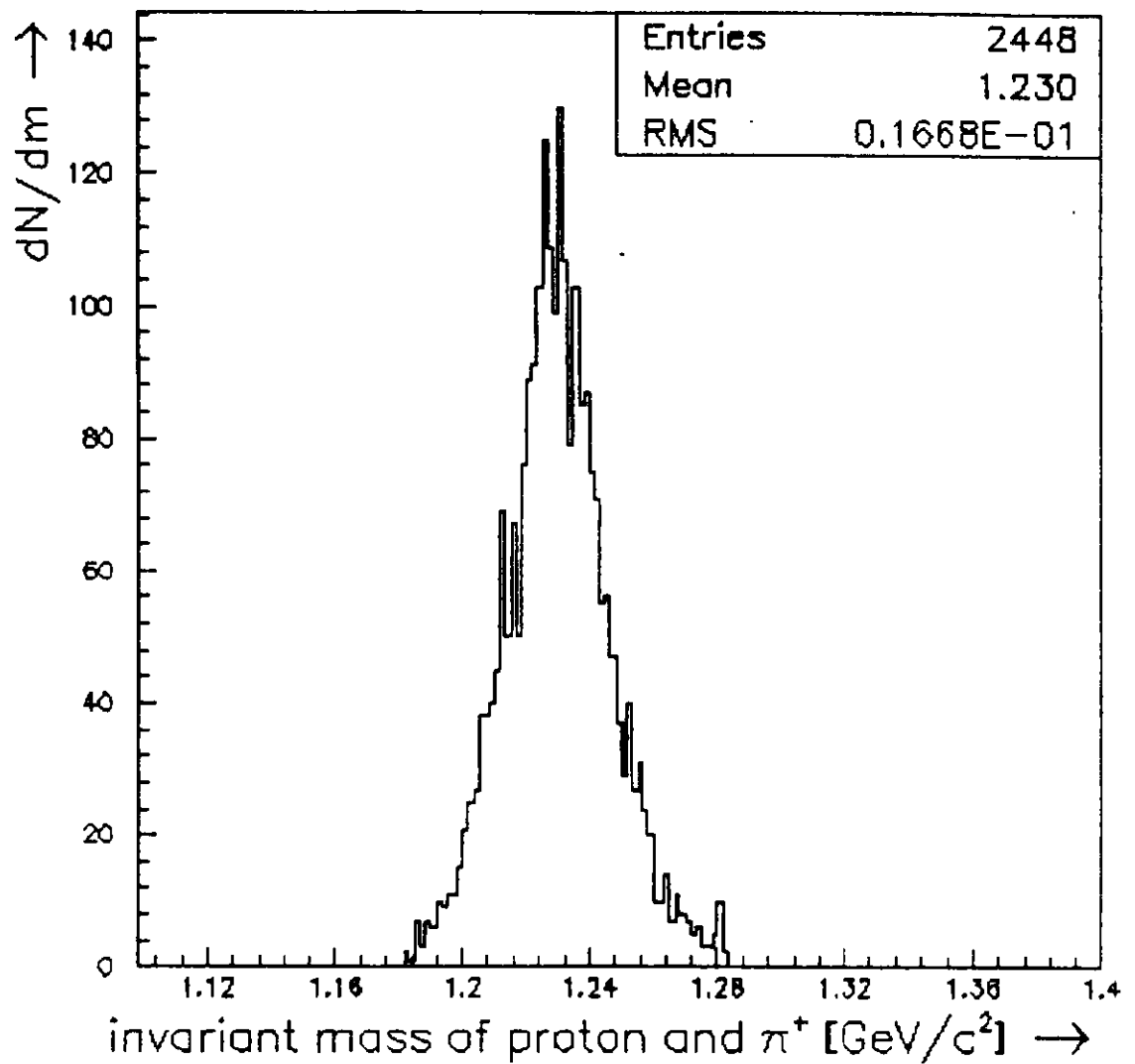


Fig. 25. Invariant-mass distribution for the  $p\pi^+$  pair from the  ${}^3\text{He}(\gamma, \Delta^{++}n)n$  reaction.

## 5. Other Reaction Channels

Although not central to the present proposal, data for a number of other reaction channels will be obtained concurrently with those discussed above. Some of these additional data pertain to problems of great current interest in nuclear physics.

### A. Coherent pion photoproduction--the ${}^3\text{He}(\gamma, \pi^+ t)$ channel

Due to the energy range covered by CEBAF, these experiments will involve large momentum transfers to the three-nucleon system. One would therefore assume that the cross section for the process  ${}^3\text{He}(\gamma, \pi^+){}^3\text{H}$  is strongly suppressed by the nuclear form factor, rendering this reaction unobservable at very large  $Q$ . However, the experimental data of (Bac73,75) indicate that this is not the case. Recent nonlocal DWIA calculations with Faddeev wave functions that include the charge-exchange mechanism explicitly (Kam91) give a very good description of these data up to  $Q^2 = 6 \text{ fm}^{-2}$ , but underestimate the data by several orders of magnitude for  $Q^2 > 10 \text{ fm}^{-2}$ . These results are shown in Fig. 26. While the computed cross section falls rapidly with increasing  $Q$  as dictated by the trinucleon form factor, the data stay flat for  $8 < Q^2 < 14 \text{ fm}^{-2}$ . This is currently the clearest signal of a new mechanism of pion photoproduction involving the simultaneous interaction of several nucleons that can share momentum transfer. It is important both to confirm the old data and to extend the measurements to higher momentum transfer. CLAS simulations for this reaction channel are underway.

### B. Pion photoproduction on correlated pairs--the $(\gamma, d\pi)$ channel

Recent unpublished data from an electrodisintegration experiment on  ${}^{16}\text{O}$  at Frascati (AngSP) show that, for electron energies between 1 and 1.5 GeV, there is an observable yield of electroproduction of deuterons (0.5% of the total hadron-emission events) in the kinetic energy range up to 400 MeV. On the other hand, a recent theoretical estimate (LagPC) indicates that for certain kinematics the direct photon interaction with a p-n or a p-p pair in the  ${}^3\text{He}$  ground state (see Fig. 27) may give a sizable contribution to the single-pion production cross section. The branching ratio to this

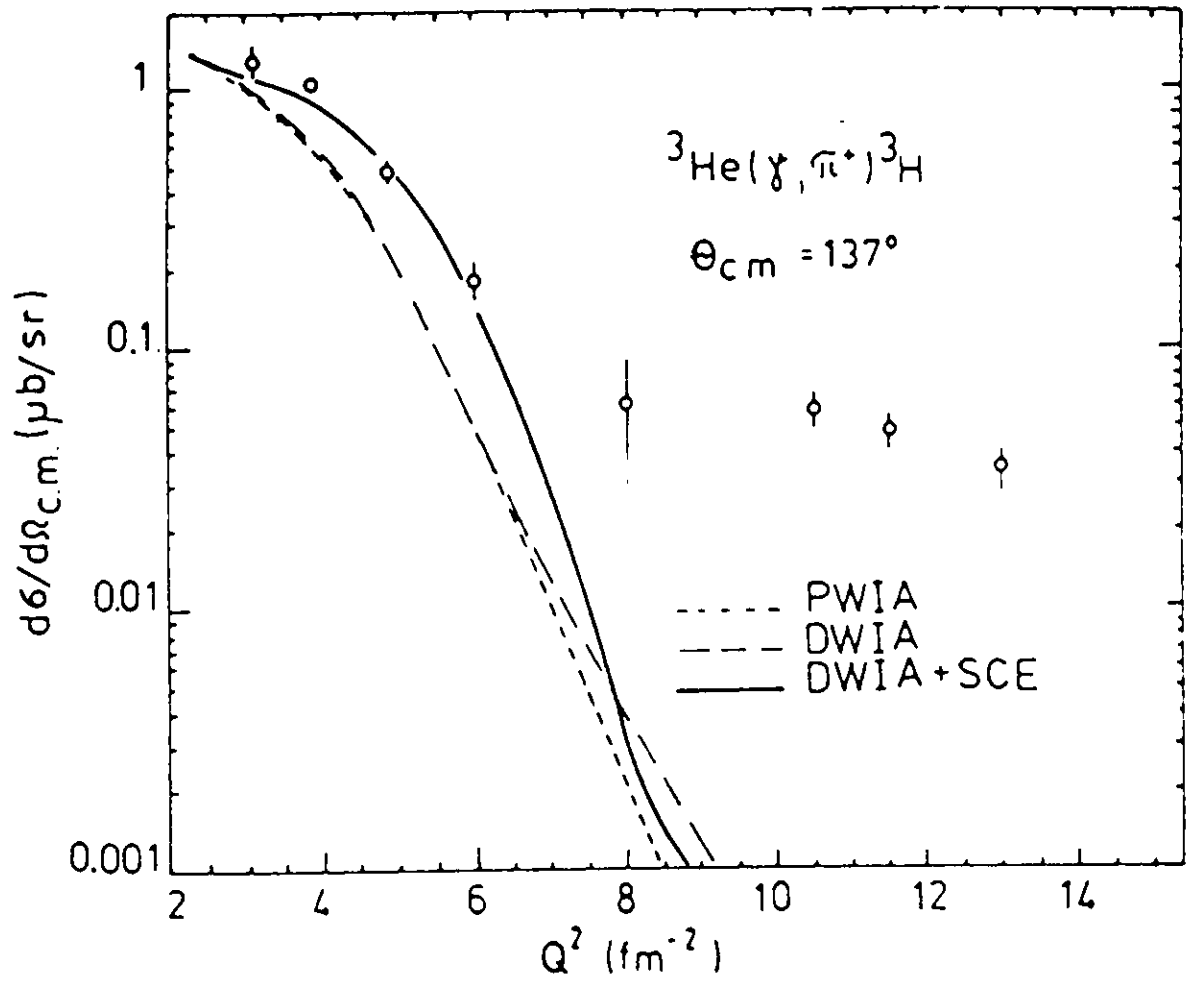


**Fig. 26.** Experimental data and theoretical calculations for the  ${}^3\text{He}(\gamma, \pi^+){}^3\text{H}$  cross section. The solid curve includes the two-step single-charge-exchange process  ${}^3\text{He}(\gamma, \pi^0){}^3\text{He}(\pi^0, \pi^+){}^3\text{H}$ .

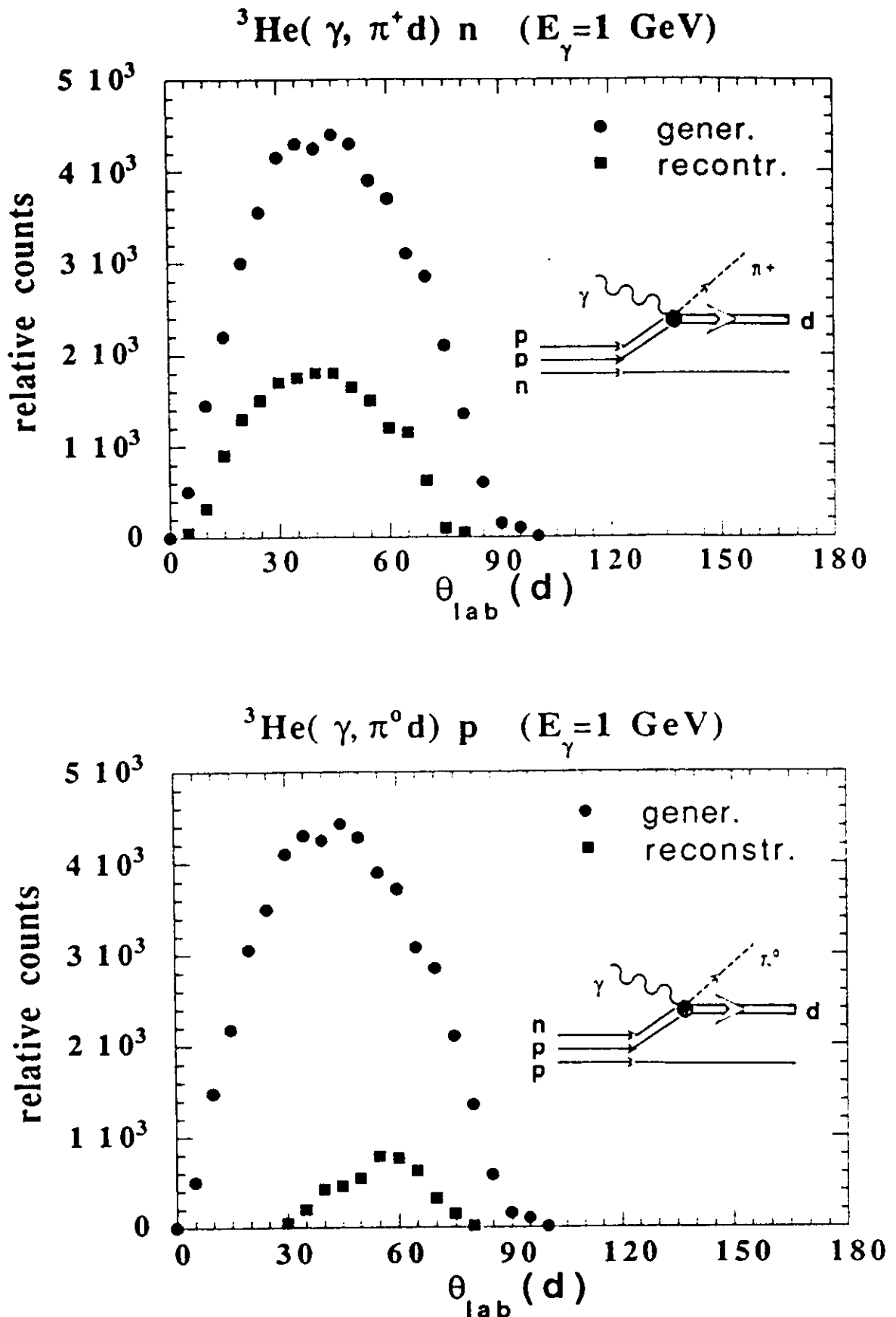


Fig. 27. Generated and accepted angular distributions of deuterons from pion photo-production from correlated nucleon pairs in  ${}^3\text{He}$ . The top figure shows the  $d-\pi^+$  channel from a correlated  $p-p$  pair; the bottom one shows the  $d-\pi^0$  channel from a correlated  $n-p$  pair.

channel at energies between 1 and 1.5 GeV should be very sensitive to short-range correlations in the three-body wave function. We therefore propose to investigate, in one- and two-pion production reactions, those channels with a high-momentum bound deuteron in the final state. In particular, the

$$\begin{aligned} & {}^3\text{He}(\gamma, d\pi^0)p, \\ & {}^3\text{He}(\gamma, d\pi^+)n, \text{ and} \\ & {}^3\text{He}(\gamma, d\pi^+\pi^-)p \end{aligned}$$

reactions should provide good experimental tests of the cross section in  ${}^3\text{He}$ . Figure 27 also shows the CLAS acceptance for the detection of the  $d$ - $\pi$  pairs at a photon energy of 1.0 GeV. Existing data on  ${}^2\text{H}(\gamma, d\pi^0)$  indicate that the cross section at  $E_\gamma = 1.0$  GeV is  $1 \mu\text{b}$  (Bou74, Laz76). Assuming comparable values of the cross section for  ${}^3\text{He}(\gamma, d\pi^+)n$  and  ${}^3\text{He}(\gamma, d\pi^0)p$ , the expected total counting rates range from  $10^{-2}$  to  $10^{-3} \text{ s}^{-1}$ , respectively, for the  $d$ - $\pi^+$  and the  $d$ - $\pi^0$  channels.

### C. Search for p-p dibaryons and N-N- $\pi$ resonances

QCD models predict the existence of six-quark resonances, but in spite of a few recent experimental indications (Boc86, Bil92), no clear evidence of these states has yet been found. Their existence would be of fundamental interest for understanding the confinement hypothesis and for describing the effect of the nuclear medium on the N-N interaction. Here we can use the CLAS for increasing the sensitivity for dibaryon detection by about two orders of magnitude compared with previous measurements. We plan to reconstruct the invariant mass of p-p or p-p- $\pi$  structures and look for a very narrow enhancement superposed on the background events. The predicted dibaryon structures have mass in the range of 2.0 to 2.1 GeV and width of 2 to 5 MeV. The background consists of those events with one or more pions and at least two high-momentum nucleons in the final state. We estimate this background using a quasideuteron model:  $\sigma_{\text{bgd}} = (NZ/A)\sigma_d\xi$ , where  $\sigma_d$  is the deuteron total cross section and  $\xi$  is the probability that two nucleons in  ${}^3\text{He}$  are closer than the wavelength of the incident photon. For  $E_\gamma = 1$  GeV and from the momentum distribution of the nucleons in  ${}^3\text{He}$  (CioPC), we obtain  $\xi \approx 5 \cdot 10^{-3}$  and  $\sigma_{\text{bgd}} \approx 1 \mu\text{b}$ . To evaluate the fraction of events detected by the CLAS in the energy interval corresponding to the dibaryon mass, we simulated the background assuming a phase-space distribution for all of the one-pion, two-pion, and

three-pion reactions. If we take into account only statistical uncertainties, then for a  $3\sigma$  confidence level the minimum detectable dibaryon cross section is  $\leq 0.2$  nb for a beam time of 400 hours.

## 6. Requirements

This experiment requires an incident electron beam of 1600 MeV. This energy is chosen for several reasons:

- 1) It is compatible with Experiment 91-014.
- 2) All parts of this experiment can be done with the same electron-beam energy.
- 3) Only one recirculation of the beam in the accelerator is required, so that the experiment can be done at an early stage of the Hall-B experimental program.

The photon beam requirements for this experiment are twofold:

- 1) 150 hours, with photons tagged from 560 to 1520 MeV, corresponding to 35%-95% of the incident electron energy.
- 2) 250 hours, with photons tagged from 320 to 1520 MeV, corresponding to 20%-95% of the incident electron energy.

The full kinematics will be measured at a single fixed electron-beam setting, thus eliminating uncertainties arising from time-dependent factors such as beam energy, charge integration, beam-spot position, and the like. The first of these runs will use a magnetic field in CLAS between 25 and 50% of its maximum positive value, and therefore will maximize the acceptance for  $p-\pi^-$ ,  $p-\pi^+-\pi^-$ , and  $p-\pi^--\pi^0$  events. This run will be fully compatible with Experiment 91-014. The second run will use the full tagger range and will therefore extend the photon energy range down to 320 MeV. This run will roughly double the number of events in the  $D_{13}$  and  $F_{15}$  resonance region, and also will overlap the  $\Delta$  for normalization purposes, will maximize the counting rate for  $p-p-n$  events, and will allow us to detect  $\Delta^{++}$  events well below the peak of their momentum distribution in  ${}^3\text{He}$ . This run also will use the full CLAS magnetic field, so that the resolution will be optimized for the  $p-p$ ,  $p-\pi^+$ ,  $n-\pi^+$ , and  $p-\pi^0$  events. The tagged-photon intensity for the first run will be  $2 \times 10^7 \text{ s}^{-1}$ ; for the second run,  $3 \times 10^7 \text{ s}^{-1}$ .

The hardware trigger will be a charged particle detected in a scintillator in coincidence with a second charged particle or with a neutral particle detected in a shower counter. This will guarantee detection of all of the kinds of events proposed here, with the sole exception of a  $\pi^+-t$  event where the triton does not emerge from the  ${}^3\text{He}$  target.

## 7. Apparatus and Commitments

In addition to the CLAS, this experiment requires the photon tagger, a liquid- $^3\text{He}$  target, and shower-counter capability at backward angles.

The photon tagger is being constructed by the Tagger Technical Working Group. The focal-plane detector array consists of 432 plastic scintillators (and 480 photomultiplier tubes), of which 384 are energy counters, overlapping to give 768 energy channels, and 48 are timing counters, sized so as to give roughly equal counting rates to maximize the tagged-photon intensity with minimum pileup. This array has been designed and is being constructed by the GWU group, at the Nuclear Detector Laboratory located at the new GWU Virginia Campus.

The cryogenic target and its associated instrumentation has been designed and will be constructed in France by the Saclay group. It will encompass capability for handling targets of liquid hydrogen, deuterium,  $^3\text{He}$ , and  $^4\text{He}$ . The target chamber will be inserted into the CLAS from the upstream side. A preliminary schematic diagram of the cryogenic target is shown in Fig. 28.

The back-angle shower counters, covering (so far) one sector of the CLAS from  $45^\circ$  to  $112^\circ$ , have been designed and are being constructed in Italy by the Genoa and Frascati groups. They consist of 33 alternating layers of lead sheets 2 mm thick and plastic scintillator sheets 15 mm thick. There are a total of 650 scintillators (and 256 photomultiplier tubes) in this array. These detectors are  $\geq 20\%$  efficient for neutron detection. Backward-angle neutron detection is particularly important for identifying and resolving  $\Delta^{++}$ -n events and for greatly enhancing the CLAS acceptance for  $\Delta^+ \rightarrow n + \pi^+$  events.

The  $^3\text{He}$  will be supplied by the Los Alamos National Laboratory. Approximately 750 liters (100 g) of very high-purity  $^3\text{He}$  is being requested (600 liters are required for operation). As of the time of this writing, 300 liters of purity 99.9% are in hand, and much more (4300 liters) is available but requires further purification. The GWU group has collaborated in recent years at LAMPF on several experiments on pion scattering from  $^3\text{H}$  and  $^3\text{He}$ .

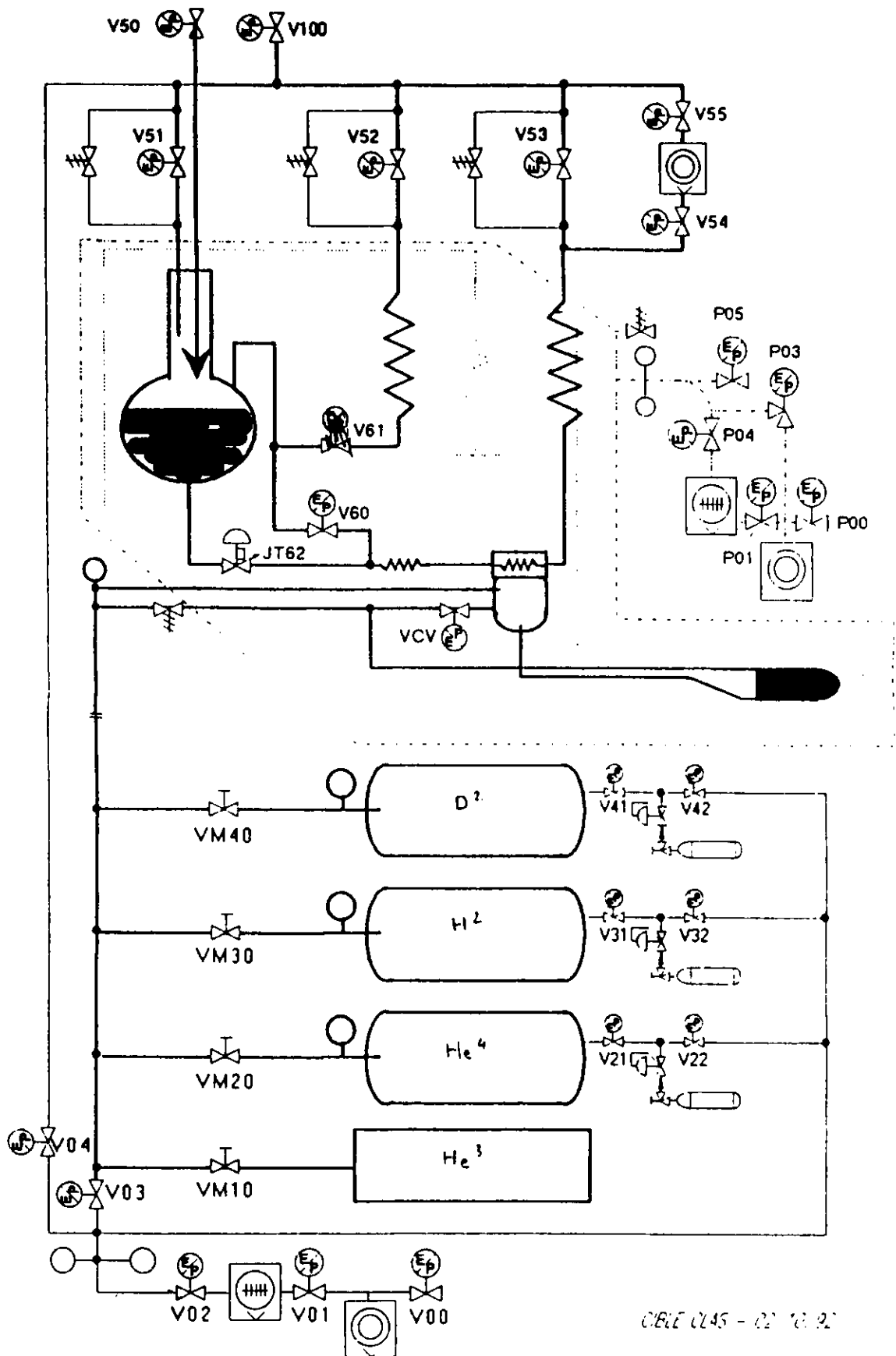


**Fig. 28.** Schematic representation of the cryogenic-liquid target for real-photon experiments with the CLAS.

## References

- (Abd90) S.K. Abdullin *et al.*, Sov. J. Nucl. Phys. **51**, 774 (1990).
- (Ang93) M. Anghinolfi *et al.*, Phys. Rev. C **47**, 922 (1993).
- (AngSP) M. Anghinolfi *et al.*, to be submitted for publication.
- (Aud89,91) G. Audit *et al.*, Phys. Lett. **227B**, 331 (1989); Phys. Rev. C **44**, R575 (1991).
- (AudPC) G. Audit, private communication.
- (Bac73,75) D. Bachelier *et al.*, Phys. Lett. **44B**, 44 (1973); Nucl. Phys. **A251**, 433 (1975).
- (Ber64) B.L. Berman, L.J. Koester, Jr., and J.H. Smith, Phys. Rev. **133**, B117 (1964).
- (Ber86) *The Three-Body Force in the Three-Nucleon System*, (B.L. Berman and B.F. Gibson, eds., Springer, Heidelberg, 1986); for a summary, see B.L. Berman, in *Theoretical and Experimental Investigations of Hadronic Few-Body Systems*, (C. Ciofi degli Atti *et al.*, eds., Springer, Vienna, 1986), p. 541.
- (Bia93) N. Bianchi *et al.*, Phys.Lett. **299B**, 219 (1993).
- (Bil92) R. Bilger *et al.*, Z. Phys. **A343**, 491 (1992).
- (Boc86) B. Bock *et al.*, Nucl. Phys. **A459**, 573 (1986).
- (Bou74) B. Bouquet *et al.*, Nucl. Phys. **B79**, 45 (1974).
- (Bri87,88) R. Brizzolara and M.M. Giannini, Few-Body Systems **3**, 49 (1987) and **5**, 1 (1988).
- (CioPC) C. Ciofi degli Atti, private communication.
- (Col93) P.L. Cole, "A Generalized FASTMC for the CLAS," CLAS note in preparation.

- (Fon92) A.C. Fonseca and D.R. Lehman, Phys. Lett. B (1992).
- (Gib84) B.F. Gibson and D.R. Lehman, Phys. Rev. C **29**, 1017 (1984).
- (Haj83a) C. Hajduk *et al.*, Nucl. Phys. **A405**, 581 (1983).
- (Haj83b) C. Hajduk *et al.*, Nucl. Phys. **A405**, 605 (1983).
- (Isg78-79) N. Isgur and G. Karl, Phys. Rev. D **18**, 4187 (1978); Phys. Rev. D **19**, 2653 (1979); Phys. Rev. D **20**, 1191 (1979).
- (Kam91) S.S. Kamalov, L. Tiator, and C. Bennhold, Few-Body Systems **10**, 143 (1991).
- (KnePC) U. Kneissel, private communication.
- (Lag85-89) J.-M. Laget, Nucl. Phys. **A446**, 4890 (1985); J. Phys. G **14**, 1445 (1988); Nucl. Phys. **A497**, 391 (1989).
- (Lag92) J.M. Laget, in *Electronuclear Physics with Internal Targets and the BLAST Detector* (R. Alarcon and M. Butler, eds., World Scientific, 1992).
- (LagPC) J.-M. Laget, private communication.
- (Laz76) C. Lazard and R.J. Lombard, Nucl. Phys. **A27**, 317 (1976).
- (Met74) W.L. Metcalf and R.L. Walker, Nucl. Phys. **B76**, 253 (1974).
- (MokPC) V. Mokeev, private communication.
- (Par91) W.C. Parke *et al.*, Few Body Systems **11**, 89 (1991).
- (RipPC) M. Ripani, private communication.
- (Str87) W. Strüve *et al.*, Nucl. Phys. **A465**, 651 (1987).
- (Wal69) R.L. Walker, Phys. Rev. **182**, 1729 (1969).
- (Wei90-92) S. Weinberg, Phys. Lett. **251B**, 288 (1990); Nucl. Phys. **B363**, 3 (1991); Univ. of Texas preprint UTTG-11-92.

## Appendix

# A Acceptance Studies of the ${}^3\text{He}(\gamma,pp)n$ Reaction

In this appendix we discuss the techniques that we have developed for separating the photoreaction  ${}^3\text{He}(\gamma,pp)n$  events from the  ${}^3\text{He}(\gamma,pp)n\pi^0$  channel. We then broach the subject of how we can accurately and expeditiously extract STAR candidates from the  ${}^3\text{He}(\gamma,pp)n$  background. Even though STARS may be likened to needles in the haystack, we firmly assert, and as will be evidenced below, that if STARS exist, we will find them.

## A.1 Event Generator and FASTMC

We employed the event generator, GENBOD, to distribute the photodisintegrated yield particles uniformly in phase space. GENBOD is a routine in CERNLIB package. The particles are then Lorentz boosted to the lab frame and fed into FASTMC. FASTMC is a parametric Monte Carlo which renders a realistic representation of the geometry and mass composition of the CLAS detector. This Monte Carlo includes such effects as particle decay, multiple scattering,  $dE/dX$  losses, detector efficiencies and geometrical acceptance. The user may select several input parameters, among which are: strength and polarity of the toroidal magnetic field, rms width of the photon beam, and dimensions and type of target.

## A.2 Acceptance Parameters

We define the acceptance in the usual way:

$$\varepsilon = \frac{N_{\text{acc}}}{N_{\text{gen}}}$$

where  $N_{\text{gen}}$  is the total number of events generated and  $N_{\text{acc}}$  represents the number of events accepted after passing all cuts. Furthermore, the acceptance,  $\varepsilon$ , depends upon the incident tagged photon energy,  $E_\gamma$ , and upon both the strength and polarity of the toroidal field of the CLAS.

$$\varepsilon = \varepsilon(E_\gamma, \vec{B})$$

For the  $ppn\pi^0$  and  $ppn$  acceptance studies, between 60 000 and 100 000 events were generated for each bin. We binned the acceptance in terms of:

1.  $E_\gamma$ : = 0.8 and 1.3 GeV
2. B field: The magnetic field was set to  $-0.25$ ,  $+0.25$ ,  $+0.50$ ,  $+0.75$  &  $1.00$  nominal strength.

We chose the following input parameters for the CLAS FASTMC detector simulation:

1. No Vertexing: The track reconstruction does not include the vertex as a constraint in the fit.
2. Error in momentum: Positional mismeasurement and multiple scattering terms included.
3. Beam: rms width of photon beam set to 1 cm.
4. Target:  $^3\text{He}$

### A.2.1 Particle Identification

For a particle that is tracked through the three separate drift chambers, and deposits energy in a TOF counter, we can calculate its mass from the relativistic relationship:

$$m^2 = |\vec{p}|^2 \frac{1 - \beta^2}{\beta^2}$$

where

$$\beta = \frac{1}{c} \frac{\ell}{\Delta t}$$

Here,  $\ell$  is the path length to the TOF counter and  $\Delta t$  is the particle's time of flight. For this study, we smeared  $\Delta t$  with a gaussian  $\sigma_t$  of between 100 and 200 picoseconds, depending upon which counter registered the hit. From the mass squared distributions, we can identify the particle. A particle with a  $m^2 > 0.65 \text{ (GeV}/c^2)^2$  is identified as a proton. In figure A1 we show the  $m^2$  distributions for phase space generated  $\gamma + ^3\text{He} \rightarrow p + p + n$  events.

### A.2.2 Singles and Doubles Proton Acceptance

After imposing the particle identification cuts for protons, we are now in the position to state the acceptance of one proton and two protons in coincidence for  $\gamma + ^3\text{He} \rightarrow p + p + n$  events. In figure A2 we show the singles acceptance for protons as a function of incident photon beam energy and magnetic field operating points. We notice that the acceptance is not a strong function of the magnetic field strength for fixed photon energy. From figure A3, we see that the acceptance is *independent* of field strength for positive polarity settings. This is because the protons are correlated. Although we distribute the nucleons randomly in phase space, we must conserve the 4-momentum of these particles, which will constrain the direction and magnitude of the three momentum of the third generated nucleon, i.e. in the cms frame:

$$|\vec{p}_3|^2 = |\vec{p}_1|^2 + |\vec{p}_2|^2 + 2p_1p_2 \cos \theta_{12}$$

where  $\theta_{12}$  is the cms angle between the first and second nucleon. And the direction of the third nucleon is opposite to the vector sum of the three momenta of the first two nucleons. So whether a proton is measured depends upon the direction the other proton.

### A.3 Cuts

In this section we discuss how we separate the signal from the noise. The primary difficulty in identifying the ppn channel is in separating the reaction  ${}^3\text{He}(\gamma, \text{pp})\text{n}$  from the process  ${}^3\text{He}(\gamma, \text{pp})\text{n}\pi^0$ . We have developed powerful cuts which allow us to unambiguously identify the ppn channel. These cuts are:

1. Two protons measured in coincidence, i.e. two charged particles with  $m^2 > 0.65 \text{ (GeV}/c^2)^2$ .
2. The missing mass squared  $\leq 1.1 \text{ (GeV}/c^2)^2$ .
3. The reconstructed energy of the incident photon agrees with the value obtained from the tagger.

Demanding a two proton coincidence and applying the missing mass cut leaves only 397 of the 60 000 ppn $\pi^0$  events generated ( $E_\gamma = 0.8 \text{ GeV}$  and  $B/B_0 = +1.0$ ). This value is to be compared to the 56.6k  ${}^3\text{He}(\gamma, \text{pp})\text{n}$  of the 100k events generated that pass these two cuts, cf. tables 2 and 3. If accidentals or  $\gamma + X \rightarrow \text{p} + \text{p} + \text{n} + X'$  contamination are not of concern, the first two cuts will suffice in eliminating the  $\pi^0$  background. If, however, we wish insure that the photoreaction yield products measured in the CLAS correspond to the measured energy of the bremsstrahlung electron in the tagger, we need to reconstruct the photon energy. In order to calculate the reconstructed photon energy, we must first determine the center-of-momentum energy.

$$E_{\text{cm}}^2 = M_{{}^3\text{He}}^2 + 2M_{{}^3\text{He}}E_\gamma \quad (1)$$

where  $M_{{}^3\text{He}}$  is the mass of the  ${}^3\text{He}$  nucleus, and  $E_\gamma$  is the energy of the tagged photon. We note, incidentally, that the energy of the bremsstrahlung photon can be tagged to within 0.1% of the incident electron energy, which is better than can be measured in the CLAS. We next calculate the proton masses from their four momentum,  $p^\mu$ . And from the quantities  $(E_\gamma, p_{p_1}^\mu, p_{p_2}^\mu, M_{{}^3\text{He}})$ , we can

determine the missing mass,  $x_{\text{miss}}$ . Namely<sup>1</sup>:

$$\begin{aligned} m_1 &= \sqrt{E_{p_1}^2 - |\vec{p}|_{p_1}^2} \\ m_2 &= \sqrt{E_{p_2}^2 - |\vec{p}|_{p_2}^2} \\ m_3 &= x_{\text{miss}} \end{aligned} \quad (2)$$

The reconstructed photon energy is then

$$E_{\gamma}^{\text{rcn}} = \frac{E_{\text{cm}}^2 - m_{\text{tgt}}^2}{2m_{\text{tgt}}} \quad (3)$$

where we have set  $m_{\text{tgt}} = -7.7 \text{ MeV} + \sum_{i=1}^3 m_i$ , and have implicitly included the 7.7 MeV binding energy of the  ${}^3\text{He}$  nucleus. We note that the reconstruction of the photon energy is very sensitive to the value obtained for the reconstructed mass of the target. Indeed, the error in the missing mass is the dominant source of error in  $E_{\gamma}^{\text{rcn}}$ .

$$|\Delta E_{\gamma}^{\text{rcn}}| = \left[ \frac{E_{\text{cm}}^2 + m_{\text{tgt}}^2}{2m_{\text{tgt}}^2} \right] \Delta m_{\text{tgt}} \quad (4)$$

For example, a 2% error in the reconstructed mass of the target (i.e. 60 MeV) will translate into a 90 MeV error in  $E_{\gamma}^{\text{rcn}}$  for a  $E_{\gamma}^{\text{true}}$  of 1.3 GeV. In figure A4, we overlay the reconstructed photon energy for the reactions  ${}^3\text{He}(\gamma, pp)n$  and  ${}^3\text{He}(\gamma, pp)n\pi^0$  at  $B/B_0 = 1.0$  and  $E_{\gamma} = 1.3 \text{ GeV}$ . Note that the distributions are normalized to their area and that no cuts have been performed; in particular the missing mass squared cut (Cut1) has not been imposed (cf. *Definition of Cuts* below). In Table A1, we tabulate the FWHM resolution of the  $E_{\gamma}^{\text{rcn}}$  and missing mass squared,  $x_{\text{miss}}^2$ , as a function of incident monochromatic photon beam energy and magnetic field operating points. These results are plotted in figures A5 and A6.

#### *Definition of Cuts*

1. Cut1: Reconstructed missing mass squared is less than  $1.1 \text{ (GeV}/c^2)^2$ .
2. Cut2:  $|E_{\gamma}^{\text{gen}} - E_{\gamma}^{\text{rcn}}| \leq 80 \text{ MeV} + \text{Cut1}$ .
3. Cut3:  $|E_{\gamma}^{\text{gen}} - E_{\gamma}^{\text{rcn}}| \leq 60 \text{ MeV} + \text{Cut1}$ .
4. Cut4:  $|E_{\gamma}^{\text{gen}} - E_{\gamma}^{\text{rcn}}| \leq 40 \text{ MeV} + \text{Cut1}$ .
5. Cut5:  $|E_{\gamma}^{\text{gen}} - E_{\gamma}^{\text{rcn}}| \leq 20 \text{ MeV} + \text{Cut1}$ .

Table 1: Resolution of missing mass squared and reconstructed photon energy as a function of incident photon beam energy and magnetic field.

FWHM of $E_{\gamma}^{\text{rec}}$ for ${}^3\text{He}(\gamma,pp)n$ [MeV]					
For $B/B_0 =$	-0.25	0.25	0.50	0.75	1.00
$E_{\gamma} = 0.8$ GeV	78	80	36	28	18
$E_{\gamma} = 1.3$ GeV	120	120	64	48	45
FWHM of $x_{\text{mass}}^2$ from ${}^3\text{He}(\gamma,pp)n$ $[(\text{MeV}/c^2)^2]$					
For $B/B_0 =$	-0.25	0.25	0.50	0.75	1.00
$E_{\gamma} = 0.8$ GeV	240	240	140	100	100
$E_{\gamma} = 1.3$ GeV	260	260	180	140	140

Table 2: Acceptance of events with two proton coincidence under various cuts. 100k events generated uniformly in phase space for the reaction  $\gamma+{}^3\text{He} \rightarrow p + p + n$

$\gamma+{}^3\text{He} \rightarrow p + p + n$										
	$E_{\gamma} = 0.8$ GeV					$E_{\gamma} = 1.3$ GeV				
$B/B_0$	Cut 1	Cut 2	Cut 3	Cut 4	Cut 5	Cut 1	Cut 2	Cut 3	Cut 4	Cut 5
-0.25	54.7k	27.0k	24.7k	20.8k	13.0k	55.7k	22.5k	19.5k	15.0k	8.3k
+0.25	55.0k	27.4k	25.0k	20.8k	13.0k	56.0k	22.4k	19.5k	14.9k	8.3k
+0.50	56.8k	28.7k	27.0k	24.5k	18.5k	58.3k	25.6k	23.9k	20.5k	13.0k
+0.75	56.7k	28.7k	27.1k	25.2k	20.9k	58.4k	25.9k	24.8k	22.5k	15.7k
+1.00	56.6k	28.6k	27.0k	25.3k	21.9k	58.4k	25.9k	24.9k	23.2k	17.3k

Table 3: Acceptance of events with two proton coincidence under various cuts. 60k events generated uniformly in phase space for the reaction  $\gamma+{}^3\text{He} \rightarrow p + p + n + \pi^0$ .

$\gamma+{}^3\text{He} \rightarrow p + p + n + \pi^0$										
	$E_{\gamma} = 0.8$ GeV					$E_{\gamma} = 1.3$ GeV				
$B/B_0$	Cut 1	Cut 2	Cut 3	Cut 4	Cut 5	Cut 1	Cut 2	Cut 3	Cut 4	Cut 5
-0.25	1224	79	58	38	19	753	46	34	29	17
+0.25	945	85	62	42	17	583	40	22	17	13
+0.50	539	40	32	18	8	382	13	8	4	2
+0.75	460	53	42	30	13	328	18	13	9	3
+1.00	397	41	28	17	5	314	25	18	13	8

Comparing tables A2 and A3, we can see how remarkably effective the  $\pi^0$  channel cuts are. In fact, should the cross section for  $\gamma+^3\text{He} \rightarrow \text{p} + \text{p} + \text{n} + \pi^0$  be 300 times greater than for the reaction  $\gamma+^3\text{He} \rightarrow \text{p} + \text{p} + \text{n}$ , the signal to noise ratio under cut4 will still be 1:1 at  $E_\gamma = 0.8$  GeV and  $B/B_0 = +0.25$ , affording our experiment an acceptance of 20.8%.

## A.4 Selection Criteria for the STAR Configurations

Now that we have a means to effectively eliminate the  $^3\text{He}(\gamma,pp)n\pi^0$  background, the next step in our acceptance studies is to correctly identify STAR candidates. We have employed Dalitz plot formalism to aid us in this endeavor.

We developed an event generator, which emulates the expected physics of the STAR configuration. In the center-of-momentum frame, the outgoing nucleons all share equal kinetic energies, since the mass difference between the proton and the neutron is less than  $1.3 \text{ MeV}/c^2$ . This implies that in the cms frame the angle between the trajectories of any two outgoing nucleons is  $120^\circ$ . The events are then generated uniformly in phase space, Lorentz boosted to the lab frame, and fed into FASTMC. For these studies we generated 25 000 events. A two proton coincidence defines an accepted event, resulting in an overall acceptance of 60%.

In figures A7 and A8 we show the results of our acceptance analysis for STAR events. In the triangular kinetic energy Dalitz plot, figure A7, the lab frame kinetic energies  $T'$  of the two measured protons and the reconstructed  $T'_{\text{neut}}$  are plotted. Here  $T'_i$  is the fractional kinetic energy that the  $i$ th nucleon carries and is equal to  $T_i/\sum_{i=1}^3 T_i$ , where  $T_i = E_{\text{lab}}^i - m$ . All STAR candidates will be contained within a circle of radius  $r$ :

$$r = \frac{\gamma[E_{\text{cm}}/3 + \beta\sqrt{(E_{\text{cm}}/3)^2 - m^2}] - m}{\gamma E_{\text{cm}} - 3m} - \frac{1}{3} \quad (5)$$

where  $m$  is the mass of a nucleon,  $\beta = E_\gamma/(M_{^3\text{He}} + E_\gamma)$ , and  $\gamma = 1/\sqrt{1 - \beta^2}$ . That is to say, in the laboratory frame, the nucleons must satisfy the condition:

$$\sqrt{T_x^2 + T_y^2} \leq r$$

where we have made the change of variable

$$T_x = \frac{T'_{p1} - T'_{p2}}{\sqrt{3}}$$

---

<sup>1</sup>We note that one could set  $m_1$  and  $m_2$  identically equal to the mass of the proton. However, since we have not modeled the effects of kaons being misidentified as protons, we chose to derive the proton masses from the 4-momentum

$$T_y = T'_n - \frac{1}{3}$$

In figure A7, we see the accepted STAR events are contained within the a circle of radius .232 for  $E_\gamma = 1.3$  GeV. We observe, moreover, that in the cms frame  $r = 0$ , which implies  $T'_i \equiv 1/3$ .

For an event that passes the above  $r$  cut, we next employ the method of the triangular invariant mass Dalitz plot to search for STAR candidates. First we form the invariant mass squared for the three pairings of the three nucleons. Where the invariant mass squared,  $m_{12}^2$ , of the first and second nucleon is:

$$m_{12}^2 = (E_1 + E_2)^2 - \sum_{i=1}^3 (p_1^i + p_2^i)^2$$

$m_{13}^2$  and  $m_{23}^2$  are similarly defined. For a STAR event:

$$m_{12}^2 = m_{13}^2 = m_{23}^2 = \frac{E_{\text{cm}}^2}{3} + m^2$$

where  $m$  is the nucleon mass. In figure A8 we plot the  $m_{ij}^2$ s (normalized to the sum of the three invariant masses). And indeed the invariant mass squared of each of the nucleon pairs are equal. In table A4, we tabulate the effects of the  $r$  and invariant mass squared cuts. Here we define:

$$m_x^2 = \frac{1}{M^2} \left[ \frac{m_{12}^2 - m_{13}^2}{\sqrt{3}} \right]$$

$$m_y^2 = \frac{m_{23}^2}{M^2} - \frac{1}{3}$$

where

$$M^2 = m_{12}^2 + m_{13}^2 + m_{23}^2$$

In table A4, we tabulate the effects of the  $r$  and invariant mass squared cuts. We see that these cuts can eliminate at least 99.4% of the  ${}^3\text{He}(\gamma, pp)n$  background for incident photon energies between 0.8 and 1.3 GeV, and the acceptance appears not to be a strong function of the magnetic operating point. As a point of reference, we subjected our STAR events to the two Dalitz cuts. We found that 67% of the two proton in coincidence accepted STAR events survived the  $r$  and  $|m_x^2| \leq 0.01$  &  $|m_y^2| \leq 0.01$  cuts for  $E_\gamma = 1.3$  GeV at  $B/B_0 = +0.75$ . The above two Dalitz techniques, moreover, do not require Lorentz boosting to the cms frame. However, once we have selected a STAR candidate, we can transform to the center-of-momentum frame to insure that  $T_1 = T_2 = T_3$ , as an additional check.

Table 4: Acceptance of events with two proton coincidence under various cuts. 100k events generated uniformly in phase space for the reaction  $\gamma + {}^3\text{He} \rightarrow p + p + n$

$E_\gamma = 0.8 \text{ GeV}$ ( $r \text{ cut} = .205$ )				
B/B <sub>0</sub>	2p Acc.	$r \text{ cut}$	$r \text{ cut}$ $ m_x^2  < 0.02$ $ m_y^2  < 0.02$	$r \text{ cut}$ $ m_x^2  < 0.01$ $ m_y^2  < 0.01$
-0.25	58.8k	22.2k	1306	325
+0.25	58.9k	22.1k	1312	337
+0.50	58.9k	22.3k	1296	351
+0.75	58.9k	22.2k	1393	333
+1.00	58.9k	22.3k	1310	347
$E_\gamma = 1.3 \text{ GeV}$ ( $r \text{ cut} = .232$ )				
B/B <sub>0</sub>	2p Acc.	$r \text{ cut}$	$r \text{ cut}$ $ m_x^2  < 0.02$ $ m_y^2  < 0.02$	$r \text{ cut}$ $ m_x^2  < 0.01$ $ m_y^2  < 0.01$
-0.25	60.0k	27.4k	845	207
+0.25	60.1k	27.4k	843	195
+0.50	60.1k	27.5k	801	186
+0.75	60.1k	27.5k	812	201
+1.00	60.1k	27.6k	814	205

## A.5 Summary

In this appendix, we have shown that we have developed extremely effective cuts, which can clearly separate  ${}^3\text{He}(\gamma,pp)n$  from the  ${}^3\text{He}(\gamma,pp)n\pi^0$  background. Moreover, our Dalitz plot techniques enable us to quickly eliminate the vast majority of uninteresting  ${}^3\text{He}(\gamma,pp)n$  events, and thereby serves to enhance the STAR signal.

## List of Figures

1	Reconstructed proton mass squared. . . . .	11
2	Singles proton acceptance as a function of incident photon energy and magnetic field operating point for the reaction ${}^3\text{He}(\gamma,p)\text{pn}$ . . . . .	12
3	Doubles proton acceptance as a function of incident photon energy and magnetic field operating point for the reaction ${}^3\text{He}(\gamma,pp)\text{n}$ . . . . .	13
4	Overlay of the reconstructed photon energy for both the reactions ${}^3\text{He}(\gamma,pp)\text{n}$ and ${}^3\text{He}(\gamma,pp)\text{n}\pi^0$ . $E_\gamma = 1.3$ GeV and $B/B_0 = +1.0$ . . . . .	14
5	Resolution (FWHM) of the reconstructed photon energy as a function of tagged photon energy and magnetic field operating point for ${}^3\text{He}(\gamma,pp)\text{n}$ . . . . .	15
6	Resolution (FWHM) of missing mass squared as a function of tagged photon energy and magnetic field operating point for ${}^3\text{He}(\gamma,pp)\text{n}$ . . . . .	16
7	Triangular kinetic energy Dalitz plot for STARs in the lab frame for $E_\gamma = 1.3$ GeV and $B/B_0 = +0.75$ . Note that the majority of events are interior to $r = .232$ for the STAR ${}^3\text{He}(\gamma,pp)\text{n}$ reaction . . . . .	17
8	Triangular invariant mass Dalitz plot for STARs in the lab frame for $E_\gamma = 1.3$ GeV and $B/B_0 = +0.75$ . Note that $m_{12}^2 \approx m_{13}^2 \approx m_{23}^2$ . . . . .	18

$E_\gamma = 1.3 \text{ GeV}$   $B/B_0 = 1.0$

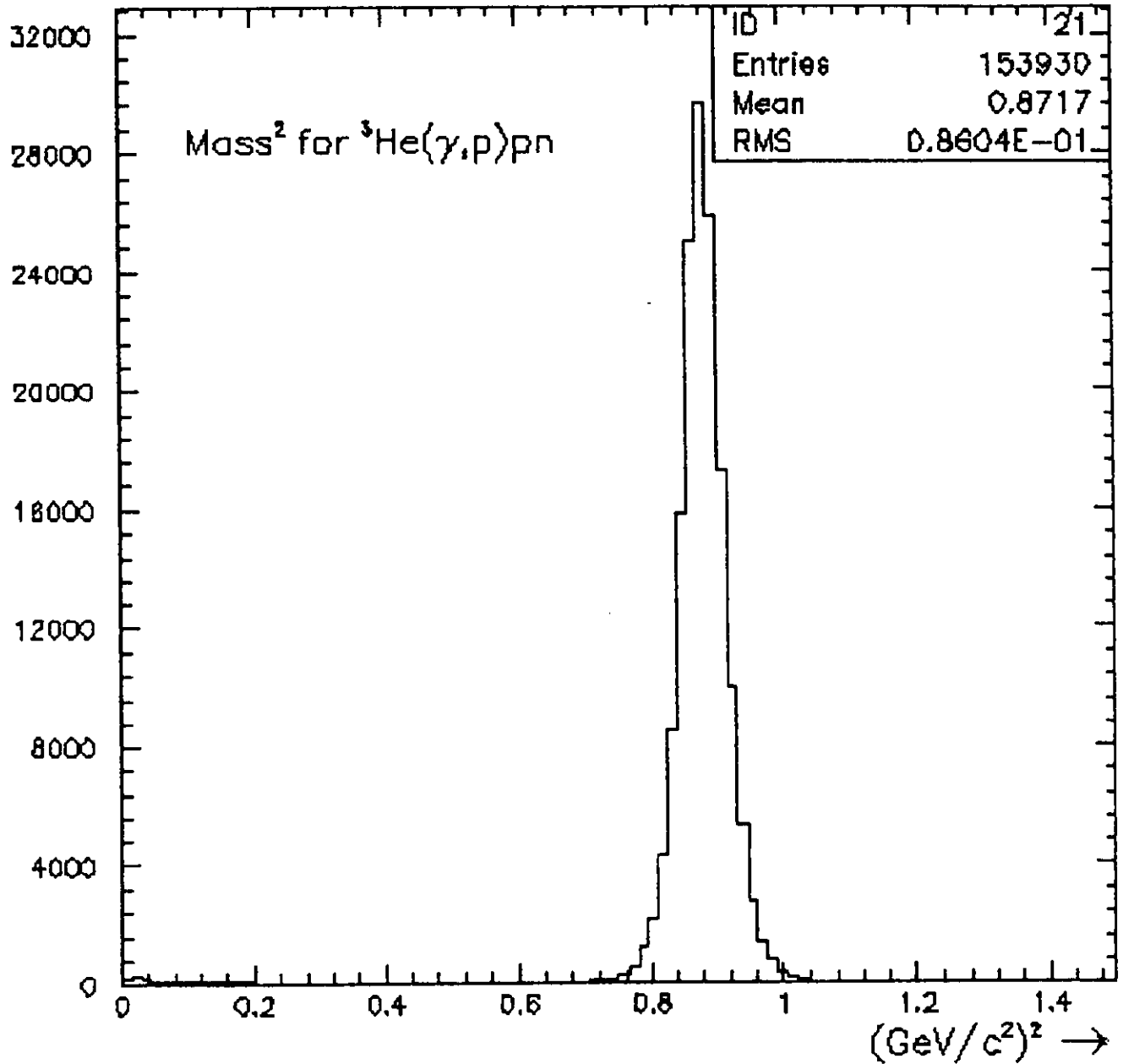


Figure 1: Reconstructed proton mass squared.

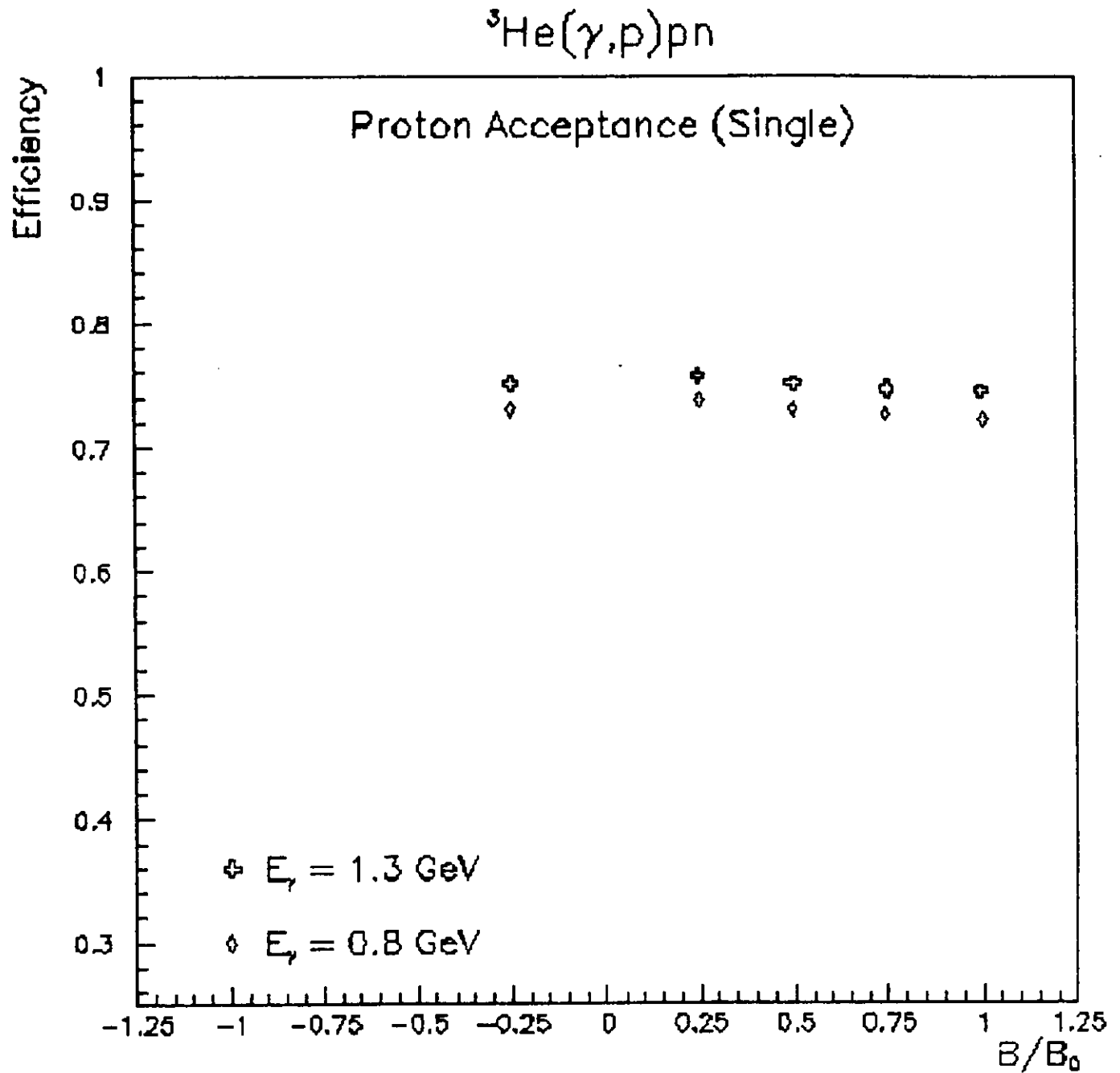


Figure 2: Singles proton acceptance as a function of incident photon energy and magnetic field operating point for the reaction  ${}^3\text{He}(\gamma, p)pn$

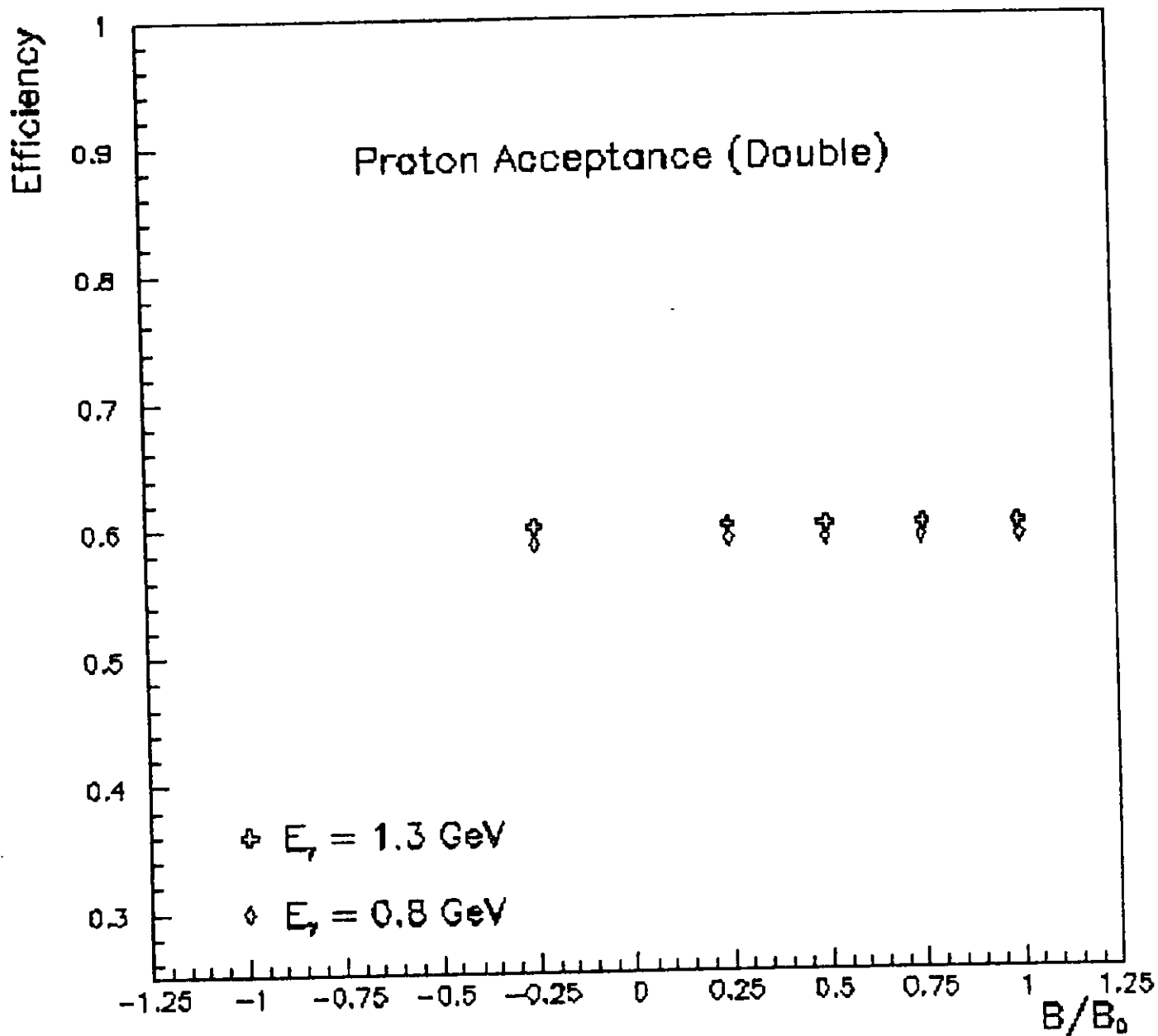
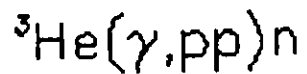


Figure 3: Doubles proton acceptance as a function of incident photon energy and magnetic field operating point for the reaction  ${}^3\text{He}(\gamma, pp)n$

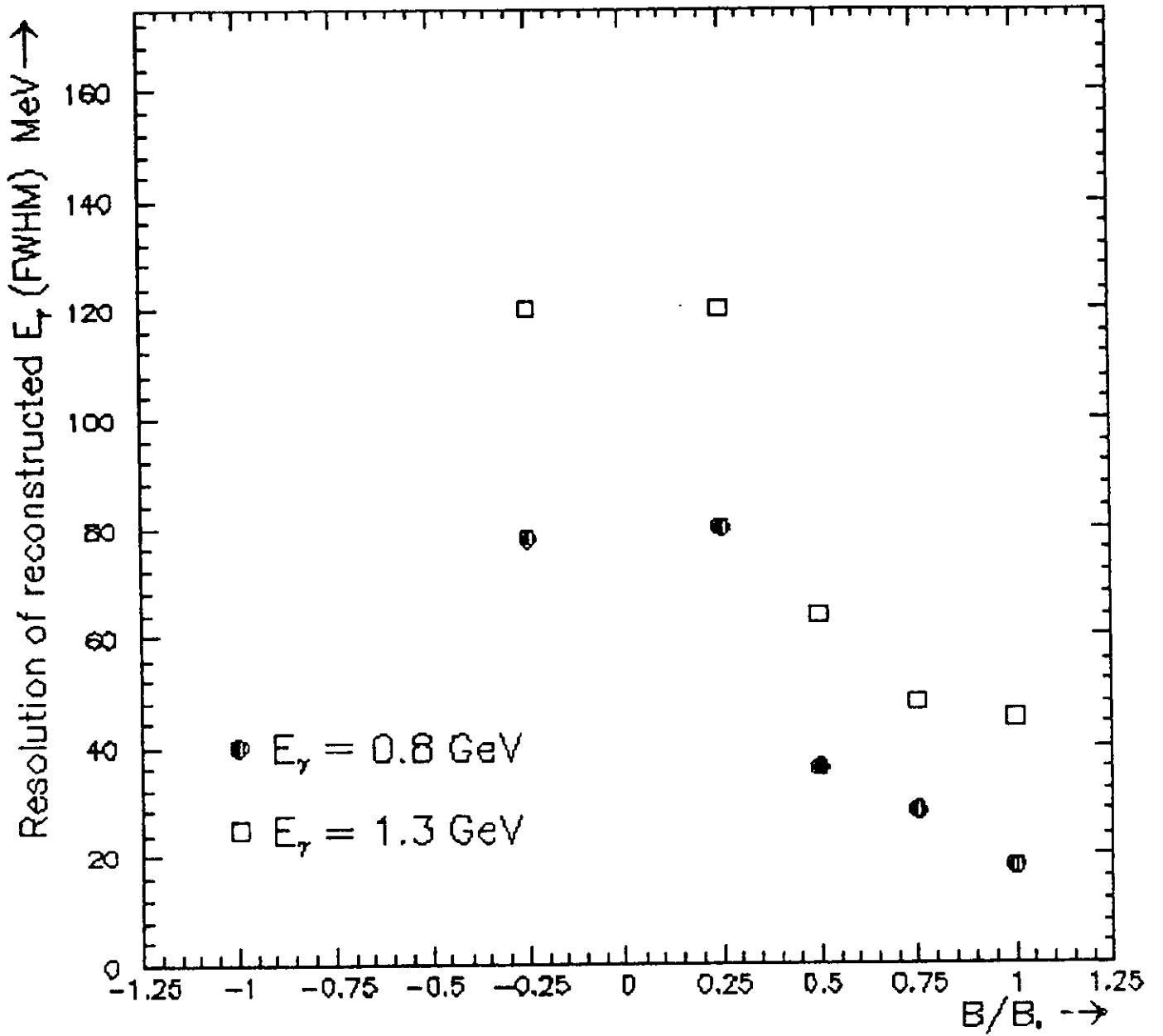


Figure 5: Resolution (FWHM) of the reconstructed photon energy as a function of tagged photon energy and magnetic field operating point for  ${}^3\text{He}(\gamma,pp)n$ .

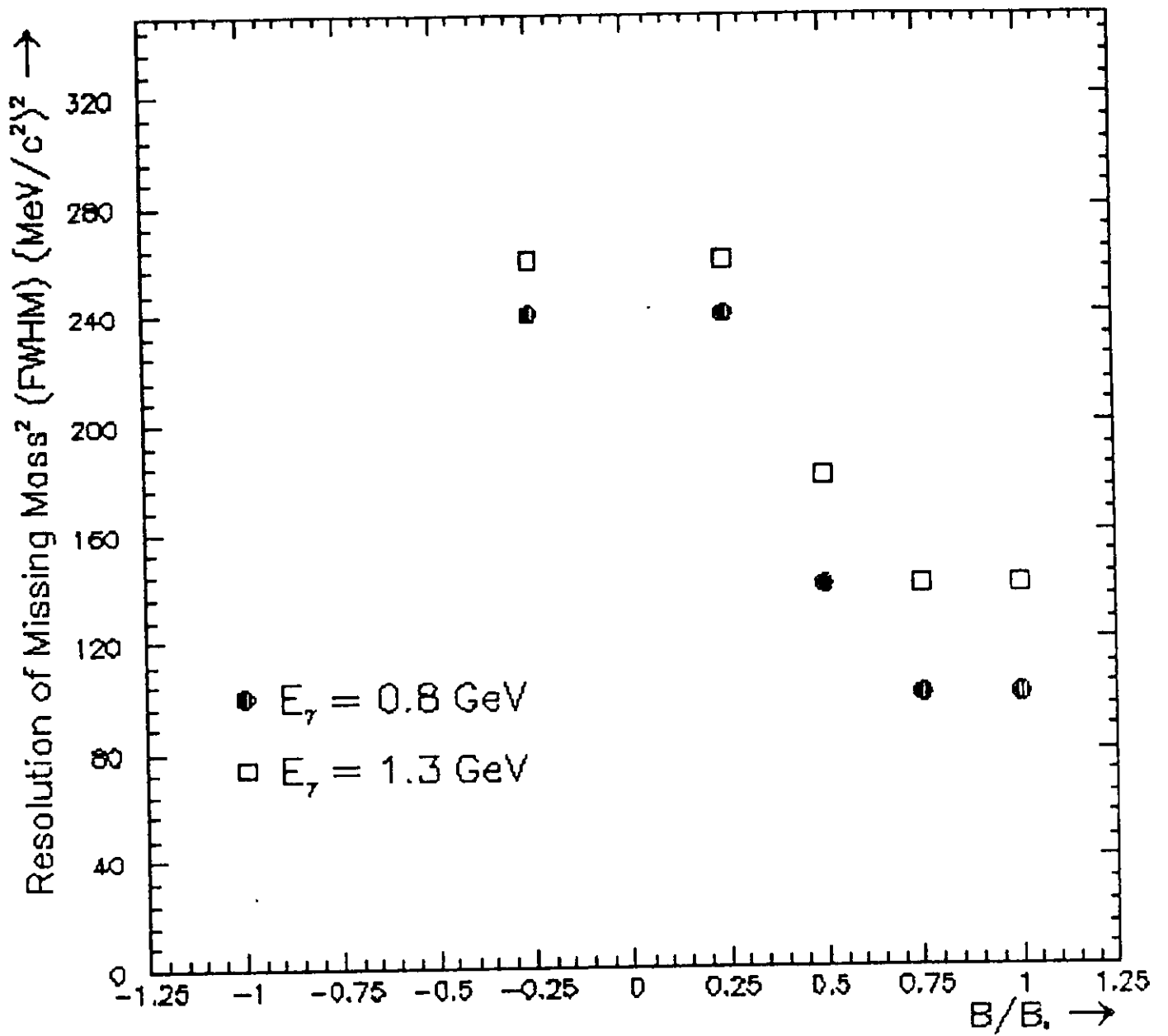


Figure 6: Resolution (FWHM) of missing mass squared as a function of tagged photon energy and magnetic field operating point for  ${}^3\text{He}(\gamma,pp)n$ .

(Comparison of 3 body breakup with  $\pi^0$ 's)

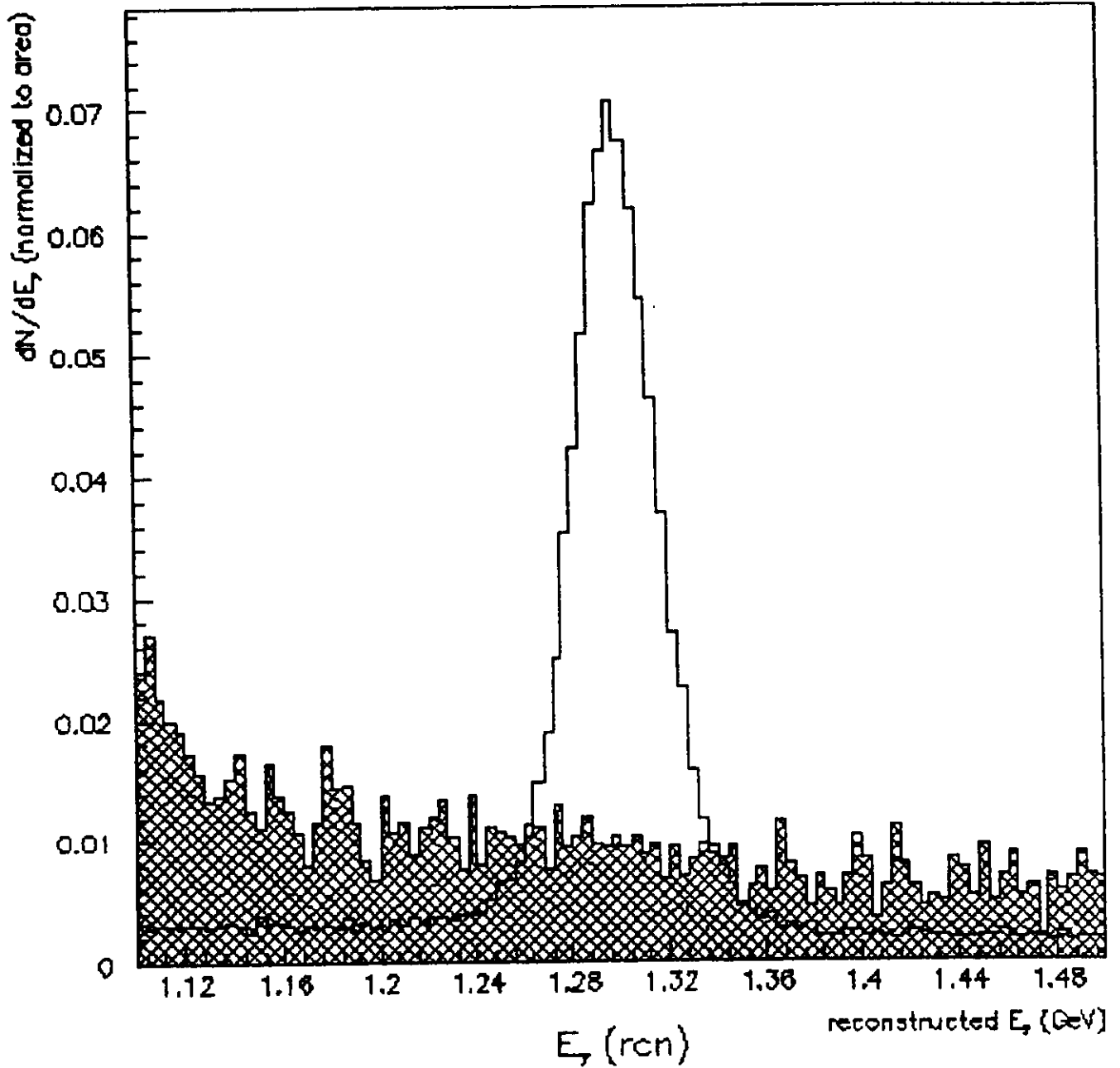


Figure 6: Resolution (FWHM) of missing mass squared as a function of tagged photon energy and magnetic field operating poing for  ${}^3\text{He}(\gamma,pp)n$ .

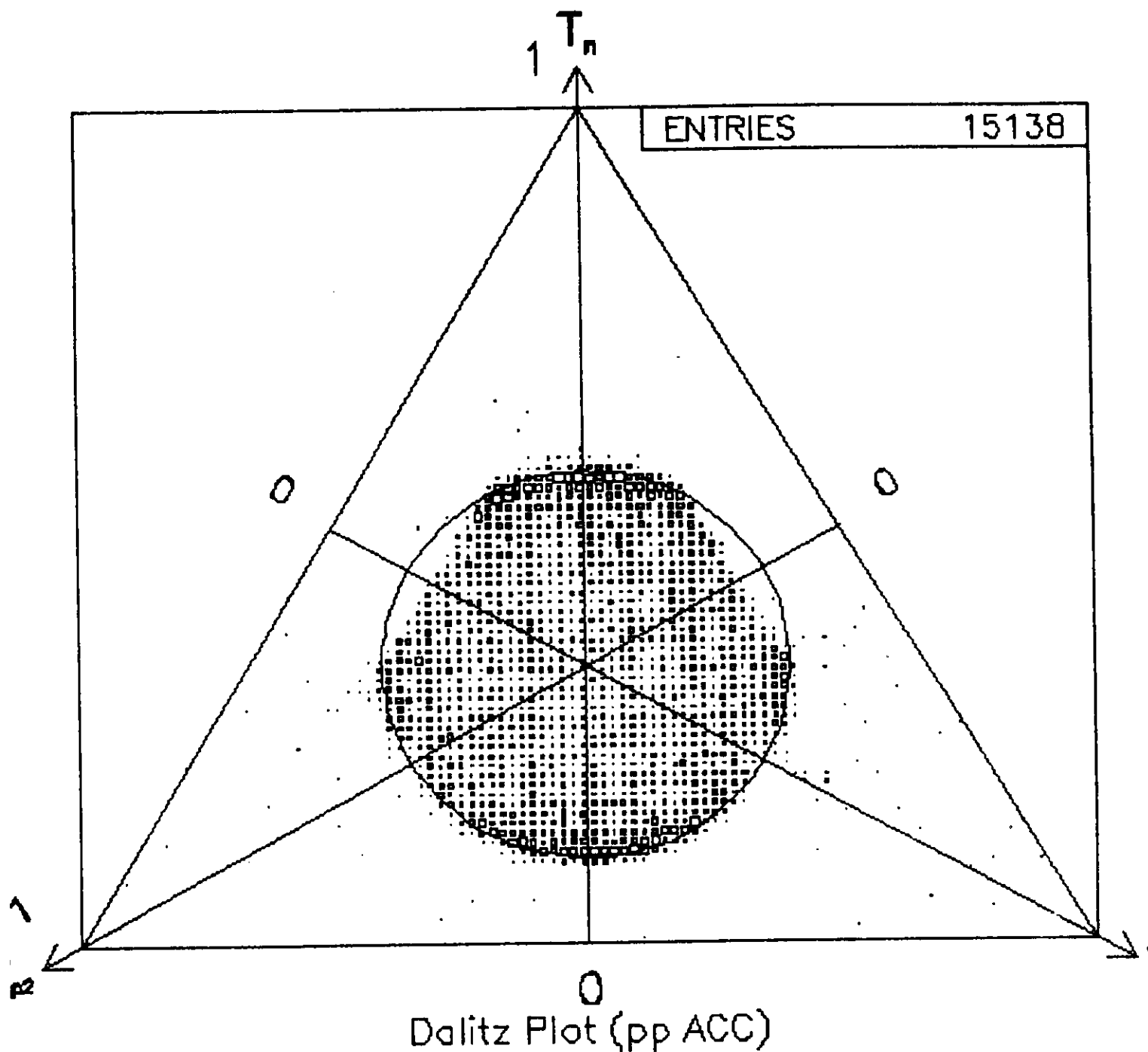


Figure 7: Triangular kinetic energy Dalitz plot for STARs in the lab frame for  $E_\gamma = 1.3$  GeV and  $B/B_0 = +0.75$ . Note that the majority of events are interior to  $r = .232$  for the STAR  ${}^3\text{He}(\gamma, pp)n$  reaction

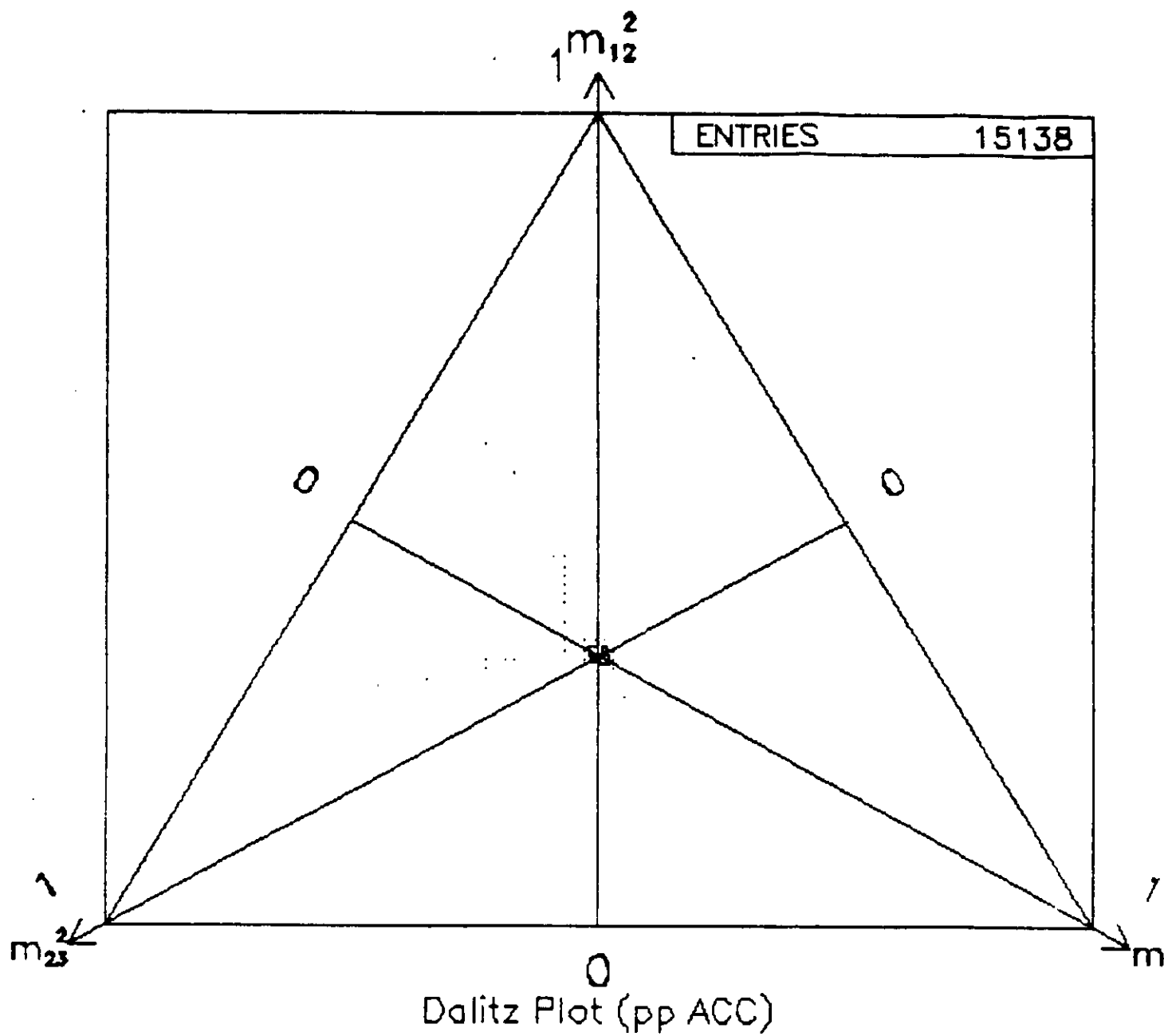


Figure 8: Triangular invariant mass Dalitz plot for STARs in the lab frame for  $\vec{E}_\gamma = 1.3$  GeV and  $B/B_0 = +0.75$ . Note that  $m_{12}^2 \approx m_{13}^2 \approx m_{23}^2$ .